A STATISTICAL THEORY OF STRENGTH FOR FIBER REINFORCED CONCRETE

by

ANTOINE E. NAAMAN
Ingénieur Diplomé de l'Ecole Centrale
des Arts et Manufactures
(Paris 1964)
Ancien Elève du Centre des Hautes Etudes
de la Construction
(Paris 1965)
S.M., Massachusetts Institute of Technology
(1970)

Submitted in partial fulfillment

of the requirements for the degree of

Doctor of Philosophy

at the

Massachusetts Institutute of Technology

September 1972

Signature of Author . . . . . .
Department of Civil Engineering, September 1972

Certified by . . . . . .
Thesis Supervisor

Accepted by . . . . . .
Chairman, Departmental Committee on Graduate Students
of the Department of Civil Engineering

ABSTRACT

A STATISTICAL THEORY OF STRENGTH

FOR FIBER REINFORCED CONCRETE

by

ANTOINE E. NAAMAN

Cementitious matrices show in general similar mechanical characteristics that distinguish them from metallic and polymeric matrices, i.e. relatively high compressive strength, poor tensile strength and brittleness at failure. Putting steel fibers in Portland cement concrete is meant to enhance its tensile properties, delay cracking and increase its toughness. Specific applications result, but are limited by the current understanding of the composite's response under load and the insufficient information on which design properties can be assessed. The scope of this study is to fill the existing gap by exploring from the microscopic to the macroscopic level the composite characteristics and presenting a rational method to predict tensile properties of fiber reinforced concrete. A detailed analytical representation is developed and simultaneously supported by an extensive experimental program.

The analytical representation is devoted to the development of a causal mathematical model that simulates the composite's response under tensile loading by taking into consideration the statistical nature of most variables involved and recognizing the extreme value characteristic of tensile strength. As the apparent ductile or brittle failure of fiber reinforced concrete depends somehow on the ratio of the fiber length to the member length, the proposed model is divided into two major parts. The first one, dealing with the ductile type failure, is based on the statistical mechanics of composite materials. It explores in detail all that is going on at the one fiber level and extrapolates results to the macroscopic response of the composite. The second part of the model covers the brittle type failure incorporating a fracture

mechanics criterion in the analysis. Each formulation leads essentially to the assessment of the composite characteristic tensile strength and its distribution functions. The chain weakest link concept of reliability theory is then applied to bound the overall model and provides results as modified by the size of the tensile member.

The experimental program is divided in four parts having various purposes as suggested by the mathematical formulation. The first part validates a major assumption of the model related to the Poisson-like distribution of the fibers in the concrete mass. The second part deals with the assessment of the bond or shear strength at the fiber matrix interface and its variation with fiber orientation. The third part is concerned with devising a reliable test to measure some fracture properties of the composite such as fracture toughness and pseudo plastic zone size. A final part is devoted to testing tensile prisms of fiber reinforced concrete where the influence of major reinforcement parameters such as volume fraction and aspect ratio of fibers is sought.

Experimental findings and consequent refinement of some of the model's assumptions lead to the conclusion that it is possible to rationally predict the tensile properties of fiber reinforced concrete using the proposed model. They also suggest that the framework of the mathematical formulation can be extended to simulate the behavior of most discontinuous fiber reinforced matrices.

Thesis Supervisor: Fred Moavenzadeh

Title: Professor of Civil Engineering

ACKNOWLEDGMENT

The author wishes to express his sincere appreciation to Professor F. Moavenzadeh, his thesis advisor, Professor F. J. McGarry and Professor M. Holley, members of his doctoral committee for their time, support and valuable guidance throughout this study.

He also wishes to thank Professor A. Argon who was most helpful in initiating this research and Professor J. Soussou who carefully reviewed the mathematical formulation and patiently discussed major implications and results.

The author is indebted to his wife, Ingrid Naaman, for typing this thesis more than once and for contributing more than her share in family affairs during his graduate studies at M.I.T.

CONTENTS

CONTENTS - continued

CONTENTS - Continued

LIST OF FIGURES

LIST OF FIGURES - continued

LIST OF FIGURES - continued

LIST OF TABLES

LIST OF MAJOR SYMBOLS

ε_{fu}	ultimate tensile strain of fiber
σ_{fu}	ultimate tensile strength of fiber
ε_{mu}	ultimate tensile strain of matrix
σ_{mu}	ultimate tensile strength of matrix
E_c	composite modulus of elasticity
ν_c	composite Poisson ratio
V_f	volume fraction of fibers
ℓ	fiber length
ϕ	fiber diameter
τ	bond or shear strength at the fiber matrix interface
A	cross section area of member or link
N	number of links in the chain model
N_s	number of fibers intersecting a unit area
N_v	number of fibers per unit volume of composite
x	pull-out length of a random fiber - also used as a variable
θ	angle of orientation of the fiber axis with the loading direction
y	efficiency factor of orientation = ratio of pull-out load resisted by a fiber oriented at θ^o to that oriented at zero degrees - also used as a variable
ρ	ratio of pull-out force associated with a random fiber to its maximum pull-out force
F_p	pull-out force associated with a random fiber
R	pseudo-plastic zone radius in plane

LIST OF MAJOR SYMBOLS - continued

δ	radius of an inherent weak area in a plane
a	$= \delta + R$ - also used as slope of a line
σ_{cc}	composite cracking strength
σ_{cu}	postcracking strength
G_{mu}	toughness of the matrix
G_{cu}	toughness of the composite
γ_c	composite surface energy = $1/2\ G_{cu}$
K_c	plane stress fracture toughness
K_{Ic}	plane strain fraction toughness
PDF	probability density function
CF	cumulative function
PMF	probability mass function
$f(\sigma)$	PDF of link strength
$F(\sigma)$	CF of link strength
$g(\sigma)$	PDF of chain strength
$G(\sigma)$	CF of chain strength
E(x)	expected value of variable x
Var(x)	variance of variable x
SD(x)	standard deviation of variable x

CHAPTER 1

INTRODUCTION

Fiber reinforced concrete is a composite material made with two major components: a Portland cement based matrix (mainly mortar) and randomly oriented and distributed short fibers (generally steel fibers).

The aim of a composite is to obtain a material having tailored properties within a range of values bound by those of the two major components. Like fiber reinforced materials, fiber reinforced concrete is both complex and versatile. It is complex by virtue of its mechanical nature and thus should be regarded not as a single material but as a materials system. Its versatility stems from a wide choice of available constituents and the variety of ways to combine them in order to achieve desirable properties that cannot be obtained in conventional Portland cement matrices. An overall efficiency in terms of specific properties can therefore be achieved.

Historically fibers have been used in building materials since ancient times such as the use of straw in sunbaked bricks and in heavy walls made with a mixture of natural lime and clay. The introduction of various types of steel fibers in Portland cement based matrices seems to have taken place in the second half of the nineteenth century. As early as 1874, Berard [13] patented an "artificial stone"

consisting of a hydraulic cement matrix reinforced with granular waste iron. Early in the twentieth century, several types of steel fibers of different shapes and purposes were proposed as reinforcement or crack inhibitors for concrete matrices. A review of some of these patents is made in [71]. The last two decades have seen a substantial growth of interest in fiber reinforcement for concrete following a similar trend in the development of fiber reinforced polymeric materials. In the U.S. this interest has been mainly promoted by the work of Romualdi and Batson [81].

The current trends in research include the use of natural fibers like bagasse, jute, and bamboo [23,90], or the development of multidimensional types of metallic fibers [71]. These investigations are encouraged by concurrent development in the modification of Portland cement concrete matrices by addition of polymers in order to increase their ductility and other mechanical properties. Both types of developments are expected to lead to a substantial increase in the efficiency of fiber reinforcement.

1.1 Effects of Fiber Reinforcement on Concrete. Mixing steel fibers with concrete matrices leads in general to an enhancement of different material properties, mainly mechanical properties such as strength, ductility, stiffness, etc. Originally, however, the addition of steel fibers was meant to increase the tensile strength of concrete with, as ultimate objective, to replace continuous reinforcement in

structural reinforced concrete members. This goal was far from being reached, but some other beneficial effects of the fibers were pointed out: they act as crack arrestors, they increase drastically the material's toughness, they enhance its wear resistance, they keep cracks from opening: their application is beneficial in impact resistant structures, linings subject to high temperature gradients, pavements [40], nuclear power plant vessels, etc.

However, improving the tensile strength of concrete and understanding the reinforcing mechanisms of the fibers remain the major goal and focus of research in this matter.

1.2 Review of Analytical Models for Strength Predictions.

On the theoretical ground a first rough method of estimating tensile strength of discontinuous fiber reinforced composites has been to use the law of mixtures which gives in general unrealistically high values. A second approach has been to modify the law of mixtures by multiplying by an efficiency factor the term corresponding to the fiber contribution [60].

Current studies of fiber reinforced materials, which were mainly developed during the last two decades for fiber reinforced polymers and metals, contain at least three models for predicting the strength of discontinuous fiber reinforced composites. These are the models of Cox, Dow, and Rosen [24, 30, 85]. They are much more realistic than the previously described models, but still

remain very restrictive: they mainly assume that the fibers are all parallel aligned, that their length is higher than the critical length, that the same strain exists in the fiber and the composite, etc. Also, they apply only to the elastic domain of loading and could be used as a first approximation to predict, for example, the cracking strength of fiber reinforced concrete.

Kelly and Davies [55] proposed an elaborate study for a model that applies to parallel oriented elastic fibers in elastoplastic matrices. Their model is realistic and complete, but cannot apply to fiber reinforced concrete due to two major restrictions: first, because concrete matrices are brittle and do not show an elastoplastic behavior, second, in the mathematical derivation the model basically assumes that the ultimate tensile strain of the fiber is smaller than that of the matrix, i.e. it considers continuity of the matrix up to the ultimate resistance of the composite. Concrete has a very small ultimate tensile strain, an order of magnitude lower than the yield strain of a steel fiber (Fig. 1). Therefore, at least two distinct stages have to be considered in describing the composite behavior under tensile loading: the precracking stage, where fibers and matrix are assumed to work almost elastically, and the postcracking stage where the fibers bridging the newly created surfaces resist the load by breaking or pulling out. In currently observed behavior and with the components' properties and proportions

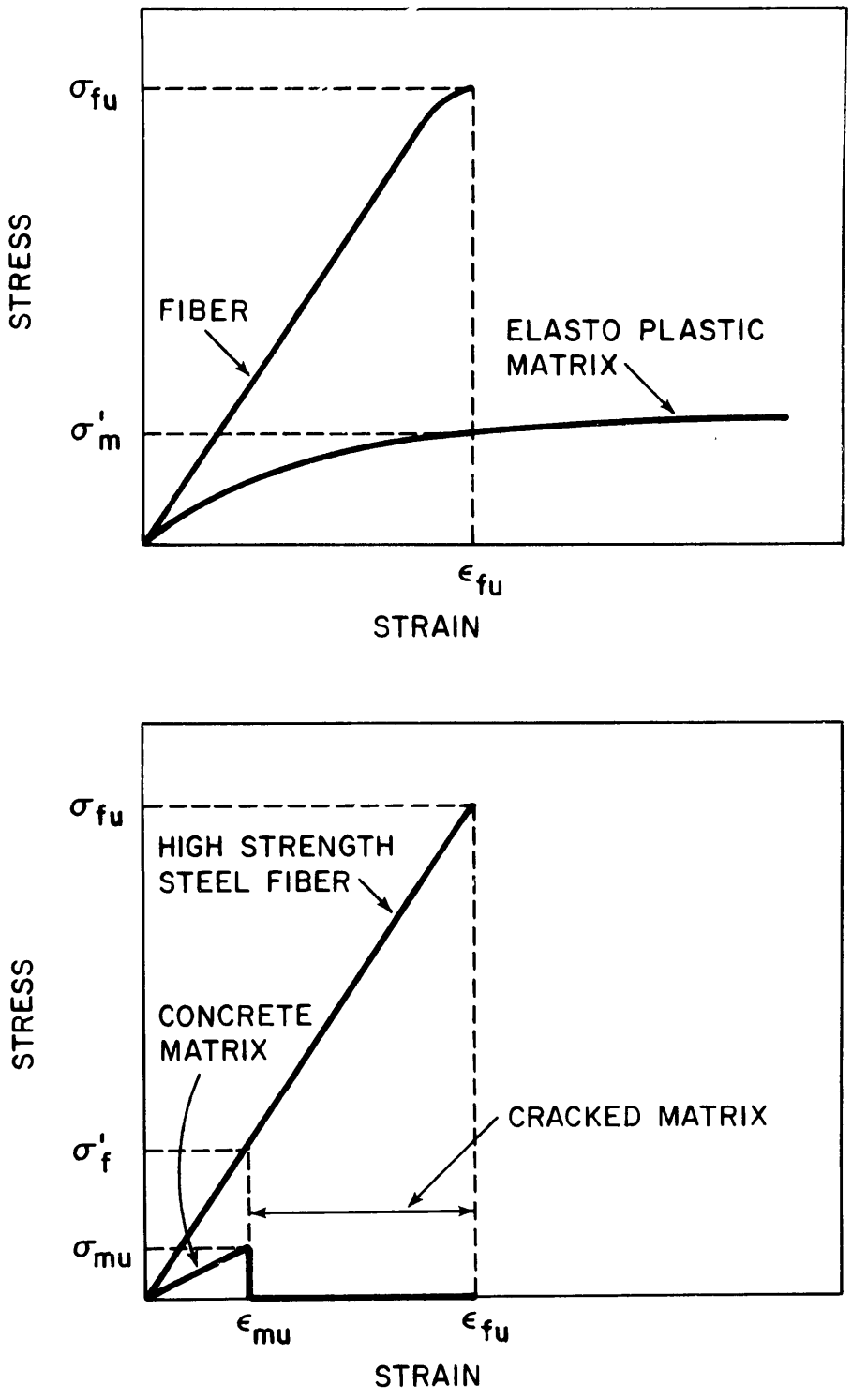

FIG. 1. TYPICAL STRESS-STRAIN DIAGRAMS OF FIBER-REINFORCED CONCRETE AS COMPARED TO MOST FIBER-REINFORCED PLASTICS.

used in practice, the steel fibers always pull out in the postcracking stage, carrying a load that is only a small fraction of their load carrying capacity.

Finally, the model proposed by Romualdi and Batson [81,82] should be mentioned, which aims to predict the composite stress at the first structural crack, i.e. at the limit of the elastic behavior. Applying Griffith's criterion of brittle fracture [41] to fiber reinforced concrete, they proposed the following formula:

$$\sigma_{cc} = \frac{K}{\sqrt{S}}$$

where σ_{cc} = composite stress at first structural crack

K = material's constant

S = average fiber spacing in space.

It is easy to notice the similarity between the proposed formula and a widely used fracture mechanics criterion, $K = \sigma\sqrt{\pi\delta}$, where K is the fracture toughness of the material, σ the nominal stress and δ the crack length or flaw size. Romualdi's formula created a controversial issue at the theoretical and experimental level among several investigators in the field [1,93]. The main disagreement can be to attributing to the effect of

spacing only the increase in cracking strength of the composite. Clearly the formula suggests that very high strength can be achieved when the fiber spacing decreases. As experimental findings are far from approaching theoretical predictions, some researchers are skeptical about the proposed theory [92,97].

Note that in a study of the yield strength of silver matrices reinforced with metal fibers, Parikh [2] observed some spacing effects but they were primarily linear with a low rate of variation.

None of the models described above covers the postcracking behavior of the fiber reinforced member and none predicts the postcracking strength, which is the major variable of interest in continuously reinforced concrete members.

1.3 On Statistical Solutions to Strength Characterization of Materials.

The factors influencing the strength properties and the behavior of material systems are numerous. They include the nature of the material as well as the geometrical configuration of the specimen. Among properties of interest are mechanical properties like tensile and compressive strengths. Size effects are also significantly pronounced in heterogeneous materials and

equivalently in composites.

A large number of theoretical investigations in mechanics have been concentrated on the development of a classical continuum concept by incorporating structural or microstructural information. While these methods have been of great help, the initiation of new approaches based on the random occurrences of microscopic properties may lead to closer expectation values and to a more realistic assessment of expected variation. These "statistical" approaches seem to have been initiated, at least for the study of tensile strength in materials, by Peirce in 1926 [75].

Peirce emphasized that any theoretical work which discusses mechanical breakdown phenomena, must take into account the fact that the observed tensile strength of a material is not a volume average quantity but rather an extremum quantity. This rule which we shall refer to as "the weakest link hypothesis" has since been thoroughly discussed and applied.

In fact, the assumption of a constant tensile strength is not supported by experimental evidence. Repeated measurements of the tensile strength of a material often result in a wide spread of values. In addition, the average tensile strength varies with

the specimen's volume or size. It is now accepted that such variation is not only due to experimental error but is rather a natural consequence of the probabilistic nature of tensile strength.

One of the most famous contributions to the statistical strength characterization of materials is that of Weibull [101]. Using Peirce's model of the weakest link, he assumed an a priori strength distribution function for the link of a tensile member made, like a chain, of a series of links. His hypothesis led to the well known result, that the tensile strength ratio of two tensile members made of the same material, is an inverse function of the ratio of their volumes. (Appendix A.1.)

Weibull's result on strength relation to size was widely applied to homogeneous materials. Equivalently successful was the weakest link concept which was applied to predict failure phenomena in fibers [19], bundles of fibers [27], and composite laminates [91]. These approaches start almost invariably with a guess as to the a priori strength distribution for a cross sectional plane in a fiber. Then the mathematical apparatus of the weakest link hypothesis is used to calculate the probability that the weakest cross sectional plane, out of a very

large sampling of planes, has a particular strength.

Comparing these methods with what could be done with a material like fiber reinforced concrete, it is evident that the a priori guess on the strength distribution function of a cross sectional plane, i.e. a link, shall take into consideration the fibers' content and properties. A composite is different from a homogeneous material mainly in that one can exogeneously change the proportions of the major components to control the strength. Assuming that the matrix composition and properties are constant, it is clear that the fibers' content and the fibers' geometrical and mechanical properties shall directly influence any causal model that aims to predict the strength distribution function of a cross sectional plane.

Therefore, a number of technical questions arise related to the distribution of the fibers in space, the distribution of the fibers' intersections with a cutting plane, the average and actual number of fibers per unit volume, etc. Clearly, the mathematical analysis of the structure of a discontinuous fiber reinforced material like fiber reinforced concrete, should start with the analysis of a network of

random lines in space. This problem is one of geometrical probability or statistical geometry. The basis to these disciplines and some other scattered applications can be found in [29,38,59].

In particular, let us mention a most successful study and application that has been generated by Corte and Kallmes [22,52] in their attempt to characterize the properties of paper. They outlined the basic approach to a quantitative description of a network of random lines in two dimensional planes and formulated the mathematical model. Their aim was to understand and correlate the controlling effect of some physical parameters of the network, like mean number of fiber crossings and mean free length, on the strength, porosity and some other properties of paper. Their contribution suggests an objective approach to handling causal relations between the fibers and the observed strength in a discontinuous fiber reinforced material.

In view of the preceding remarks and discussions, it seems that a newly developed model that predicts the strength of discontinuous fiber reinforced materials, with a particular emphasis on fiber reinforced concrete, will present a number of improvements over existing ones and will be more realistically descriptive of observed experimental results.

1.4 Objective and Scope of Study.

The overall objective of this thesis is to develop an analytical model to predict the tensile strength of fiber reinforced concrete as a function of the characteristics of its major components, focusing mainly on the reinforcing mechanisms of the fibers. Specifically, the model would predict the causal effect of given dominant variables, like fraction volume and aspect ratio of fibers, bond and tensile strength of the matrix, size of the structure, on the composite strength through the use of dependent variables derived from the data and from the assumptions on which the model is based. Dependent variables are, for example, the actual number of fibers per unit volume of composite, the actual number of fibers intersecting a unit area, the real distribution of the fibers in a concrete mass, the efficiency factor of orientation associated with a random fiber, etc. As these dependent variables are not directly controllable, the model necessitates the use of statistical methods to represent them and will therefore be probabilistic in nature.

The theoretical approach developed in this study is primarily based on the mechanics of composite materials and fracture mechanics: first, it takes into consideration the statistical nature of the variables involved, and, second, it recognizes the statistically extreme

value of observed strength as stated in the chain's weakest link hypothesis. As the observed response of fiber reinforced concrete tensile prisms is either brittle or ductile depending on the ratio of the fiber length to the specimen length under test, two different failure criteria were used in the analysis: A composite material approach for the ductile type failure, and a fracture mechanics approach for the brittle type failure. Therefore, the analytical formulation is divided in two major parts, simulating each type of failure.

The mathematical formulation of the model leads to the full determination of the characteristic strength distribution functions of the material as related to a random cross section, or link. Then the chain's weakest link method provides the theoretical distribution functions of strength for a tensile member of a given size. The expected value of strength as well as other related variables, surface energy, fracture toughness, etc. are given as a function of major input parameters and the properties of the material components. Some normalized distribution curves are also derived and plotted as a means for rapid estimating purposes.

An extensive experimental program has been performed in order to correlate theoretical predictions with experimental observations. The first part of this program deals with the experimental validation of one of the major assumptions of the model related to the random distribution of the fibers

in the concrete mass following a Poisson process. Histograms of the number of fibers intersecting a cutting plane are plotted veruus the assumed theoretical distribution and compared through a χ^2 goodness of fit test. Another section of the experimental program deals with the determination of one of the most important exogeneous variables assumed to be a given data in the model: the bond or shear strength at the fiber matrix interface. A large number of pull-out tests on single oriented fibers lead to the estimation of the frequency distribution as well as the expected value and variance of the bond strength. Similar pull-out tests on inclined fibers covering a range of orientation from zero to ninety degrees provide the relation between pull-out force and fiber orientation. Most of this information is used to assess values to the bond strength and the efficiency factor of orientation involved in the theoretical model, in order to correlate theoretical predictions and observed results on tensile strength of fiber reinforced concrete prisms.

The central part of the experimental program is concerned with tensile tests of fiber reinforced concrete specimens. It focuses first on the characterization of the physical response of the material under tensile loading and shape of the load elongation curve up to complete separation. Then, the influence of most important reinforcement parameters, the fraction volume and the aspect ratio of the

fibers are widely investigated. Four different values of aspect ratios and corresponding to each, three different fraction volumes of fibers are used. Relations between these parameters and observed mean values of cracking strength, maximum postcracking strength and toughness are plotted and compared to theoretical predictions. Discussion of observed correlations or discrepancies between both results and refinement of some of the assumptions are a part of the model's validation.

A final part of the experimental program deals with devising a new test to determine the fracture toughness and the pseudo plastic zone size of fiber reinforced concrete. These variables are in fact the only unknown variables used in the second part of the mathematical model, part which simulates the brittle type failure in the composite. The main objective here is to propose a successful testing method in order to experimentally measure the above mentioned variables. This goal is achieved through the use of cleavage or double cantilever type beams.

The analytical model and the experimental methodology developed herein may be used to characterize the tensile behavior of most discontinuously fiber reinforced materials having brittle matrices like ceramics or brittle polymers. The framework of the mathematical

formulation can be easily extended to cover the case of ductile type matrices.

1.5 The Structure of the Thesis.

Chapter 2 describes the general framework of the mathematical formulation, states the assumptions on which the model is based and discusses their important implications. Chapter 2 provides the basic framework for Chapter 3 and 4 where the two distinct parts of the theoretical study are presented respectively in detail. Chapter 3 treats the case of the ductile type failure while Chapter 4 covers the brittle type failure. Chapter 5 describes the experimental program and related methods of testing. Chapter 6 discusses observed results and correlates them with theoretical predictions. Finally, Chapter 7 summarizes the findings, contains the major conclusions, and states recommendations for future research.

CHAPTER 2

FRAMEWORK OF THE MODEL'S MATHEMATICAL FORMULATION

This Chapter describes the framework of the mathematical formulation which will be developed in full detail in the following two chapters. It states the general assumptions on which the theoretical model is based and discusses some of their important implications. The last section is devoted to the validation of the assumption on the Poisson distribution of fibers in space.

The objective here is to characterize the tensile behavior of a fiber reinforced concrete member by developing a mathematical representation of the fiber reinforced material. We will therefore always assume in this study, except when stated otherwise, that the applied loading is of the tensile type.

2.1 The Approach.

The apparent brittle or ductile failure of fiber reinforced concrete under tensile loading is dependent on the size of the specimen under test. More specifically this scale effect is due to the ratio of the fiber length to the length of the reinforced member. For relatively small size members, the failure is ductile-like while for large size members it looks brittle. It is easy to understand

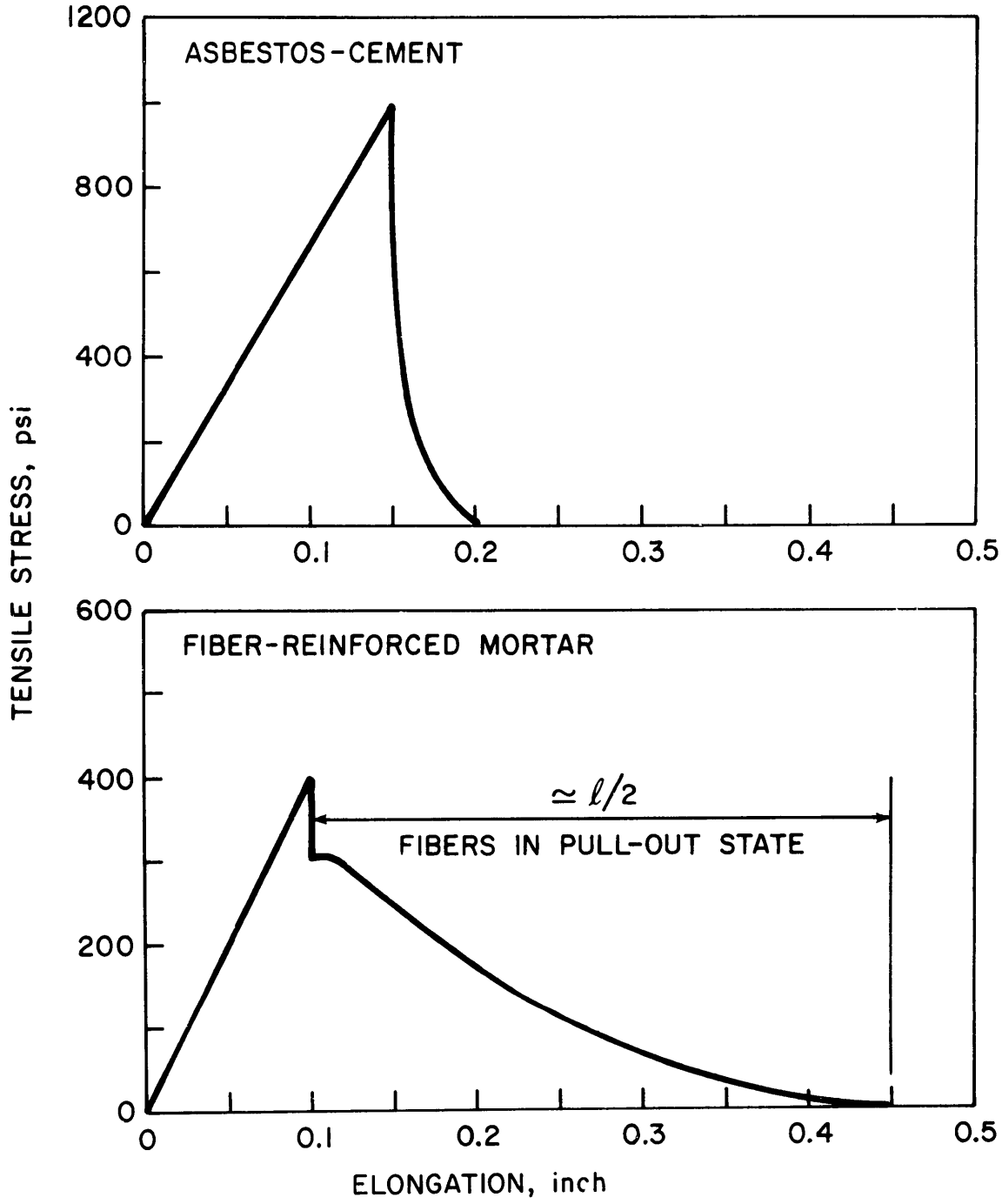

FIG. 2. TYPICAL STRESS ELONGATION CURVES AS INFLUENCED BY FIBER LENGTH.

this observation by comparing the load elongation curve of a mortar specimen reinforced with 0.75 inch steel fibers, to that of a similar specimen of asbestos cement where the fibers are less than a millimeter in length. (Fig. 2.)

In order to take into account these size effects, the mathematical model is divided in two major parts. The final solution to either part requires the synthesis of different concepts and approaches.

The first part (developed in Chapter 3) covers the case of a ductile failure and uses as basic criteria for analysis the statistical mechanics of composite materials. It explores in detail all that is going on at the fiber level, assigns values to most relevant variables and extrapolates results to the macroscopic behavior of the composite. In this part, the precracking and postcracking stages, as observed in the specimen behavior under loading, are treated distinctly.

The second part of the model covers the case of a brittle type failure where stress concentration effects take place. A fracture mechanics criterion is used in the analysis and no distinction is made between the precracking and postcracking behavior. The strength is defined as the nominal stress at the onset of rapid crack propagation leading to a complete separation of the material.

Each of these formulations leads to a determination of the distribution function of strength for a cross sectional

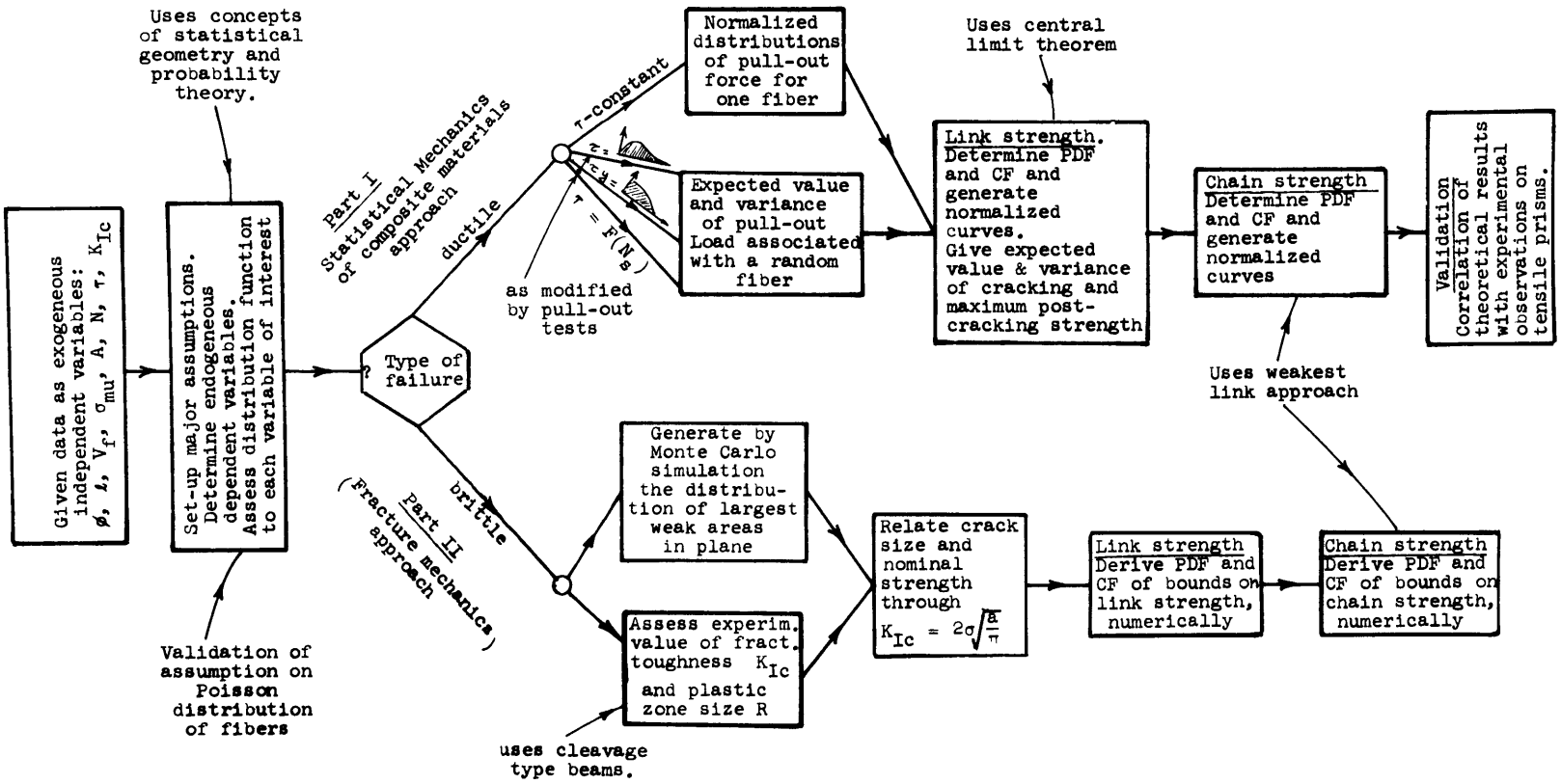

Fig. 3 Framework of the Mathematical Formulation

plane (or link) of the tensile member, assumed to be made like a chain of a series of links. The chain's weakest link concept of reliability theory is then applied to bound the overall model and provide the distribution functions of strength for the member.

The general framework of the mathematical formulation and other relevant remarks or details, are shown in a flow chart in Fig. 3 . This chart will help understand and keep track of the logical steps followed in Chapters III and IV.

2.2 General Assumptions.

A number of assumptions are implicitly made throughout the mathematical formulation. They are stated with some explanatory remarks as follows:

1. The tensile member is assumed to be made like a chain of a series of links. The mathematical implications of this hypothesis and methods of estimating the number of links are covered in the following paragraphs.

2. The tensile and shear or bond strengths of the concrete matrix, whether given by a constant or a frequency distribution, are assumed to be isotropic properties.

3. The reinforcing fibers have a constant length ℓ and diameter ϕ. The model may be extended in order

to handle other possible alternatives when ℓ and ϕ are given by a distribution function.

4. It is assumed that under loading a crack will propagate along a smooth plane perpendicular to the loading direction. The amplitude of the crack roughness in relation to the fiber length is neglected. In practice, this is realistic for fiber reinforced mortar or paste but subject to limitations for fiber reinforced concrete with relatively large size aggregates.

5. The smaller portion x of a fiber length on either side of a crack is uniformly distributed between zero and half the fiber length that is $0 \leq x \leq \ell/2$.

6. The fibers have an equal probability of making all possible angles with any arbitrary chosen fixed axis (for example, the loading direction). This is realistic if no vibration or only a slight one is applied during the pouring operation [32].

7. The fibers in the concrete mass and equivalently their points of intersection with a cutting plane are randomly distributed following a Poisson process. The mathematical justification of this assumption is given in Appendix A.2 and an experimental validation is made in section 2.5 and Appendix A.3.

2.3 Mathematical Implication of the Weakest Link Hypothesis.

We shall refer to Chapter 1 and Appendix A.1 to recall the origin and the mathematical development of the weakest link hypothesis. Here we will mainly use the major assumption and the derived results as follows:

a. The tensile member under study consists of a chain of N consecutive links in series.

b. The link strength has a statistical distribution described by a probability density function (PDF), $f(\sigma)$, and a cumulative function (CF), $F(\sigma) = \text{Prob.}(\Sigma \leq \sigma)$.

c. The probability distribution function and cumulative function of strength for the chain are given respectively by:

$$g(\sigma) = N f(\sigma) [1. - F(\sigma)]^{N-1}$$

$$G(\sigma) = \text{Prob.}(\Sigma \leq \sigma) = 1. - [1. - F(\sigma)]^{N}$$

Therefore the determination of the link PDF and CF functions will lead to the determination of the chain functions of interest, if the number of links N is known.

2.4 Assessment of the Number of Links N.

There are a number of ways to determine or at least to

set bounds to the number of links N that make a tensile member.

Sometimes the tensile member may naturally contain weak sections that may be considered the center of a link slice. Experimentally, as we did in our test, one can put notches along the specimen creating very weak sections and so fixing the desired number of links N.

If, however, a tensile prism of a constant cross section and a given length is considered, an upper bound value to N can be assessed. One can consider that the member is reinforced with the same fraction volume of fibers assumed continuous and oriented in the loading direction. Using existing reinforced concrete theories of cracking, it is then possible to determine the average crack spacing and so the average number of cracks developed along the loaded member. This number may be considered as an upper bound value to the number of links N.

Another, less constraining upper bound value is given by the ratio of the member length to the fiber half length, $L/(\ell/2)$. This results from the assumption that the transfer of load from the fiber to the matrix from an existing crack is such that another crack will not develop along the fiber embedded length. This bound may provide a realistic value if fibers of average length are used.

A lower bound value to N seems to be realistically defined as follows. Consider a crack across the member.

The stress field is disturbed locally on either side of the crack and becomes uniform only at a certain distance from the crack. This distance can be estimated after Saint Venant as, for example, twice the smallest dimension of the member d. The corresponding link dimension is twice the value found. Therefore $N \geq L/(4 \times d)$.

Finally, the assessment of the number of links can be made experimentally by determining in a sufficiently long tensile prism the observed average number of cracks under loading. This method implies that the postcracking stress is higher than the cracking stress, such that more than one structural crack develops. Similarly, an extensive experimental program may lead to some empirical formula relating reinforcement parameters to average crack spacing, as in conventional reinforced concrete members.

It seems a priori, that defining an upper and lower bound to N if the exact value is unknown, can still provide a very good estimation to the assessment of the strength distribution. We will see later in this study that, if N is high, the obtained normalized curves for $g(\sigma)$ and $G(\sigma)$ are much less sensitive to an increase in N. (Fig. 9 and 10).

2.5 Validation of the Assumption on the Poisson Distribution of Fibers.

This assumption is the most important stated and needs experimental validation. It implies first that the fibers

are distributed in the mass following a Poisson process, second, that on the average, the number of fibers found in a volume, is equal to the known average number of fibers thrown into the matrix and directly related to the fraction volume V_f, length ℓ and diameter ϕ of the fibers. Let's call N_V the number per unit volume of composite.

This is equivalent to saying that the fiber points of intersections with a cross sectional plane are Poisson distributed in the plane and that on the average the number found per unit area is equal to the average theoretical number, say N_S, directly derived from the knowledge of N_V.

However, these last two consequences are easier to check experimentally.

Slices of fiber reinforced mortar specimens cut from already tested beams with known reinforcement parameters were analyzed.

For at least four different sections taken from different specimens of the same batch, the numbers of fiber intersections were determined, added, and the average number per square inch derived. In most instances the average found was within a range of 15% of the theoretically predicted values.

The random arrangement of the fibers over a cross sectional area was verified by laying a grid of small squares (Fig. 4b) on the section under study and showing that the frequency of the fiber intersections per square is Poisson like.

(a)

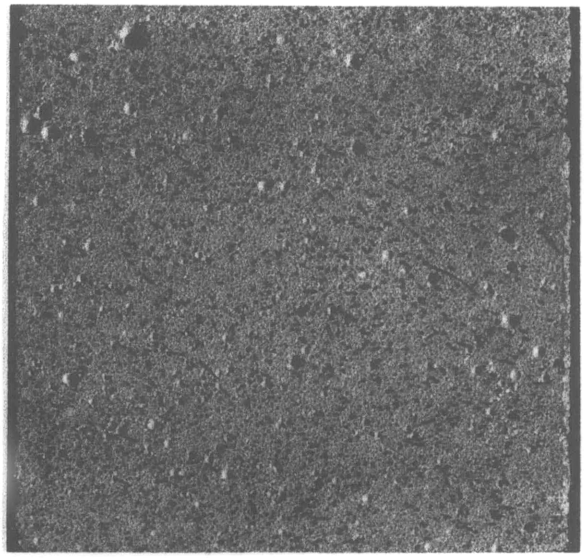

ϕ = 0.006" ℓ = 0.5" V_f = 3%

(b)

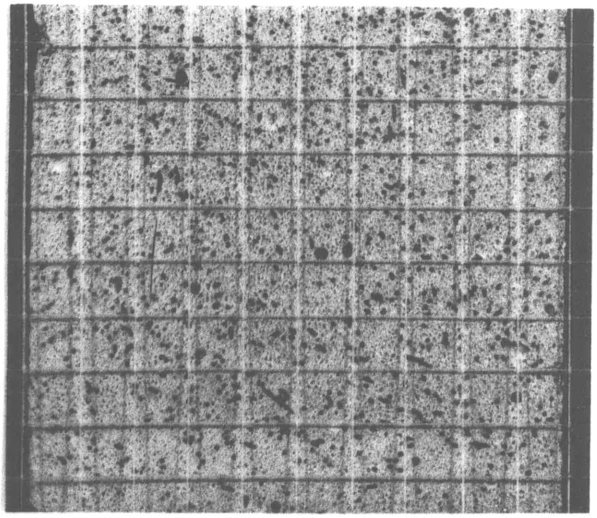

ϕ = 0.10" ℓ = 0.75" V_f = 3%

Fig. 4 a) Typical Cross Section of Fiber Reinforced Mortar

b) Example of Counting Grid for Determination of Fiber Distribution

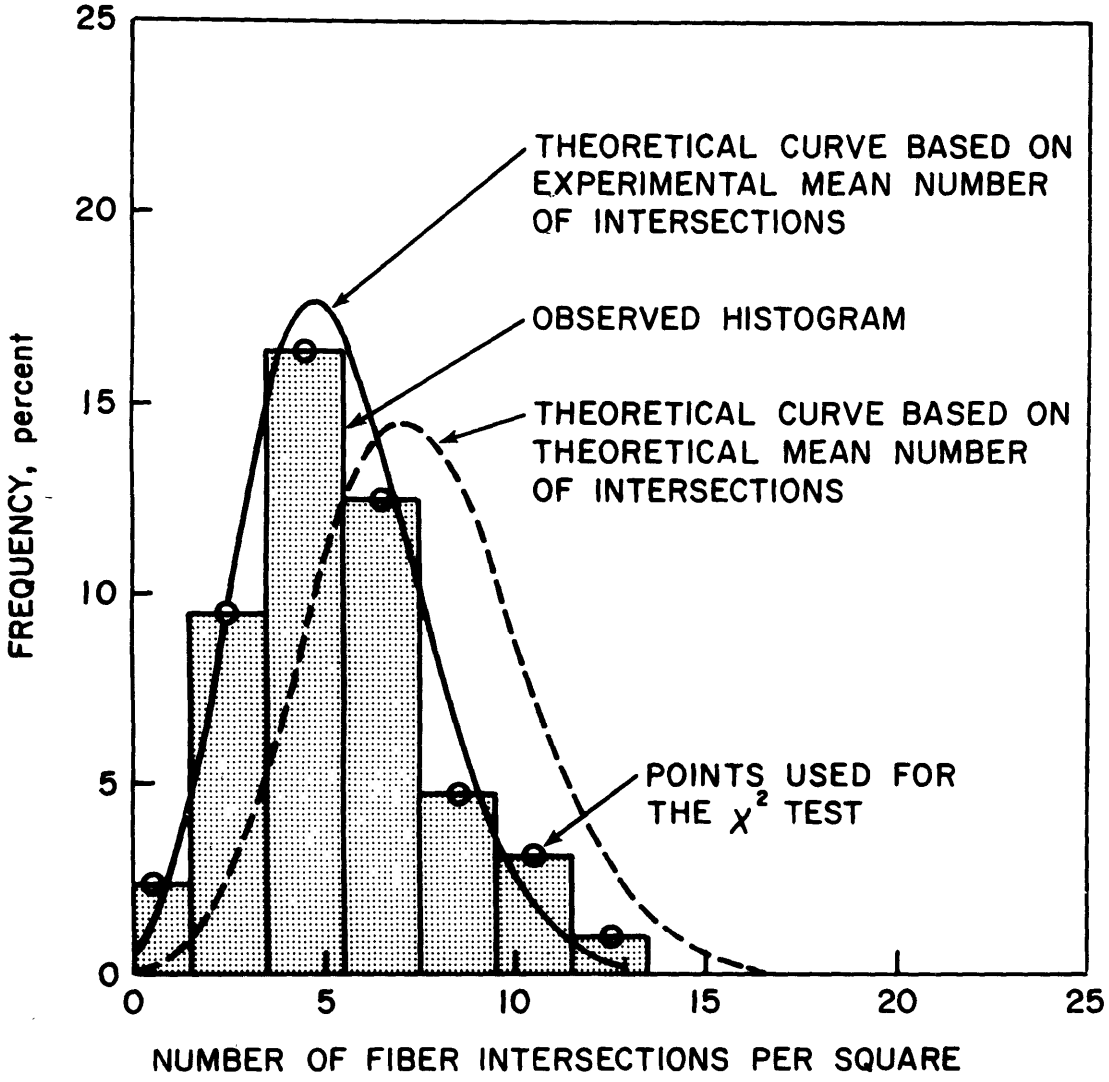

FIG. 5. POISSON-LIKE DISTRIBUTION OF THE FIBER INTERSECTIONS IN A CROSS SECTION.

In this case the theoretical curve to which the observed histogram is compared, is obtained using as a parameter the actually observed mean number of fiber intersections per square. The χ^2 goodness-of-fit test was used on a large number of histograms, to validate the hypothesis. In most cases the 95% confidence level was passed and in many the 90% was passed. A typical example of a histogram and a corresponding theoretical distribution of interest are shown in Fig. 5 . Also an example of the χ^2 goodness-of-fit test as applied in this study is treated in Appendix A.3.

CHAPTER 3

PROBABILISTIC MODELING OF THE DUCTILE TYPE FAILURE IN FIBER REINFORCED CONCRETE

This chapter describes the first part of the mathematical formulation as shown on the flow chart, Fig. 3. It applies to fiber reinforced members in which the ratio of the fiber length to the member's dimensions is small, i.e., members that fail in a ductile manner. Two stages in the material's response under tensile loading are identified: the precracking and the postcracking stage. The latter will be covered first in the following analytical treatment.

The major steps in the theoretical development are described in detail in a flow chart, Fig. 6. Part I of the chart is concerned with the assessment of the maximum postcracking strength of the material. It shows how the relevant mechanical variables lead to the determination of the maximum pull-out force for a random fiber. It also shows how a random number of fibers in a state of pull-out contribute to the link and chain strength.

In part II of Fig. 6, it is shown that the strength at cracking is made up of the contribution of the two major components, the fiber and the matrix. It is assumed that the fiber contribution function contains the same parameters used to determine the pull-out force associated with

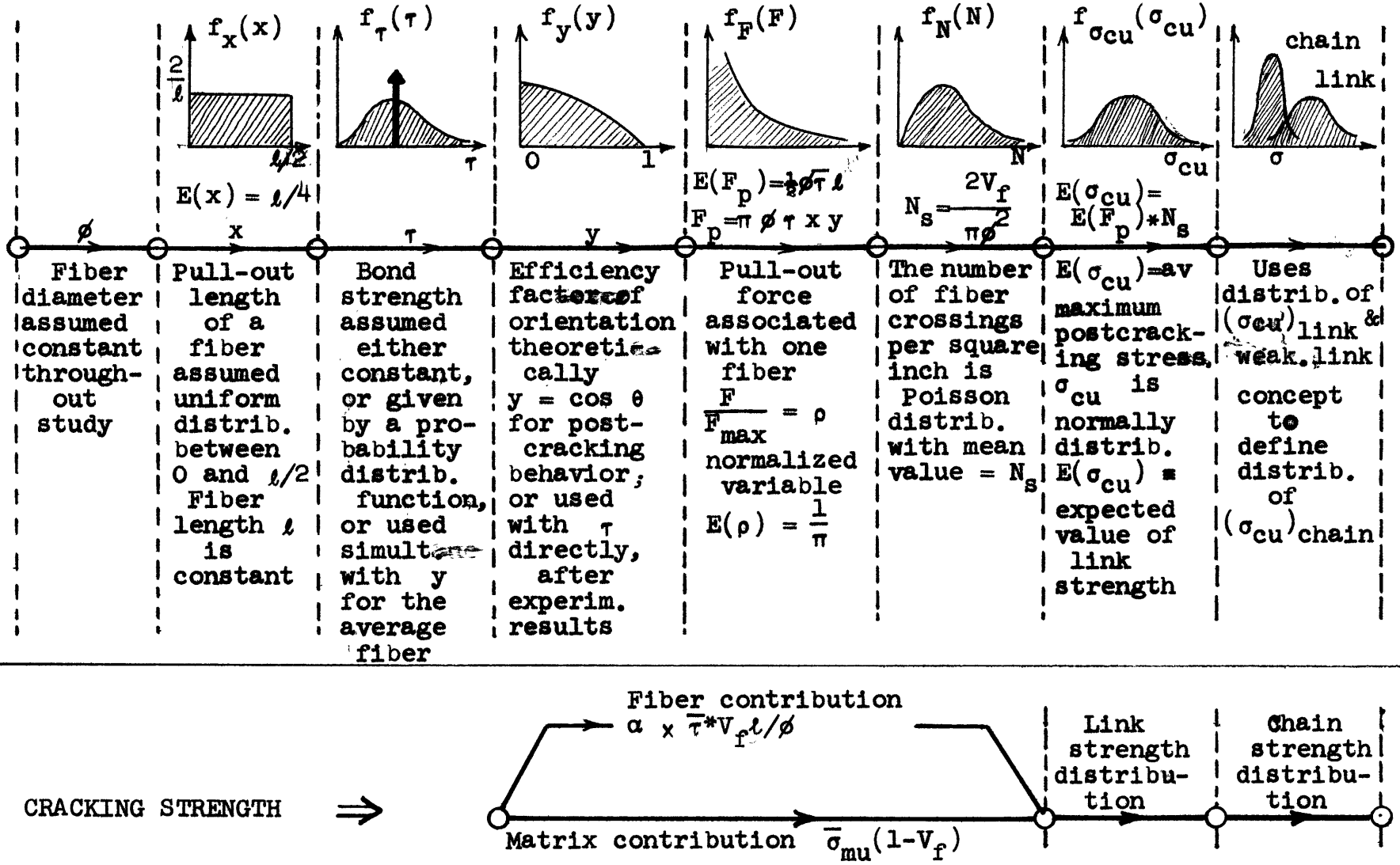

Fig. 6 Logical Approach to Modeling Ductile Failure

a fiber but with different distributions or values. Referring to the upper branch of the figure, the efficiency factor of, for example, orientation y, will be equal to $\cos^2\theta$ rather than $\cos\theta$ in the precracking state. The fiber contribution function before cracking is therefore related to the pull-out force by a factor. Later on in this chapter, we will discuss the matrix contribution to the precracking strength.

3.1 Definition of Relevant Data.

Given data as used herein are in general independent variables that are known or that can be controlled exogeneously. They describe mainly the component properties, dimensions or proportions. Following is a list of the most relevant variables, as used in this chapter.

V_f = fraction volume of fibers

ℓ = fiber length inch

ϕ = fiber diameter inch

τ = bond or shear strength at the fiber matrix interface psi

σ_{mu} = ultimate tensile strength of the matrix psi

ε_{mu} = ultimate tensile strain of the matrix

N = number of links of the tensile member

A = cross section area of the tensile member sq.inches.

From part of these data and the assumption on the Poisson distribution of the fibers in space, we will first

determine two endogeneous or dependent variables of interest, the number of fibers per unit volume and the number of fibers intersecting a unit area.

3.2 Number of Fibers per Unit Volume and Corresponding Number of Fibers Intersecing a Unit Area.

Given the fraction volume V_f, the length ℓ, and the diameter ϕ of the fibers, it is straightforward to deduce the average number of fibers per unit volume as related to these parameters

(1) $$\boxed{N_V = \frac{4V_f}{\pi \ell \phi^2} .}$$

In fact, the real number of fibers found in a unit volume of the composite, say R, is statistically distributed and related to N_V by the following Poisson distribution function

(2) $$P(R) = \frac{N_V^R e^{-N_V}}{R!} .$$

P(R) is the probability of finding exactly R fibers per unit volume knowing that on the average there are N_V fibers per unit volume. The number of fibers intersecting a unit area of a cutting plane, say N_S, depends on N_V.

Assume the R fibers are randomly oriented with uniform distribution over the hemisphere, and independent

of each other. Consider a cutting plane. If the center of gravity of the fiber is at a distance t from the plane, the probability that the fiber will intersect the plane is related to the ratio of areas of a zone on a sphere to the sphere. The area of a zone is proportional to the height h, and we have the following result:

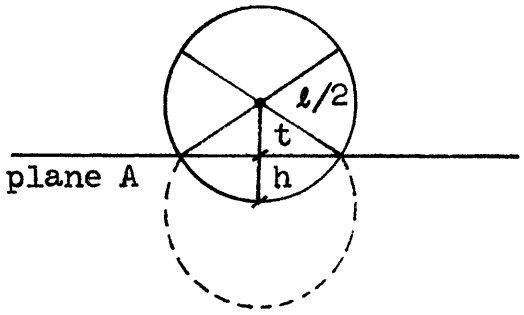

$$\text{Prob(fiber cut plane}|\text{given its center is at dist t)} = \frac{\ell/2 - t}{\ell/2}$$

$$\text{i.e.} \quad \text{Prob(intersect}|\ t) = 1 - \frac{2t}{\ell} \quad \text{for} \quad t \leq \ell/2$$
$$= 0 \qquad\qquad \text{for} \quad t > \ell/2.$$

Note that the distance t is uniformly distributed between zero and $\ell/2$.

Considering a unit volume on one side of the plane, the expected number of fibers intersecting an area A in the plane is

$$\int_0^{\ell/2} (1 - \frac{2t}{\ell}) N_V A \, dt = N_V A \frac{\ell}{4}$$

and for a unit area $A = 1 \Rightarrow N_V \frac{\ell}{4}$.

Now if we consider the fibers on either side of the plane, the expected number of fibers that intersect a unit area on that plane is given by

(3) $$\boxed{N_s = 2N_v \frac{\ell}{4} = N_v \frac{\ell}{2} = \frac{2V_f}{\pi \phi^2} .}$$

As N_v is the mean value of a number R of fibers that have a Poisson distribution, N_s is the mean value of a number q of fibers that have also a Poisson distribution. Therefore we have

(4) $$P(q) = \frac{N_s^q e^{-N_s}}{q!} .$$

This is the probability of finding exactly q fiber intersections per unit area knowing that on the average there are N_s fiber intersections.

3.3 Characterization of Relevant Variables Associated with a Fiber in a State of Pull-out.

Let us consider a random fiber in space (Fig. 7), of length ℓ and diameter ϕ constants, and let us define its orientation by the angle θ of its axis with the loading direction zz. Also, let us describe the relative position of the fiber with respect to a cutting plane normal to the loading direction by a variable x. The cutting plane materializes a cracking plane and x represents the smallest length of the fiber on either side of the plane. It is the fiber part that will pull out after cracking. We shall first assess to each of these variables a distribution function,

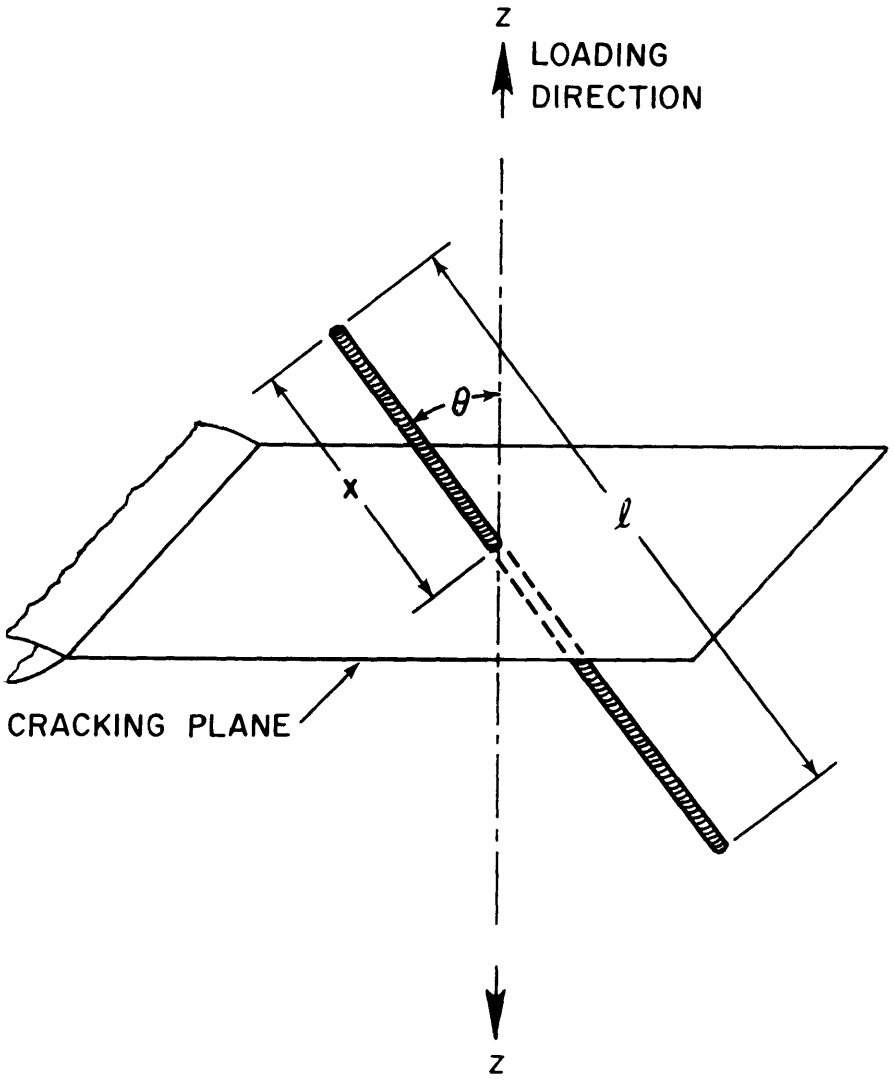

FIG. 7. TYPICAL REPRESENTATION OF A FIBER IN SPACE.

in order to be able to define the distribution function of the pull-out load associated with one fiber.

3.3.1 Statistical Characterization of x

x is the smaller fiber length on either side of a cracking plane. It has a uniform distribution between 0 and $\ell/2$.

So the probability density function of x

$$f_x(x_0) = \frac{2}{\ell} dx = \text{Prob}(x_0 \leq x \leq x_0 + dx)$$

and the cumulative function of x

$$F(x_0) = \frac{2}{\ell} x_0 = \text{Prob}(x \leq x_0).$$

Values of interest are given below:

$$(5) \quad \begin{cases} \text{Expected value} = E(x) = \bar{x} = \int_0^{\ell/2} x\, f_x(x_0)dx = \frac{\ell}{4} \\ \text{Second moment} = E(x^2) = \frac{\ell^2}{12} \\ \text{Variance} = \text{Var}(x) = E(x^2) - E^2(x) = \frac{\ell^2}{48} \\ \text{Stand. deviation} = SD(x) = \sqrt{\text{Var}(x)} = \frac{\ell}{4\sqrt{3}} \end{cases}$$

3.3.2 Statistical Characterization of y.

y is defined as the efficiency factor of orientation. It is the ratio of the pull-out load sustained by a fiber

oriented at an angle θ to that of a fiber oriented at $\theta = 0$. For a fiber in a state of pull-out, y is theoretically equal to $\cos\theta$.

It was assumed earlier that the fibers in space have equal probability of being oriented in any direction. So the angle θ in space has a uniform distribution between 0 and $\pi/2$. Therefore the PDF of θ is:

$$f_\theta(\theta_0) = \frac{2}{\pi}\, d\theta$$

and the CF is

$$F(\theta_0) = \frac{2}{\pi}\,\theta_0 \,.$$

Let's determine the PDF of $y = \cos\theta$.

$$f_y(y_0) = \text{Prob}(y_0 \le y \le y_0 + dy_0)$$

$$f_y(y_0) = \left|\frac{d\theta}{dy}\right| f_\theta(\theta_0)$$

$$\left|\frac{d\theta}{dy}\right| = \frac{1}{\sin\theta} = \frac{1}{\sqrt{1-\cos^2\theta}} = \frac{1}{\sqrt{1-y^2}}$$

so $$f_y(y_0) = \frac{2}{\pi\sqrt{1-y^2}}\, dy$$

and $$F(y_0) = \int_0^{y_0} f_y(y_0)dy = \frac{2}{\pi}\quad \sin^{-1}(y_0).$$

Values of interest are given below:

$$(6)\qquad \begin{cases} y = \cos\theta \\ E(y) = \overline{y} = \dfrac{2}{\pi} \\ E(y^2) = \frac{1}{2} \\ Var(y) = \frac{1}{2} - \dfrac{4}{\pi^2} \\ SD(y) = \sqrt{\frac{1}{2} - 4/\pi^2} \end{cases}$$

3.4 Statistical Characterization of the Pull-out Force F_p Associated with a Random Fiber.

In a most general form, the pull-out force associated with one fiber can be written as follows:

$$(7)\qquad \boxed{F_p = \pi \phi \tau x y .}$$

We already mentioned that the diameter ϕ is a given constant. This section aims at characterizing the statistical values of interest for F_p.

Let us note at this point that it is not necessary to determine the full distribution function of F_p in order to derive that of the link strength. As the link strength is made up of the addition of pull-out forces associated with a big number of fibers, and as these forces have the same distribution, the central limit theorem of probability theory tells us that the link strength distribution will be Gaussian.

The Gaussian or normal distribution will be fully determined if its two parameters, the mean and the standard deviation, are determined. In our attempt to characterize F_p we will mainly concentrate on determining these two parameters when the full distribution function seems to be analytically out of hand. We will distinguish a number of cases leading us from a purely theoretical form to a form that is more closely adapted to experimental observations.

3.4.1 Case where τ = constant and $y = \cos\theta$.

This case is based on the widely used assumption that the shear or bond strength is a constant and that the efficiency factor of orientation varies as theoretically predicted following $\cos\theta$. In this case

$$F_p = \pi \phi \tau x y = c^t \times x y = c^t \times z$$

where $z = x y$ and $0 \leq z \leq \frac{\ell}{2}$. We shall determine the distribution of z first in order to find that of F_p.

x and y are independent variables. Their joint probability density function is equal to the product of their individual PDFs. Therefore

$$f_{x,y}(x_0,y_0) = f_x(x_0) f_y(y_0) = \frac{4}{\pi \ell} \frac{1}{\sqrt{1 - y^2}} \, dx \, dy$$

with $0 \leq x \leq \ell/2$ and $0 \leq y \leq 1$.

The method of solution [31] is to find first the Prob($z \leq z_0$), i.e. the CF of z and differentiate it with respect to z to get the PDF. In order to determine the Prob($z \leq z_0$) we have to integrate the joint PDF of x and y over the domain of interest as shown in our sketch.

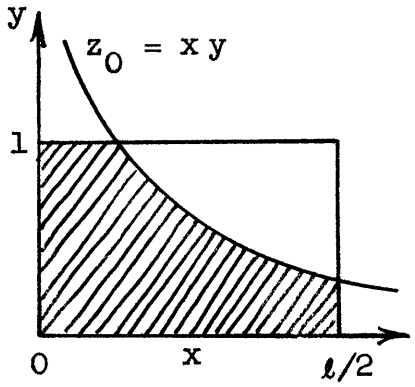

Therefore:

$$\text{Prob}(z \leq z_0) = 1. - \frac{4}{\pi \ell} \int_{x=z_0}^{\ell/2} dx \int_{y=z_0/x}^{1} \frac{dy}{\sqrt{1-y^2}} .$$

Integration gives the cumulative function

$$\text{Prob}(z \leq z_0) = F(z_0) = \frac{2}{\pi} \sin^{-1}\left(\frac{z_0}{\ell/2}\right) - \frac{2}{\pi}\frac{z_0}{\ell/2} \ln\left(\frac{1-\sqrt{1-(z_0/\ell/2)^2}}{z_0/\ell/2}\right)$$

and by differentiating F(z) we obtain the PDF of z:

$$f_z(z_0) = -\frac{4}{\pi \ell} \ln\left(\frac{1-\sqrt{1-(z_0/\ell/2)^2}}{z_0/\ell/2}\right) dz \qquad 0 \leq z \leq \ell/2.$$

Values of interest for z are given below:

$$(8) \qquad \begin{cases} E(z) = \dfrac{\ell}{2\pi} \\ E(z^2) = \ell^2\left(\dfrac{1}{16} - \dfrac{1}{6\pi^2}\right) \\ \text{Var}(z) = \ell^2\left(\dfrac{1}{16} - \dfrac{5}{12\pi^2}\right) \\ \text{SD}(z) = \ell\sqrt{\dfrac{1}{16} - \dfrac{5}{12\pi^2}} \end{cases} .$$

As $F_p = c^t \times z$, the descriptors of interest for F_p are directly derived below:

$$(9)\quad \begin{cases} E(F_p) = \phi\, \tau\, \ell/2 \\ E(F_p^2) = (\pi\phi\tau\ell)^2[\frac{1}{16} - \frac{1}{6\pi^2}] \\ Var(F_p) = (\pi\phi\tau\ell)^2[\frac{1}{16} - \frac{5}{12\pi^2}] \\ SD(F_p) = \pi\phi\tau\ell\sqrt{\frac{1}{16} - \frac{5}{12\pi^2}} \end{cases}$$

Instead of deriving the PDF and CF of F_p, it seems of more interest to derive those of a normalized variable ρ defined as

$$(10)\qquad \rho = \frac{F_p}{F_p max} = \frac{\pi\phi\tau z}{\pi\phi\tau\ell/2} = \frac{z}{\ell/2}$$

where $F_p max$ is the maximum value that F_p can take, corresponding to $z = \ell/2$. From the PDF and CF of z we derive the corresponding distribution functions for ρ as follows

$$F(\rho_0) = Prob(\rho \leq p_0) = \frac{2}{\pi}\sin^{-1}(\rho_0) - \rho_0 \ln\left(\frac{1-\sqrt{1-\rho_0^2}}{\rho_0}\right)$$

$$f_\rho(\rho_0) = -\frac{2}{\pi}\ln\left(\frac{1-\sqrt{1-\rho^2}}{\rho}\right)d\rho$$

with $0 \leq \rho \leq 1$.

Normalized curves representing these two functions have been plotted for use in Fig. 8.

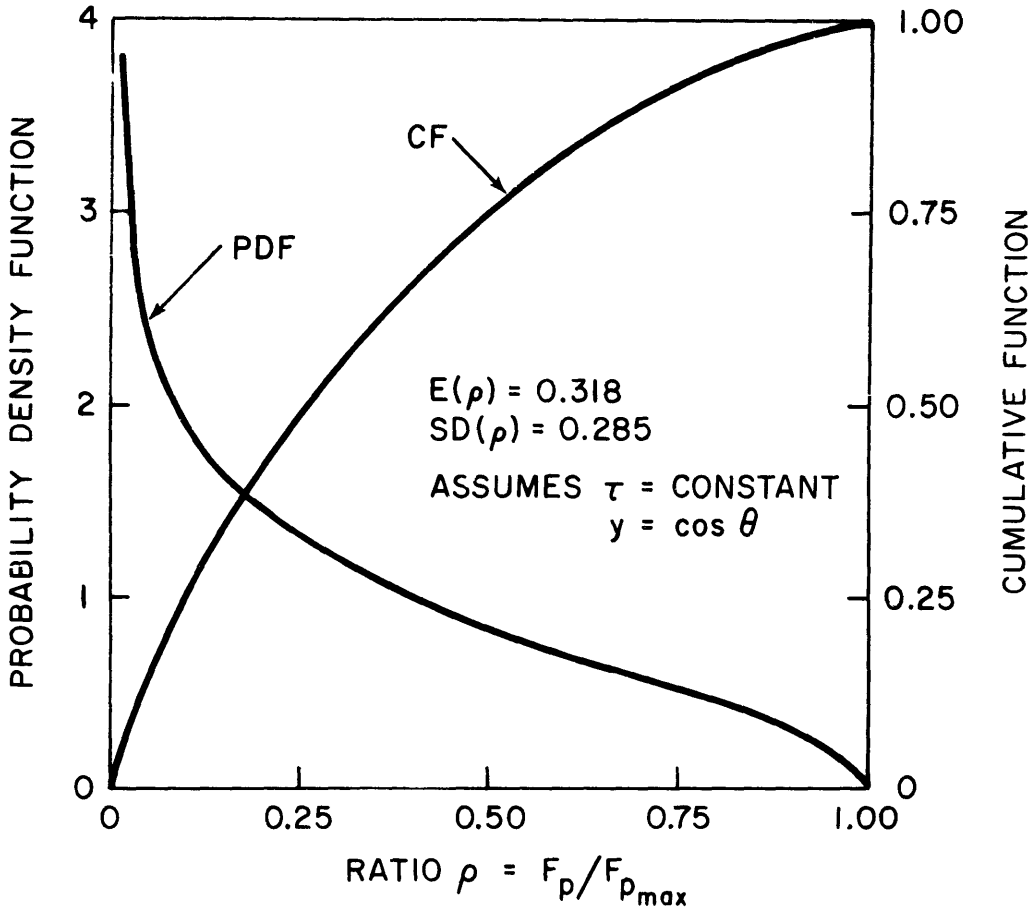

FIG. 8. DISTRIBUTION FUNCTIONS OF THE RATIO OF A FIBER PULL-OUT LOAD TO ITS MAXIMUM PULL-OUT LOAD.

Note that

$$(11)\qquad \begin{cases} E(\rho) = \frac{1}{\pi} = 0.318 \\ Var(\rho) = 4(\frac{1}{16} - \frac{5}{12\pi^2}) = 0.081 \\ SD(\rho) = \sqrt{Var(\rho)} = 0.284 \ . \end{cases}$$

3.4.2 Case where τ is statistically distributed and $y = \cos\theta$.

Like any other property of the material, the bond strength τ as observed in practice is not a constant but rather a statistically distributed variable. In general we have at least a histogram of results for τ from which we can determine the expected value $\bar{\tau}$ and the variance $Var(\tau)$. These will allow us to derive the statistical descriptors of interest for F_p:

$$(12)\qquad \begin{cases} E(F_p) = \phi\,\bar{\tau}\,\ell/2 \\ Var(F_p) = (\pi\phi)^2[Var(\tau)E(z^2) + Var(z)E(\tau^2) \\ \qquad\qquad + Var(\tau)\,Var(z)] \\ SD(F_p) = \sqrt{Var(F_p)} \\ E(F_p^2) = Var(F_p) + (\phi\,\bar{\tau}\,\ell/2)^2 \end{cases}$$

Note that $E(\tau^2) = Var(\tau) + \bar{\tau}^2$.

3.4.3 Case where the product τy can be represented by a single variable, say u.

This case may result from the experimental determination of τ versus the angle of orientation θ. Defining y, the efficiency of orientation, as the ratio of the bond strength associated with a fiber pulling out at an angle θ over that of a fiber pulling out at $\theta = 0$, the product $\tau y = u$ represents the experimental value of a bond strength associated with a randomly oriented fiber. Assuming we know the expected value $\bar{u}$, and variance $\mathrm{Var}(u)$ of the variable u, we can derive the statistical descriptors of interest for F_p

$$E(F_p) = \frac{\pi \phi \ell \bar{u}}{4}$$

$$\mathrm{Var}(F_p) = (\pi\phi)^2[\mathrm{Var}(x)E(u^2) + \mathrm{Var}(u)E(x^2) + \mathrm{Var}(u)\,\mathrm{Var}(x)] \tag{13}$$

$$= \frac{(\pi\phi\ell)^2}{48}\,[E(u^2) + 5\,\mathrm{Var}(u)]$$

3.4.4 Case where τ is a function of the amount and properties of the reinforcing fibers.

We have assumed so far in the model that the apparent bond strength, whether given by a constant or by a distribution, is independent of the reinforcement parameters. In a number of investigations dealing with the bond

strength associated with conventional reinforcing rods in concrete [106], it was pointed out that the observed result was very dependent on the size of the embedding matrix volume. Translating this to fiber reinforced concrete, it is to be expected that the concentration and properties of the fibers pulling out simultaneously from the same surface, will directly influence the normalized pull-out load per fiber and the apparent bond strength associated with it. In practice we observe a high level of deterioration and disruption of the matrix, on either side of a crack, after the complete pull-out of the fibers. The level of deterioration seems to be a function of the fiber properties (length, diameter, flexibility), the number of fibers bridging the crack and the local resistance of the matrix. Given a certain type of fiber, this observation suggests that the apparent bond strength per fiber will be dependent on the number of fibers pulling out per square inch. The a priori and subjective relation is very likely to be a decreasing function. Therefore, given the reinforcement parameters, one can define ranges of values for the average number of fibers per square inch, inside which the corresponding bond strength will be assumed constant. Then the final solution to the pull-out force per fiber F_p will be similar to one of the cases already treated.

3.5 Determination of the Link Postcracking Strength & Toughness.

The maximum postcracking force F_L associated with a cracked cross section or link is made up of the sum of pull-out forces F_p associated with a random number N_r of (Poisson distributed) fibers bridging this section. As all F_p have the same distribution function, F_L will, after the central limit theorem, have a normal distribution. Also the maximum pull-out strength σ_{cu} which is equal to F_L/A where A is the cross section area, will have a normal distribution. It will be fully defined if its two descriptors, the mean and the standard deviation, are known. Normalized standard tables then provide the full distribution functions.

In the most general case, the sum of a random number of independent, identically distributed random variables has the following moments:

$$E(F_L) = E(N_r)\, E(F_p)$$

$$Var(F_L) = E(N_r)Var(F_p) + E^2(F_p)Var(N_r)$$

which give for the maximum postcracking stress

$$E(\sigma_{cu}) = \bar{\sigma}_{cu} = E(\frac{F_L}{A}) = E(\frac{N_r}{A})E(F_p) = N_s E(F_p)$$

$$Var(\sigma_{cu}) = \frac{1}{A^2}\, Var(F_L) = \frac{N_s}{A}\, [Var(F_p) + E^2(F_p)]$$

that is

$$(15)\qquad \begin{cases} \bar{\sigma}_{cu} = \dfrac{2V_f}{\pi\phi^2}\, E(F_p) & \le \sigma_{fu} V_f \\ \mathrm{Var}(\sigma_{cu}) = \dfrac{2V_f}{\pi\phi^2}\, \dfrac{1}{A}[\mathrm{Var}(F_p) + E^2(F_p)] \ . & \end{cases}$$

Note the upper bound on $\bar{\sigma}_{cu}$ as we are assuming that the fibers are in a state of pull-out, otherwise the composite postcracking strength will be equal to the load carrying capacity of the fibers bridging a unit area.

For the theoretical case where the efficiency factor of orientation y equals cos θ and where τ is assumed constant or given by a frequency distribution, from (12) and (15), the expected value of the maximum postcracking stess is

$$(16)\qquad \boxed{\bar{\sigma}_{cu} = \frac{1}{\pi}\,\bar{\tau}\, V_f\, \frac{\ell}{\phi} \le \sigma_{fu}\, V_f}$$

Note that for the case where τ is assumed constant, the variance will be

$$(17)\qquad \mathrm{Var}(\sigma_{cu}) = \frac{\pi}{A}\, V_f\, \tau^2\, \ell^2 \left(\frac{1}{8} - \frac{1}{3\pi^2}\right)$$

where A is the area of the cross section under study.

The work at fracture per unit area, G_{cu}, called also the toughness, can be calculated as the sum of the

work to fracture the concrete matrix and the frictional energy dissipated by the pull-out of the fibers up to complete separation. Assuming that the pull-out force decreases linearly with the pull-out distance, the frictional work associated with one fiber can be written as follows

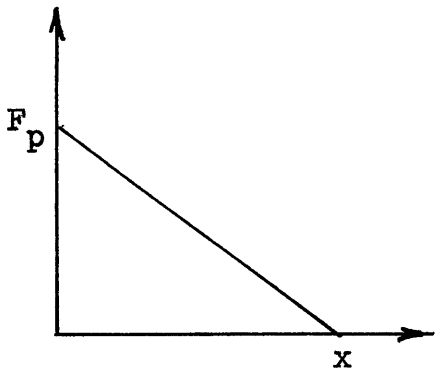

$$G_p = F_p \frac{x}{2} = \tfrac{1}{2} \pi \phi \tau x^2 y \ . \tag{18}$$

For a random number of fibers N_r intersecting an area A we have in the most general case

$$G_{pr} = N_r G_p$$

$$\begin{aligned} E(G_{pr}) &= \overline{G}_{pr} = E(N_r)E(G_p) \\ Var(G_{pr}) &= E(N_r)Var(G_p) + E^2(G_p)Var(N_r) \end{aligned} \tag{19}$$

and the normalized values per unit area will be

$$G_{ps} = \frac{G_{pr}}{A} = \frac{N_r G_p}{A}$$

$$\begin{aligned} E(G_{ps}) &= \overline{G}_{ps} = N_s E(G_p) \\ Var(G_{ps}) &= \frac{N_s}{A} [Var(G_p) + E^2(G_p)] \ . \end{aligned} \tag{20}$$

For the theoretical case where $y = \cos\theta$ and τ is constant or given by a distribution function we have

$$(21) \qquad \overline{G}_{ps} = \frac{1}{6\pi}\,\overline{\tau}\,V_f\,\frac{\ell^2}{\phi} = \overline{\sigma}_{cu}\,\frac{\ell}{6}\,.$$

For $\tau = ct$ the variance takes the following form

$$(22) \qquad Var(G_{ps}) = \frac{\pi V_f \tau^2 \ell^4}{320\,A}\,.$$

In order to calculate the energy at fracture or toughness of the composite (G_{cu}), we have to take the matrix contribution G_{mu} into account

$$(23) \qquad \begin{aligned} E(G_{cu}) &= E(G_{mu}) + E(G_{ps}) \\ Var(G_{cu}) &= Var(G_{mu}) + Var(G_{ps}) \end{aligned}$$

For the theoretical case of $y = \cos\theta$ and τ constant or statistically distributed

$$(24) \qquad \boxed{\overline{G}_{cu} = \overline{G}_{mu} + \frac{1}{6\pi}\,\overline{\tau}\,V_f\,\frac{\ell^2}{\phi} = 2\overline{\gamma}_c}$$

where $\overline{\gamma}_c$ is the expected surface energy of the composite.

From the values of $\overline{G}_{cu}$ or $\overline{\gamma}_c$ one can directly derive the expected value of the composite fracture toughness as follows

(25) for plane stress $K_c = \sqrt{2\bar{\gamma}_c E_c}$

plane strain $K_{Ic} = \sqrt{\frac{2\bar{\gamma}_c E_c}{1 - \nu_c^2}}$

where E_c and ν_c are the composite modulus of elasticity and the Poisson ratio, respectively.

3.6 Estimation of the Link Strength at Cracking.

The cracking strength of fiber reinforced concrete is made up of the contribution of the matrix and the fibers, respectively. As the matrix is assumed to have isotropic properties, its contribution to the composite strength is generally given by $\bar{\sigma}_{mu}(1-V_f)$. The fiber contribution, however, requires more consideration.

An attempt has been made (Appendix A.4) to predict the cracking strength of fiber reinforced concrete using a composite material approach similar to that of Kelly and Davies but taking into account the randomness of the fibers in space. The model assumes that the tensile stress in the fiber is induced by a minimum differential strain at the fiber matrix interface, which will allow the full development of the bond or shear strength. This also means that a minimum tensile strain shall be inflicted on the composite in order to allow the shear stress at the interface to reach its maximum value. Corresponding calculations lead to

the conclusion that the necessary strain to be applied on the composite is an order of magnitude higher than the ultimate cracking strain of the concrete matrix alone. Therefore this method cannot currently be applied to concrete matrices and will be best suited to matrices having a higher tensile strain at ultimate.

However, in order to realistically estimate the fiber contribution in the precracking stage, the following assumption is made: the term corresponding to the fiber contribution shall contain the same major variables as in the postcracking strength, but with different distributions. For example, variable x will be replaced by $\ell/2$, y will be equal to $\cos^2\theta$ instead of $\cos\theta$, and τ will be partially present. Therefore, the fiber contribution in the precracking stage will be equal to the postcracking strength multiplied by a factor. This factor can be experimentally estimated, as was done in Chapter VI for the tensile prisms tested in this study.

In view of the preceding remarks the expected value of the composite cracking strength has the following general form

$$(26) \qquad \bar{\sigma}_{cc} = \bar{\sigma}_{mu}(1-V_f) + \alpha'\bar{\sigma}_{cu} \leq \bar{\sigma}_{mu}(1-V_f) + \sigma_{fu}V_f$$

that is

$$\bar{\sigma}_{cc} = \bar{\sigma}_{mu}(1-V_f) + \frac{\alpha'}{\pi}\,\bar{\tau}\,V_f\,\frac{\ell}{\phi}$$

or

$$\boxed{\bar{\sigma}_{cc} = \bar{\sigma}_{mu}(1-V_f) + \alpha \bar{\tau} V_f \frac{\ell}{\phi}} \tag{27}$$

subject to $\alpha \bar{\tau} \frac{\ell}{\phi} \leq \sigma_{fu}$.

This last constraint limits the contribution of the fiber to that obtained by continuous reinforcement.

Assuming that the variance of the matrix tensile strength has been experimentally determined and that it is independent of the fiber reinforcing parameters; we have

$$Var(\sigma_{cc}) = (1-V_f)^2 Var(\sigma_{mu}) + \alpha'^2 Var(\sigma_{cu}) \tag{28}$$

where $Var(\sigma_{cu})$ has been calculated in section 3.5 Furthermore the cracking stress σ_{cc} may be assumed to be made up of, for example, a big number of cracking forces associated with elemental areas containing on the average one random fiber. The distribution of σ_{cc} will therefore be Gaussian, as that of σ_{cu}.

In fact some experimental observations [15,16,65,70] show a significant relation between reinforcement parameters and the apparent cracking strain of the matrix. This seems to result from the high distribution of the fibers in the matrix. In general the apparent cracking strain increases with V_f and $\frac{\ell}{\phi}$ and therefore the cracking stress of the matrix shall be modified correspondingly. The following

formula is appropriate

$$\boxed{\bar{\sigma}_{cc} = \bar{\sigma}^{*}_{mu}(1-V_f) + \alpha\,\bar{\tau}\,V_f\,\frac{\ell}{\phi}} \tag{29}$$

where $\bar{\sigma}^{*}_{mu}$ is the modified matrix strength.

The determination of $\bar{\sigma}^{*}_{mu}$ may be obtained by measuring the apparent tensile strain of the composite at cracking and the elastic matrix modulus, or by extrapolating results obtained on cracking stress versus V_f and ℓ/ϕ. In the case of fiber reinforced concrete V_f and ℓ/ϕ have relatively small values. Moreover, they cannot have a large range of variation without modifying the matrix strength through addition of water for mixing purposes. Therefore formula (27) is still useful for a first approximation estimation.

3.7 Determination of the Chain Strength.

Most of this chapter has been devoted to prove that the link's pre- and postcracking strengths are normally distributed and to determine their statistical descriptors, the expected value and the standard deviation. These parameters allow us to fully determine the strength distribution functions PDF and CF or to refer to normalized standard tables to determine them. The distribution functions of the chain strength have been given in function of those of the

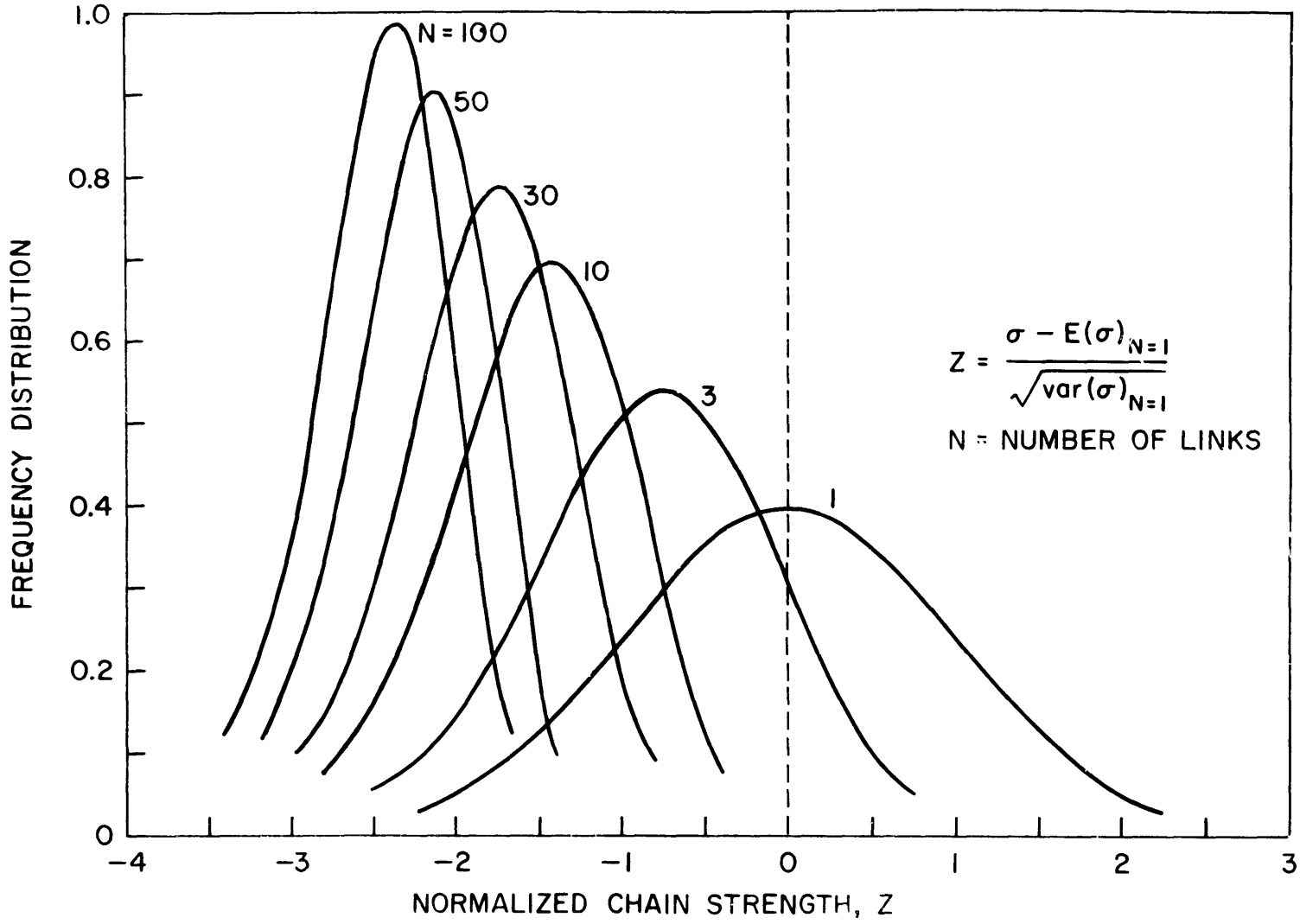

FIG. 9. NORMALIZED PROBABILITY DENSITY FUNCTIONS OF CHAIN STRENGTH.

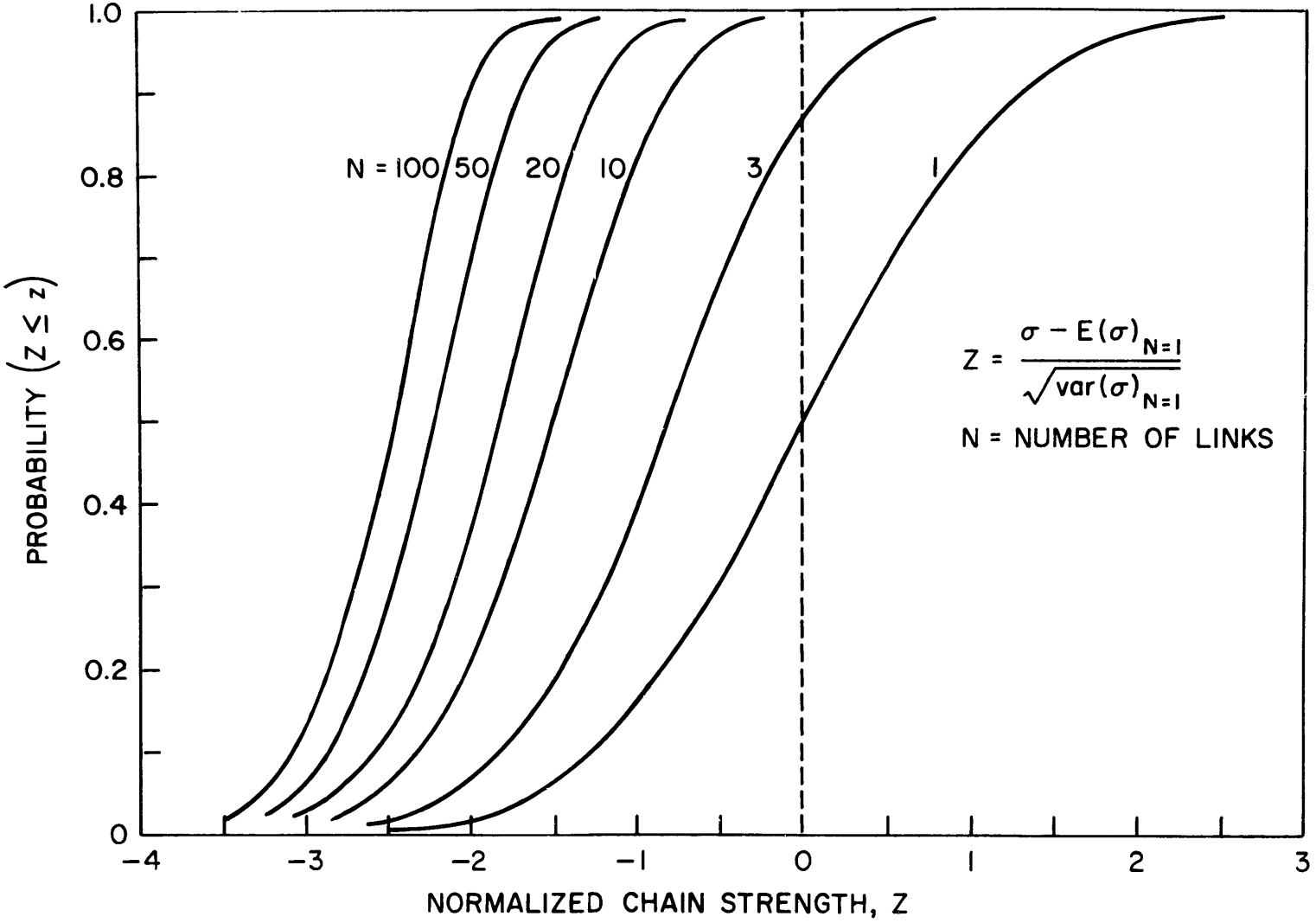

FIG. 10. NORMALIZED CUMULATIVE FUNCTIONS OF CHAIN STRENGTH.

link in section 2.3. Note that there is no direct formula to determine the expected value of the chain strength, but it can be calculated numerically. It is given by:

$$(30) \quad E(\sigma_{cu})_{chain} = \int_{-\infty}^{+\infty} \sigma\, g(\sigma)d\sigma = \int_{-\infty}^{+\infty} N\, \sigma[1 - F(\sigma)]^{N-1} f(\sigma)d\sigma.$$

In order to present an easy-to-use tool, some normalized curves of probability density functions and cumulative functions of the chain strength have been numerically calculated and plotted. (Fig.9 and 10), for a chain having various numbers of links. The normalized variable used is the normalized Gaussian variable z and it is defined by

$$(31) \qquad z = \frac{\sigma - E(\sigma)_{N=1}}{SD(\sigma)_{N=1}} \quad .$$

Let us note that for $N = 1$ the PDF curve is symmetrical (normal distribution), while for $N > 1$ it is not, even though it gives that impression on the graph.

CHAPTER 4

A SIMULATION MODEL FOR THE BRITTLE TYPE FAILURE IN FIBER REINFORCED CONCRETE

This chapter is concerned with the second part of the mathematical formulation as shown on the flow chart Fig. 3. Its objective is to present what the author considers basic principles and physical observations involved in understanding the way fiber reinforced cementitious materials fracture, with a particular emphasis on fiber reinforced concrete. It begins with a very brief review of fracture mechanics and its application to homogeneous and composite materials. A description of the fracture behavior of concrete and fiber reinforced concrete, necessary for the full understanding of the proposed model, follows. The proposed model for the brittle fracture of fiber reinforced concrete is then presented and solutions proposed either through a mathematical lower bound solution or by a simulation method. A final section is devoted to discussing a specific example with fiber reinforced concrete.

4.1 Some Background on Fracture Mechanics.

The body of knowledge known as fracture mechanics is a relatively new one and there are many problems of concern that remain unsolved. Moreover, the analysis of fracture

in composites is one of great complexity [4 ,10,77] involving many possible failure mechanisms and the process is by no means completely understood.

Fracture mechanics started with the famous relationship on energy balance in brittle homogeneous materials provided by Griffith [41] using an available stress analysis developed by Inglis. An extension of the result by Orowan, Irwin, and co-workers led to the following relation that applies to an infinite plate containing a sharp crack and subjected to tensile loading

$$\sigma_{nom.crit.} = \left(\frac{2E\gamma_p}{\pi c}\right)^{\frac{1}{2}} \tag{1}$$

where

$\sigma_{nom.crit}$ = nominal stress at fracture

E = elastic modulus

γ_p = plastic work term

c = half the crack length.

Note that this equation can be rewritten as $\sigma_{nom.crit.}(\pi c)^{\frac{1}{2}} = (2E\gamma_p)^{\frac{1}{2}}$ separating materials properties E and γ_p from geometric properties. The quantity $(2E\gamma_p)^{\frac{1}{2}}$ is called the notch toughness and is commonly designated by K_c. At fracture

$$K_c = \sigma_{nom.crit.}(\pi c)^{\frac{1}{2}} . \tag{2}$$

K_c is also commonly called fracture toughness or stress intensity factor. For levels of stresses σ below the $\sigma_{nom.crit.}$ required for crack extension, K is defined as the stress field intensity parameter and is equal to $K = \sigma\sqrt{\pi c}$. In its most general form, however, the notch toughness is given by $\sigma\sqrt{\alpha\pi c}$ where α is a factor dependent on specimen geometry and boundary conditions. For relatively large size members α is taken equal to unity. The critical value of K in the opening mode (tensile field) is called K_{Ic} where the subscript I denotes that the applied stress causes the crack to "open".

The notion of stress intensity factor, which was mainly developed for the two dimensional case of a crack in a plate, has been extended by Sneddon [6,94] to the tridimensional case of a circular disk crack of radius c in an infinite solid subject to a uniform tension normal to the crack plane. His result for the crack tip stress expansion leads to the following expression

$$K_{Ic} = \sigma_{nom.crit.}\sqrt{\frac{4c}{\pi}} \quad . \tag{3}$$

The principles of linear elastic fracture mechanics can be used [99] to relate the critical value of K to the critical value of G, where G is the work done per unit area of crack formed during the separation process. Note that K_c characterizes a critical stress field intensity while G_c characterizes a critical energy release rate. Depending whether

conditions of plane stress or plane strain exist K_c and G_c are related as follows

$$(4) \qquad \begin{cases} \text{for plane stress} & K_c = \sqrt{EG_c} \\ \text{for plane strain} & K_c = \sqrt{\dfrac{EG_c}{1-\nu^2}} \end{cases}$$

where E and ν are the elastic modulus and Poisson's ratio of the material.

A review of the application of fracture mechanics to concrete as well as determination of the critical values of K, γ and G is made in [68]. More general applications to composite materials can be found in [8,10,72].

4.2 Fracture Behavior of Concrete and Fiber Reinforced Concrete as Compared to Other Materials.

A general feature of the fracture process in cementitious matrices is the accumulation of very fine porosities or holes into larger faults. According to Griffith's theory these holes are far too small to enlarge rapidly. In particular, the fracture of concrete involves three processes:

a) The initial growth of microcracks at low stresses [36,50,54].

b) The linking of microcracks with other microcracks of similar size under increasing stress or strain to form a macrocrack.

c) The unstable propagation of a macrocrack up to

complete fracture.

A macrocrack can be visualized as the concentration of holes or weak adhesion portions.

One way of increasing the strength of cements and concretes is to increase the dissipation of energy at fracture which can be done by inserting fibers. Apparently the presence of numerous and fine fibers constrains local failures at weak portions and enables cementitious matrices to display higher strains and/or stresses at fracture. Therefore the statistical distribution of weak portions could be considered as an important parameter in determining the strength.

There has been a limited amount of theoretical work on the extension of fracture mechanics to fiber reinforced materials [4,66,72]. Presently the analyses applied are those of homogeneous fracture mechanics modified to simulate more closely a typical composite. A very crucial point is in general concerned with the determination of the composite's toughness which is intimately related to not only the behavior and properties of the individual components but to their mutual interaction. Frequently a distinction is made whether the fiber and the matrix are brittle or ductile, whether the fiber will break or pull out under loading, whether there is debonding or delamination along a certain portion of the fiber before fracture, etc. A summary

of available information on the subject is made by Tetelman in [98].

Describing fracture in fiber reinforced concrete it can be said that fracture is generally initiated by a matrix tensile fracture followed by an interface shear fracture or fiber debonding. Debonding adds a significant amount to the energy absorbed or toughness of the composite.

The analysis of the stress field at the tip of an advancing crack in homogeneous materials identifies in general two zones of interest: the plastic and the elastic zone. Immediately surrounding the tip of the crack the plastic zone represents a region where high strains are induced and where the material has yielded locally. Outside the plastic zone, the elastic zone represents the portion of material in which the elastic stress field predicted by the theory exists. Conventionally, the plastic zone in a homogeneous isotropic material has been estimated by computing the distance from the crack tip to the point where the longitudinal stress equals the tensile yield strength of the material [6 , 7]. Depending on the degree of brittleness of the material, the plastic zone size may be very small. For example, it is of the order of one millimeter in brittle steel while in ductile steel it is an order of magnitude higher [74,76]. In composite materials a pseudo plastic zone is generally visualized where miniature tensile specimens represented by the fibers are assumed to contribute to the

toughening mechanisms [72,57]. Here too the analysis is different whether the fibers debond, delaminate or break.

In fiber reinforced concrete the plastic zone represents an area where the matrix is cracked and where the fibers are in a local state of pull-out. An attempt has been made to describe qualitatively in Fig.11 the stress distribution in the two zones of interest. In the plastic zone the material is locally in its "postcracking state" as compared to the "precracking state" which characterizes the elastic zone. Note that the stress distribution in the plastic zone is not uniform but reflects the relationship between the pull-out resistance of the fibers and the crack tip opening. However, an average stress value can be assessed to simplify the problem. In order to estimate the size of the plastic zone in a fiber reinforced material where fibers pull out as in concrete, one can use a cleavage specimen [46,66] and measure the crack extension for an opening at the crack tip equal to half the fiber length. Therefore, depending on the fiber length and other geometrical and material characteristics, the measured plastic zone size will be more or less important. For fiber reinforced concrete it is certainly of the order of a few inches while for asbestos cements it may be an order of magnitude smaller.

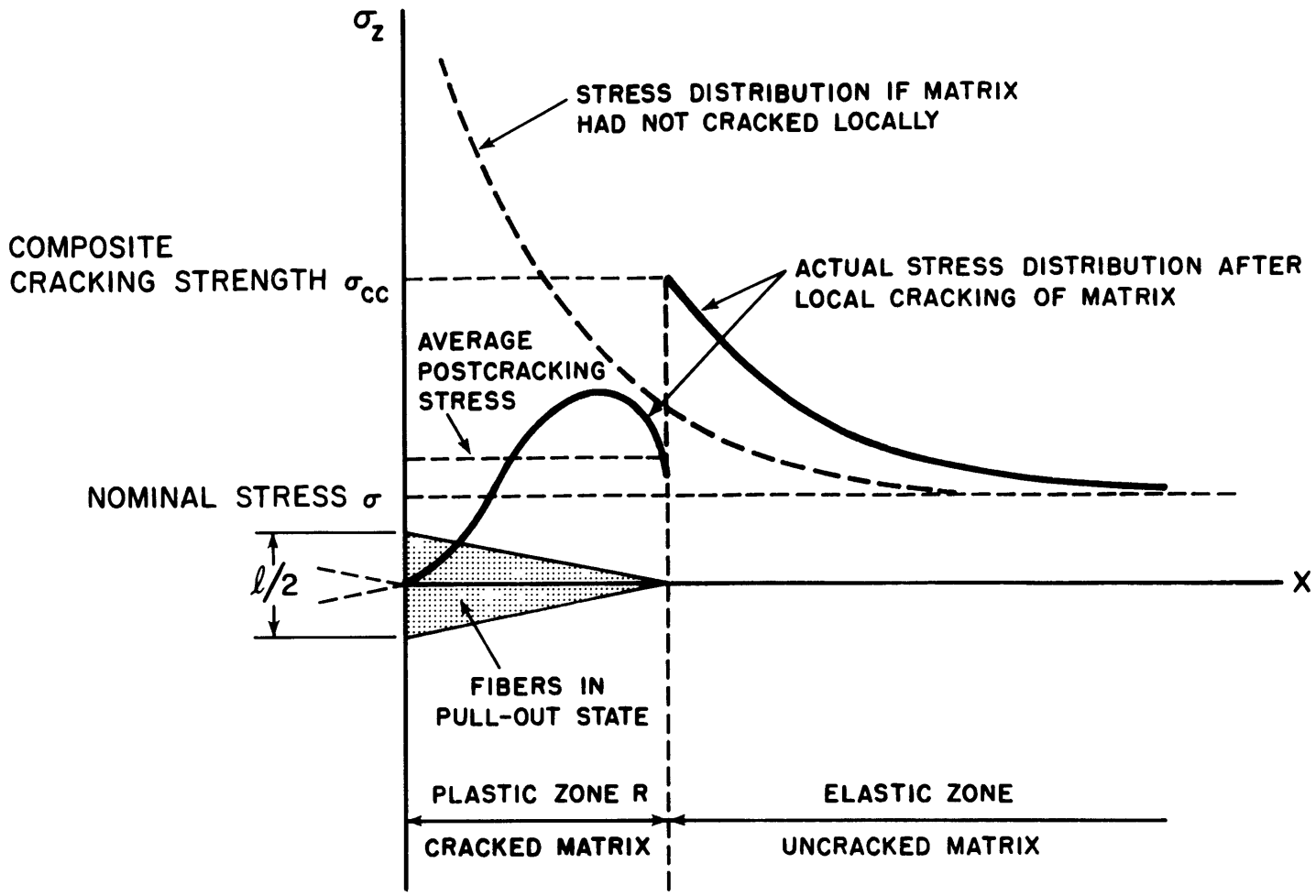

FIG. 11. DISTRIBUTION OF LONGITUDINAL STRESS AHEAD OF A CRACK IN A FIBER-REINFORCED CONCRETE COMPOSITE.

4.3 Proposed Fracture Model and Major Assumptions.

The proposed model is based on the understanding of some of the remarks and observations made earlier. Due to the small volume fraction of fibers generally used, it is assumed that the crack initiation and extension process in fiber reinforced concrete is qualitatively similar to that of concrete alone. Macrocracks in the matrix are going to form and extend under loading but complete fracture of the composite cannot occur without the necessary energy to pull out the fibers.

Another important consideration relates to the distribution of "inherent weak areas" in the composite. An inherent weak area is defined herein as a portion of the member cross section where there is no fiber intersection. In a more general definition, it is an area where the number of fiber intersections is less than or equal to a minimum value characteristic of the material. This value corresponds to the critical volume fraction [55] in discontinuous fiber reinforced composites and is explained on the sketch on the right. The existence of inherent weak areas is due to

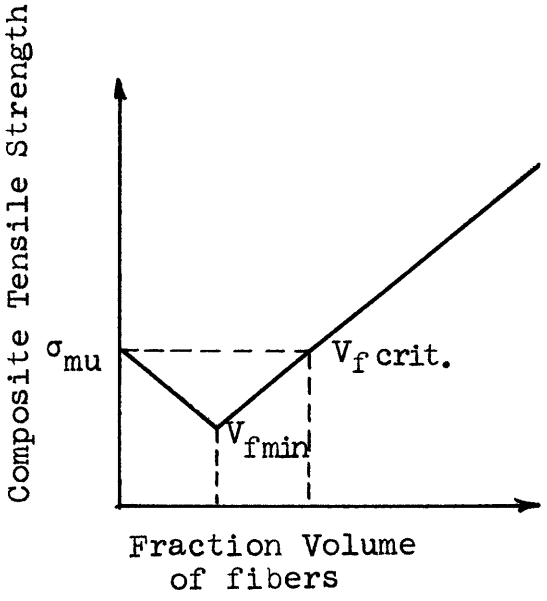

the random nature of the fiber distribution. The distribution of largest weak areas in the links of a chain member may have a critical importance on the observed composite strength. Therefore the following assumptions are made:

1. Potential cracks are more likely to generate in portions of the link cross section containing no or a small amount of fibers depending on the material characteristics.
2. The minimum length of a crack $2a$ that may become critical is very likely to be at least equal to the plastic zone length $2R$ plus the diameter of the largest inherent weak area 2δ. (Fig. 12). Including the plastic zone size in the value of the critical crack length is a consequence of the fact that the matrix is really cracked in the pseudo plastic zone described earlier.
3. The strength of the fiber reinforced member is assumed to be controlled by the worst "crack", the one having the largest diameter, among the large number present. Assumption 2 allows us to estimate a lower bound on the length of the worst crack as $2a = 2\delta + 2R$ and its distribution can be determined from that of δ assuming R constant for a given composite.
4. The fundamental fracture mechanics relation, relating half crack length $a = \delta + R$, strength σ and the fracture toughness K_{Ic},

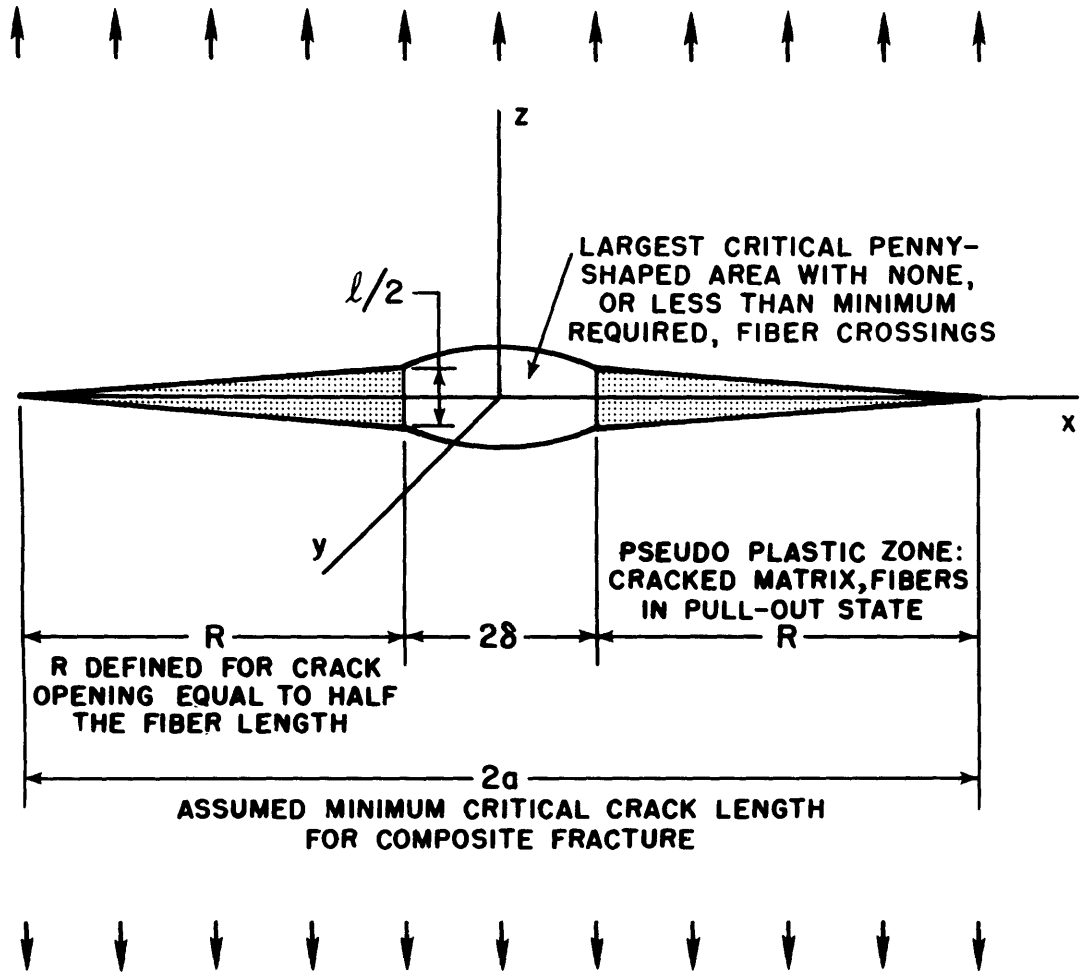

FIG. 12. ASSUMED CRITICAL CRACK MODEL CONTROLLING FRACTURE OF FIBER-REINFORCED CONCRETE.

in the tridimensional case holds, that is

$$K_{Ic} = \sigma_{nom.crit.}\sqrt{\frac{4(\delta+R)}{\pi}} \quad . \tag{5}$$

5. The fracture toughness K_{Ic} (or equivalently G_{Ic}) as well as the plastic zone radius R can be determined experimentally for a fiber reinforced material. For given component proportions and characteristics K_{Ic} and R are considered average composite material properties.

6. From assumptions 3, 4 and 5 an upper bound distribution on the link strength at composite fracture can be established. Note that the probability that the link strength is less or equal to σ_0 is equal to the probability that the radius of the largest critical crack a is higher or equal to a_0.

7. The distribution functions of strength for the chain can then be derived numerically from those of the link as described in 2.3.

Let us note that we have stated an upper bound value criterion on the composite strength. This is not the only upper bound however. The value of the composite strength derived in Chapter III is also an upper bound solution as it considers the ideal case where a crack propagates instantaneously through the matrix and where a perfect redistribution of load between all fibers and equal strain on the link cross

section exist. These two values can be compared and the lowest one used. Moreover, a lower bound value on the strength can be obtained by using the $\sigma_{nom.crit.}$ of the non-reinforced matrix.

Let us finally mention that the only experimental values that are needed for the proposed model are the fracture toughness K_{Ic} and the plastic zone radius R and they can be obtained by running a single experiment, that is a double cantilever cleavage type beam [66,67]. The determination of the distribution of δ, the radius of the largest inherent weak area, is treated in the next section. Depending on the relative magnitude of R and δ, the fracture process may be more or less influenced by one term or the other. If δ/R is high, the statistical distribution of the inherent weak portions will have a major influence on the fracture process while if δ/R is small only the plastic zone size will be important.

4.4 Distribution of Largest Inherent Weak Areas in a Link Cross Section.

Let us recall that "inherent weak area" refers to portions of the link cross section containing no fiber intersections or a number less than or equal to a required minimum; we are interested in defining the distribution of the largest weak portion in a link cross section, knowing the area of the

link and the average number of fiber intersections per square inch. In the following section an attempt is made to define a mathematical lower bound solution, as the exact solution is of extreme complexity. However, a fairly good solution can be obtained through a Monte Carlo simulation model which is explained in section 4.4.2.

4.4.1 A Lower Bound Mathematical Solution.

The definitions of major terms as used in this section are:

A = cross sectional area of the prismatic member or the link in square inches

N_s = average number of fiber intersections per square inch $\qquad N_s = \frac{2V_f}{\pi \phi^2}$

λ = elemental area containing on the average one fiber intersection

ϵ_0 = weak area assumed to be a crack nucleus. It contains zero fibers or depending on the material, a proportion of fibers less than or equal to a minimum characteristic value, $p\, n_0$.

n_0 = number of elemental areas contained in the basic grid under consideration. Also, equal average number of fiber intersections in a square of the basic grid.

δ_0 = radius of weak area .

In order to simplify the following computations it is assumed that the link cross section is square. The method described can be applied to other forms of sections.

Let us divide the cross sectional area of the link, say A, into small square areas called "elemental areas", say λ, containing on the average one fiber intersection. The distribution of fibers in the cross section of a link as well as in the elemental areas, is of Poisson type. Similarly, one can consider dividing the link cross section into larger squares of area $n_0\lambda$ and containing on the average n_0 fiber intersections. We are interested in the probability of finding in the link cross section a "weak" area of size $n\lambda$ larger than or equal to $n_0\lambda$. Here "weak" means empty or containing a number of fiber intersections r less than or equal to $p\,n_0$, assuming $p\,n_0$ rounded to the closest integer, and p is a fixed proportion assumed to be characteristic of the material.

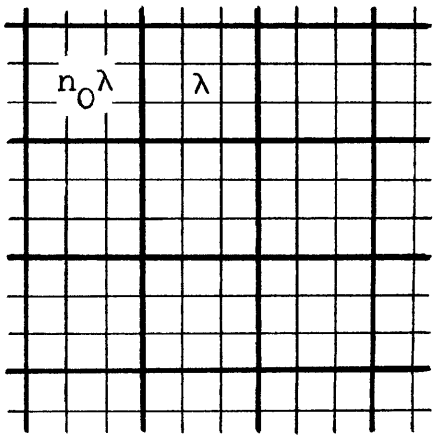

Let us lay a grid on the link cross section made of squares of size $n_0\lambda$, i.e. n_0 times the elemental area. There will be $\frac{N_L}{n_0}$ such squares in the link cross section.

Also, let us consider the actual number of fiber intersections r in a random sample of these squares. We have the following

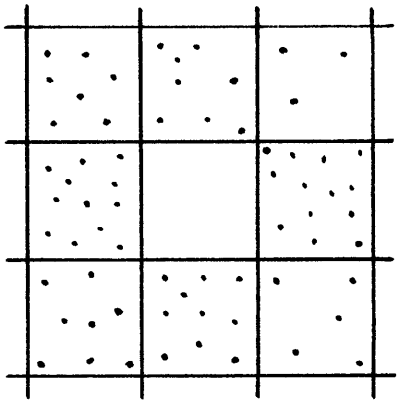

$$p_r(r) = \frac{n_0^r e^{-n_0}}{r!} .$$

This is the probability of finding r fiber intersections knowing that on the average there are n_0 fiber intersections. Therefore

$$p_r(0) = \frac{n_0^0 e^{-n_0}}{0!} = e^{-n_0}$$

$$p_r(pn_0) = \frac{n_0^{pn_0} e^{-pn_0}}{pn_0!}$$

and

$$\text{Prob}(r \leq pn_0) = \sum_{r=0}^{pn_0} \frac{n_0^r e^{-n_0}}{r!} = P_0 . \tag{6}$$

Note that for $r = 0$ $P_0 = e^{-n_0}$.

Let us then perform the following Bernoulli test on each of the squares of size $n_0\lambda$ of the given grid :

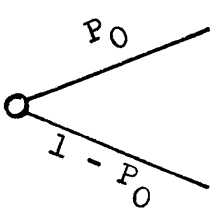

$x = 1$ success: area of size $n_0\lambda$ contains a number of fiber intersections $\leq pn_0$

$x = 0$ failure: it contains more than pn_0.

where x is the Bernoulli variable.

Let S be the sum of $\frac{N_L}{n_0}$ independent Bernoulli random variables x. The probability mass function (PMF) of S is described by the binomial PMF which in terms of our variables is given as follows

$$p_S(S_0) = \binom{\frac{N_L}{n_0}}{S_0} (P_0)^{S_0} (1 - P_0)^{N_L/n_0 - S_0}.$$

We are mainly interested in the probability of $S \geq 1$, i.e. in the probability of finding at least one "weak" area of size larger than or equal to $n_0\lambda$. Therefore

$$\text{Prob}(S \geq 1) = 1. - \text{Prob}(S=0)$$

but $$\text{Prob}(S=0) = (1. - P_0)^{N_L/n_0}.$$

So $$\text{Prob}(S \geq 1) = 1. - (1.-P_0)^{N_L/n_0}$$

In terms of the size of the weak area of interest ϵ we have

$$\text{Prob}(S \geq 1) = \text{Prob}(\epsilon \geq \epsilon_0) = \text{Prob}(n\lambda \geq n_0\lambda) = \text{Prob}(n \geq n_0).$$

So the final expression in terms of n_0 is

$$(7) \qquad \text{Prob}(\epsilon \geq \epsilon_0) = \text{Prob}(n \geq n_0) = 1. - \left(1. - \sum_{r=0}^{pn_0} \frac{n_0^r e^{-n_0}}{r!}\right)^{N_L/n_0}.$$

Note that this is a very lower bound value as the scheme of

the grid may be modified. The point of origin of the grid may be chosen in n_0 different ways inside a square of size $n_0\lambda$ (see sketch), the orientation of the grid axis may be changed and the forms of the basic areas of size $n_0\lambda$ may be modified to rectangles or otherwise. The problem becomes extremely intricate and no exact mathematical solution seems to be possible. Furthermore, any mathematical attempt at a solution is made more difficult as dependencies exist between events if more than one grid scheme is considered.

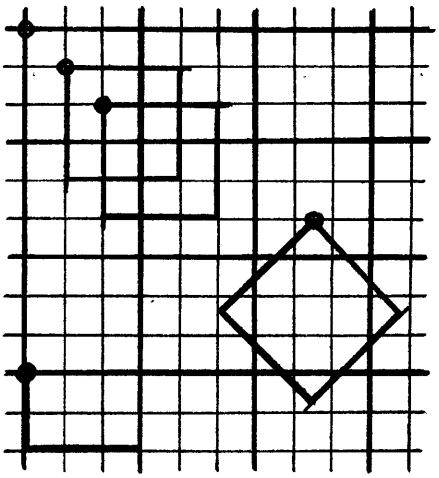

Another lower bound value, based on the strong assumption that independence exists between two overlapping squares of two different grid schemes, leads to consider $\frac{N_L}{n_0} \times n_0$ Bernouilli tests and therefore

$$(8) \quad \text{Prob}(\varepsilon \geq \varepsilon_0) = \text{Prob}(n \geq n_0) = 1. - \left(1. - \sum_{r=0}^{pn_0} \frac{n_0^r e^{-n_0}}{r!}\right)^{N_L}.$$

In order to derive the distribution function of the crack radius associated with a weak area, one can, for example, make the following assumption: the crack size 2δ is equal to the diameter of the circle having the same

area as the square under consideration. Therefore

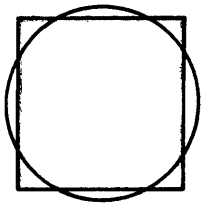

$$\epsilon_0 = n_0 \lambda = \pi \delta_0^2$$

and as $N_s = \frac{1}{\lambda} \Rightarrow n_0 = \pi N_s \delta_0^2$.

So we replace in equation (7) n_0 by its value in function of δ_0.

In the particular case where it is known that the plastic zone size R of the composite is negligeable or very small one can directly assess the cumulative function of link strength σ by replacing $a = \delta_0$ by its value in function of K_{Ic} and σ_0, that is:

$$n_0 = \pi N_s \delta_0^2$$

and from equation (5) we get

$$\delta_0^2 = \frac{\pi^2}{16} \left(\frac{K_{Ic}}{\sigma_0}\right)^4 \tag{9}$$

and

$$n_0 = \frac{\pi^3}{16} N_s \left(\frac{K_{Ic}}{\sigma_0}\right)^4 \tag{10}$$

so that

$$\text{Prob}(\sigma \leq \sigma_0) = 1. - (1. - P_0)^{\frac{N_L}{N_S} \frac{\pi^3}{16} \left(\frac{K_{Ic}}{\sigma_0}\right)^4}$$

and as $\frac{N_L}{N_s}$ = area of the link cross section A, we end up with

$$(11) \qquad \text{Prob}(\sigma \leq \sigma_0) = 1. - (1. - P_0)^{A \frac{\pi^3}{16} \left(\frac{K_{Ic}}{\sigma_0}\right)^4}$$

where P_0 is given in function of σ_0.

For the particular case where $P_0 = e^{-n_0}$, i.e. where the weak areas are completely empty we will have

$$(12) \qquad P(\sigma \leq \sigma_0) = 1. - \left(1. - e^{-\frac{\pi^3}{16} N_s \left(\frac{K_{Ic}}{\sigma_0}\right)^4}\right)^{A \frac{\pi^3}{16} \left(\frac{K_{Ic}}{\sigma_0}\right)^4}$$

4.4.2 Simulation Model for the Determination of the Distribution of Largest Weak Areas in a Link Cross Section

As it is impossible to derive an exact mathematical solution to the distribution of the largest weak portions in a link cross section, a simulation method is proposed in order to get at least a numerical solution to the problem. This is achieved by the Monte Carlo simulation method. The Monte Carlo method [44,62] is a simulation technique that has been used in a variety of disciplines to study and predict the behavior of both deterministic and stochastic phenomena. With the development of high speed computers and the random number generation routines, this method has become an invaluable tool in the fields of operations research and systems engineering. Its application to civil engineering problems in order to take into account

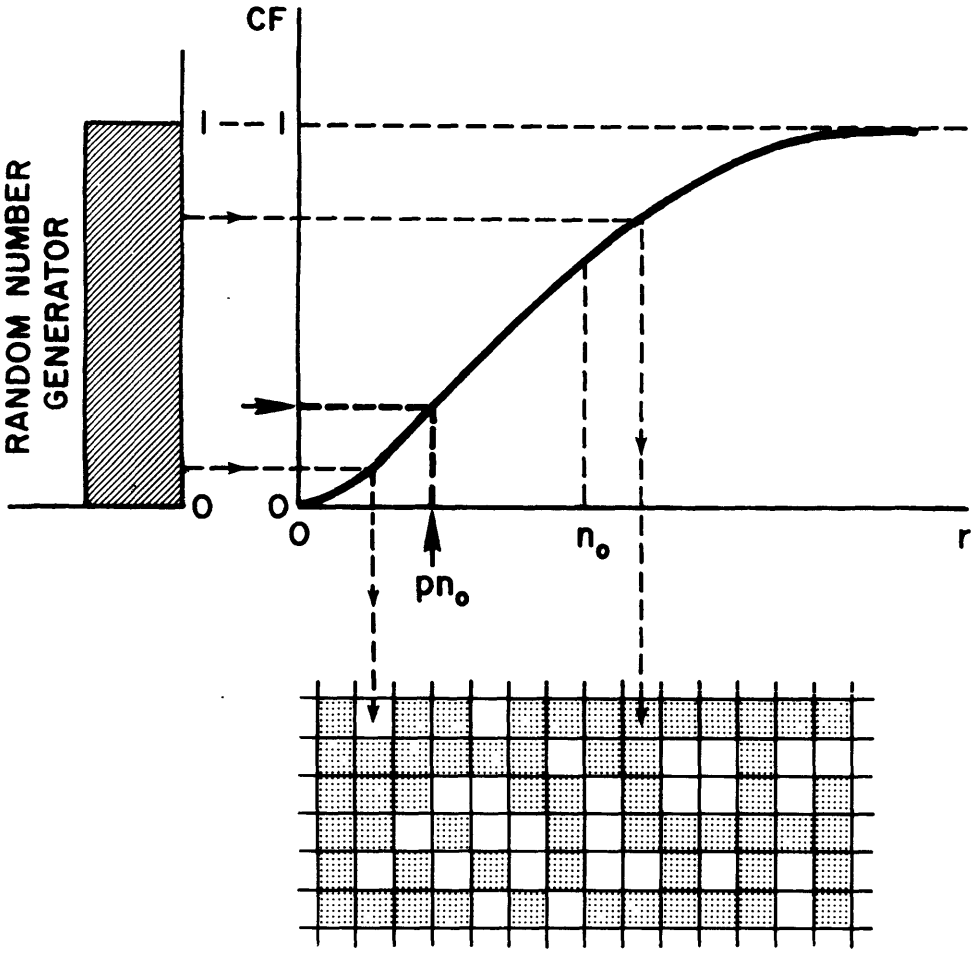

n_o = AVERAGE NUMBER OF FIBER INTERSECTIONS PER SQUARE

r = ACTUAL NUMBER OF FIBER INTERSECTIONS PER SQUARE

FIG. 13. MONTE CARLO SIMULATION FOR THE DISTRIBUTION OF WEAK AREAS.

material and structural variabilities is relatively recent [21, 51, 100].

This method as used herein is relatively very simple. The problem is to find the distribution of largest weak portions in the link cross section. As we know a weak portion is an area containing no fibers or a number of fibers less or equal to a specified limit, say pn_0 rounded to the closest integer. We also know that the fibers are Poisson distributed in the link cross section. Given data related to cross section area A (assumed square, for example), and average number of fibers per square inch N_s, the method involves the following steps:

1. Divide the link cross sectional area by a grid of a relatively large number of small squares that will contain each on the average n_0 fiber intersections.
2. Calculate the probability that each of these squares contains a number of fiber intersections less than or equal to pn_0, i.e. $\sum_{r=0}^{pn_0} \frac{n_0^r e^{-n_0}}{r!} = P_0$
3. Generate a random number RN, with a uniform probability distribution between zero and one. (Fig. 13)
4. Compare result.

   If $RN \geq \sum_{r=0}^{pn_0} \frac{n_0^{-r} e^{-n_0}}{r!}$ → fill corresponding square with a star

$$\text{If} \quad RN < \sum_{r=0}^{pn_0} \frac{n_0^{-r} e^{-n_0}}{r!} \quad \rightarrow \quad \text{leave blank}$$

5. Repeat steps 3 and 4 for every small square of the cross section.

6. Repeat step 3, 4, 5 for a big number of runs, say 100, of the same cross section.

7. Analyze results as directly drawn on paper (Fig. 13) by a computer routine. Find the frequency distribution of largest blank areas. Limit search, for example, to convex areas with ratio of diagonals between one and four.

Having the distribution of the largest weak portions one can derive the distribution of the largest radius δ associated with them and then, using equation (5) derive the distribution function of strength knowing K_{Ic} and R.

4.5 An Example of Application to Fiber Reinforced Concrete.

The manner by which the proposed model can be applied to steel fiber reinforced concrete is demonstrated by a simple example below.

The distribution of the largest diagonal 2δ associated with the largest weak area in a link cross section has been obtained using the simulation program described earlier for the following particular data:

Link area = 20 x 20 = 400 square inches

Average number of fiber intersections

N_s = 100/Square inch

Critical proportion p = 0.2.

The frequency distribution of 2δ as obtained is drawn on Fig. 14. It shows that 2δ varies mainly from 0.3 to 1.6 inches with a peak value at around .7 inches.

The plastic zone radius R can be estimated from the cleavage tests described in the following chapter. The test results suggest that for a specimen reinforced with 3% fibers having a diameter of 0.006 inch and a length of 0.5 inch, the plastic zone radius R is of the order of 20 inches. Therefore the ratio δ/R for a representative fiber reinforced concrete sample, is negligeable and one can ignore the value of δ in the calculations.

For a value of R assumed constant and equal to 20 inches, and a value of K_{Ic} of the order of 5000 psi$\sqrt{in}$ (Table B3 Appendix B) equation (5) indicates that an upper bound value of the link strength will be given by

$$\sigma = K_{Ic}\sqrt{\frac{\pi}{4R}} = 5000\sqrt{\frac{\pi}{80}} \simeq 960 \text{ psi} .$$

Note that a second upper bound value on the strength as predicted by equations (3.16) or (3.27) is in the order of 400 psi. (The highest result of the two equations is considered.)

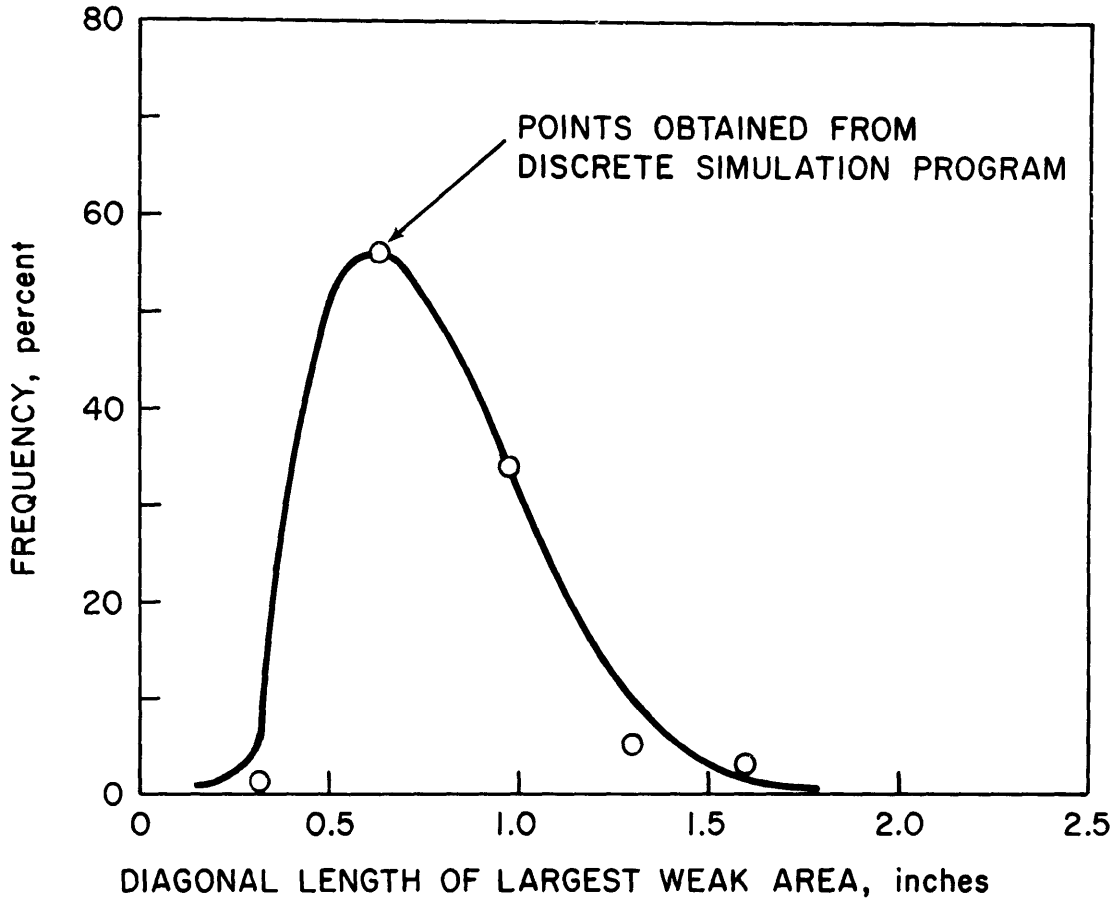

FIG. 14. TYPICAL DISTRIBUTION OF LARGEST CRACK LENGTH ASSOCIATED WITH LARGEST WEAK AREAS, AS GENERATED BY SIMULATION.

Finally, a lower bound value can be assessed using the strength of the non-reinforced concrete matrix that is of the order of 300 psi.

It can be concluded that the overall model leads to rather realistic bounds in predicting the strength characteristics of the material.

CHAPTER 5

EXPERIMENTAL PROGRAM

The experimental program described in this chapter comprises three types of experiments: pull-out tests on fibers, tensile tests on fiber reinforced concrete prisms and cleavage beam tests. Pull-out tests as well as cleavage beam tests are mainly concerned with assessing experimental values to important variables or parameters given as input data in the analytical model. Tensile tests represent the major part of the experimental program, results of which will be correlated with theoretical predictions in Chapter 6.

5.1 Matrix Composition and Curing History.

Essentially the same mortar matrix was used throughout this investigation. High early Portland cement type III and fine graded Ottawa silica sand (ASTM C-109) were mixed with water in the following proportions: water to cement ratio by weight = 0.6, sand to cement ratio by weight = 2.5. The high water-cement ratio was necessary to keep the mix workable when fibers were added.

The fibers were thoroughly mixed with the mortar matrix using a food mixer with a pan capacity of approximately five gallons.

All specimens were poured into especially designed plexiglas molds, except the pull-out specimens for which standard ASTM briquette molds were used.

Less than twenty-four hours after pouring, specimens were removed from their molds, cured in a moisture room at 100% relative humidity and 75° Fahrenheit for six days and tested on the seventh day. In the case where specimens had to be cut and/or notched, these operations were performed under wet conditions, sometime during the curing period.

5.2 Pull-out Tests on Fibers.

The method used to perform the pull-out tests was chosen in order to simulate closely the way the fibers pull out in the postcracking state. It was achieved by using ASTM standard molds for tensile briquettes in which only one half of the specimen was poured, the other half being closed with a styrofoam sandwich holding the fiber. Some experimental details of preparation and testing are shown in Fig. 15.

The experimental program included a large number of tests on single oriented fibers in order to assess as precisely as possible the mean value of the bond strength $\bar{\tau}$ at the fiber matrix interface. The influence of the angle of orientation θ on the bond strength was also investigated by testing in pull-out a group of two symmetrically

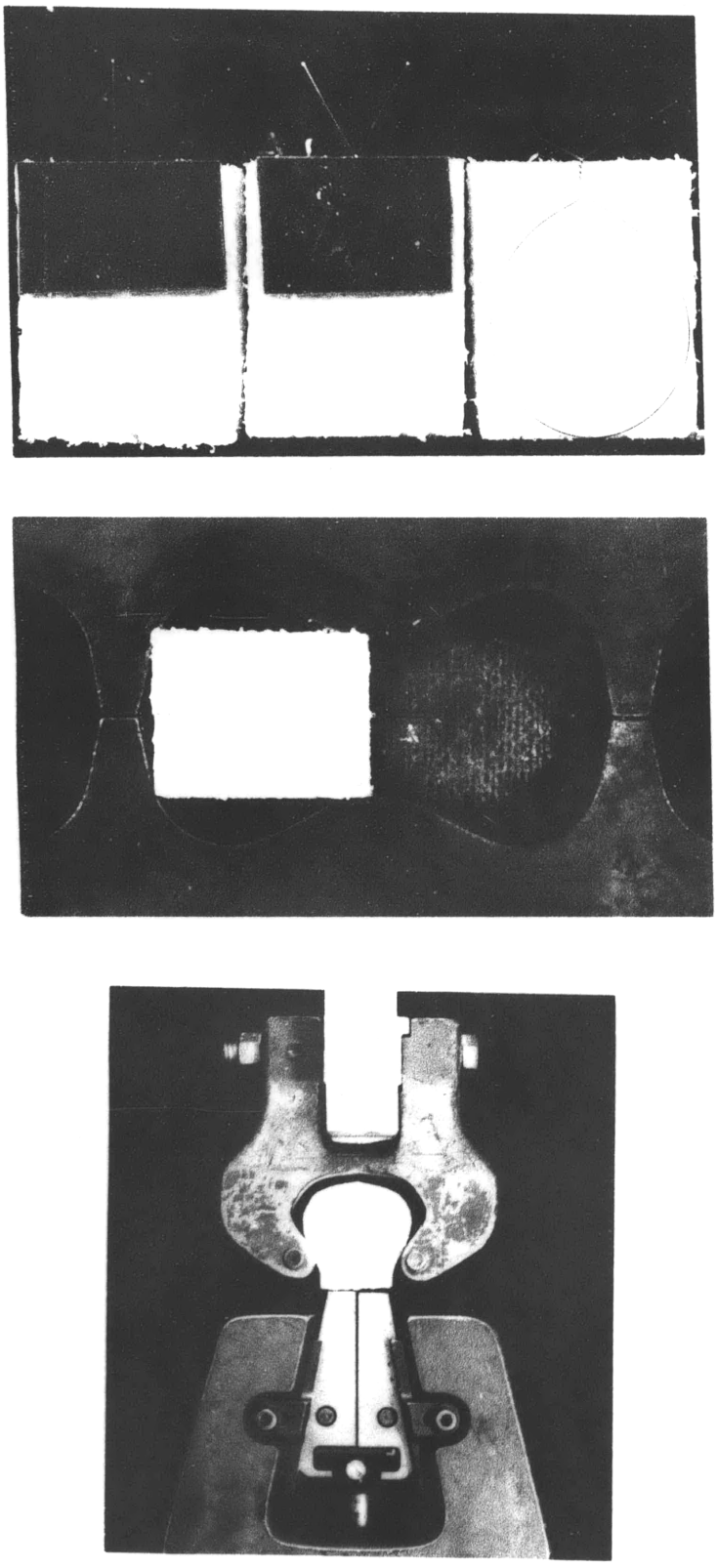

Fig. 15 Typical Preparation and Testing of Pull-Out Specimens

oriented fibers. The values of the angle θ were chosen as 15, 30, 45, 60, and 75 degrees. In all cases the fiber diameter and the embedded fiber length were taken equal to 0.01 and 0.50 inches, respectively. As in a first series of experiments the fibers oriented at 60 and 75 degrees either broke or slipped out of the tightening jaws under loading, it was decided to prepare them differently, using a two step pouring procedure. The first step was similar to the one described earlier. The second consisted in taking out the styrofoam pieces after twelve hours, putting a piece of polyethylene separator along the middle section of the briquette and pouring mortar into the second half. For these specimens the standard ASTM grips for briquette were used for testing. In general extreme care was taken in handling the specimens in order to avoid torsion or twisting of the fibers and ensure reliable results.

All results, mean values, and standard deviations are given in Appendix B Table B1. Their interpretation is discussed in 6.

5.3 Tensile Tests on Fiber Reinforced Concrete Prisms.

Most investigators in the field of steel fiber reinforced concrete derived tensile properties indirectly from observations on flexural or splitting cylinder tests. The objective here was to obtain the direct tensile properties

through pure tensile tests. As no standard shape specimen of a reasonable size was available, it had to be especially designed for the experiment. The shape and dimensions chosen are described in Fig. 16. Corresponding plexiglas molds and wedge type grips were built to perform the experiment (Fig. 17a).

The molds were designed so that a 7-inch-thick block profile was poured at a time, from which 3 two-inch-thick slices, representing each a specimen, were cut with a thin diamond saw under wet conditions. Endpieces of $\simeq$ 3/8 inch thickness were disregarded. This slicing method was chosen in order to facilitate pouring conditions, decrease variabilities, and diminish the influence of the mold sides on the orientation of the fibers. Furthermore, on the two opposite sides of the middle part of each specimen, that were not sawed, three 1/4 inch deep notches, spaced one inch apart, were cut. The purposes of these notches are the following: first, to ensure that a nice plane crack developes at fracture along one of the notched sections, second, to guarantee that inside this section the fibers would all be randomly oriented (as the influence of the sides of the molds is eliminated), third, to simulate a chain member made out of three consecutive links, and finally, to allow the measurement of the composite surface energy from the recorded load elongation curve.

Four series of experiments indentified as A, B, C, and

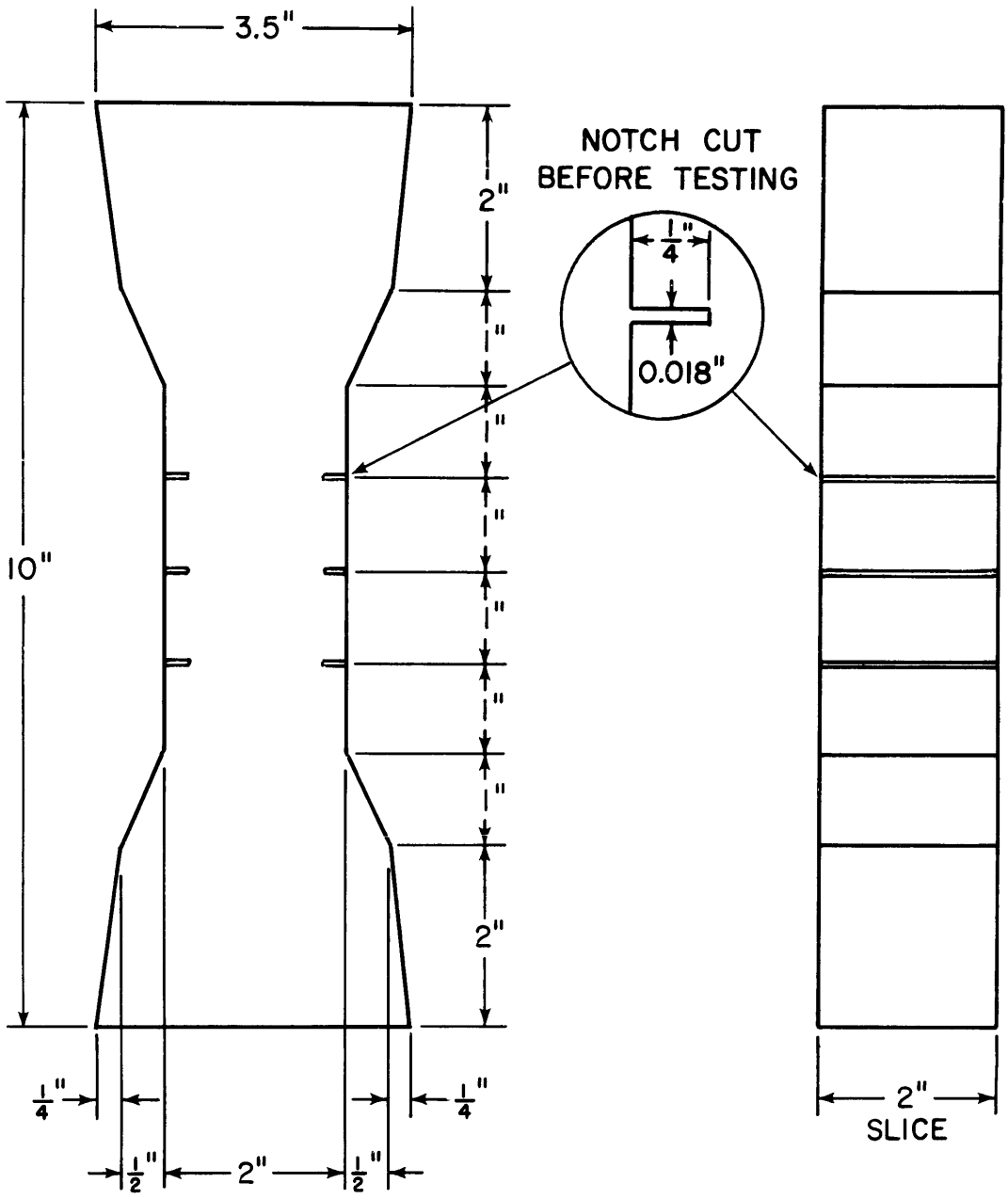

FIG. 16. DIMENSIONS OF TENSILE SPECIMEN.

(a)

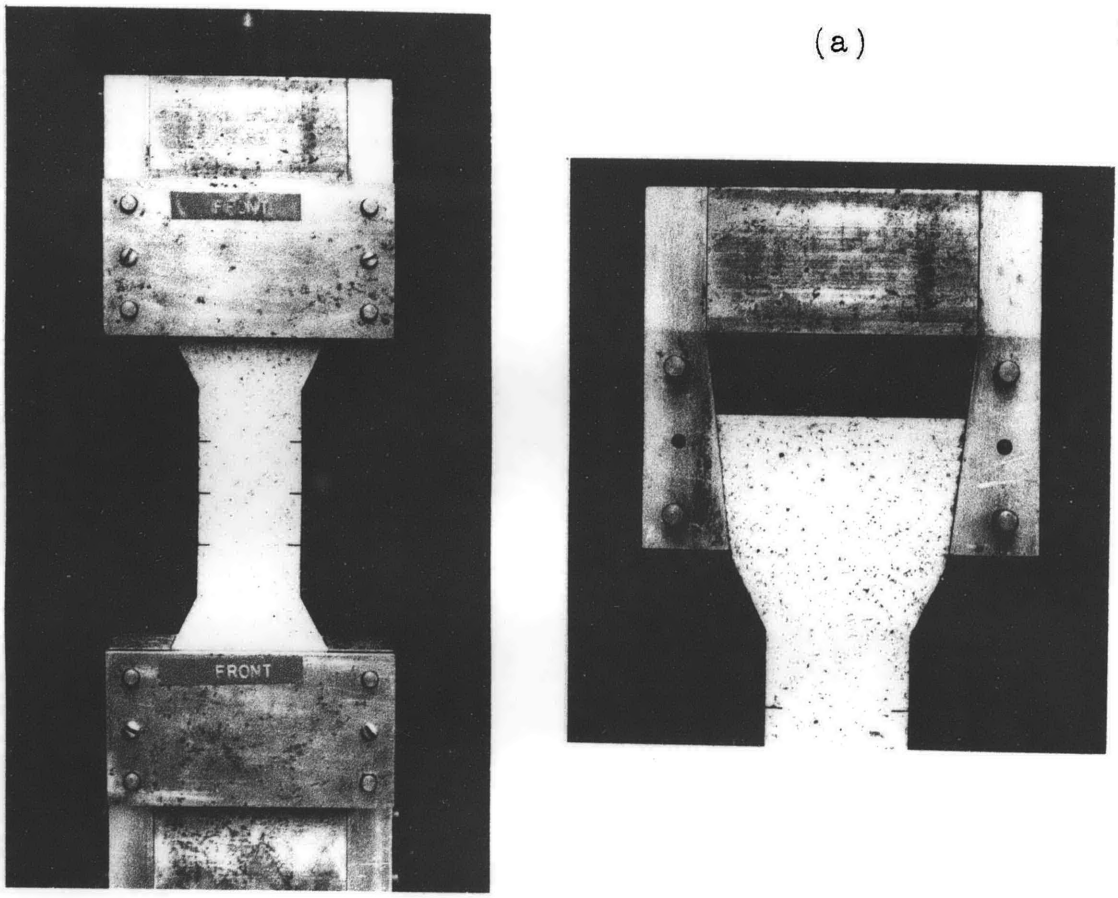

(b)

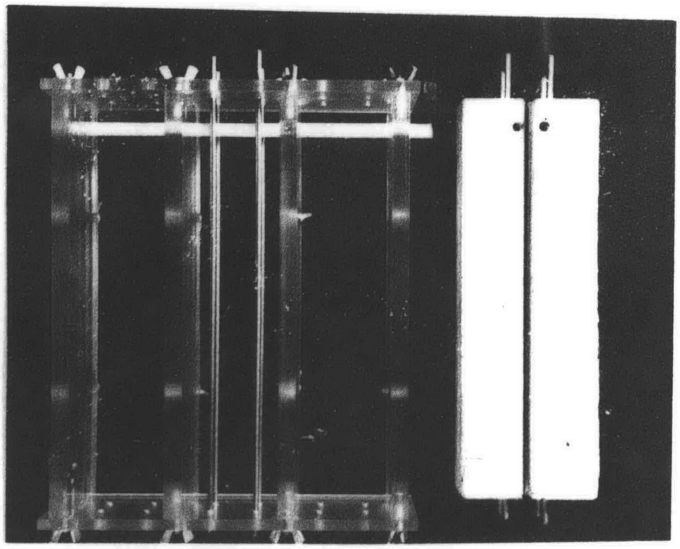

Fig. 17 a) Typical View of Tensile Specimen and Grips
b) Typical View of Cleavage Specimen and Mold

D were performed. The description of reinforcement parameters and other relevant variables as described in this study is given in Table 1. The four series of experiments correspond to four different fiber aspect ratios (three with the same fiber diameter). For each aspect ratio three different volume fractions of fibers were used. An average of six to eight specimens was prepared for each sample.

Testing was performed on the INSTRON universal testing machine, using the 10,000 pound load cell. The load was applied at a rate of 0.05 inch per minute for a chart speed of 2 inches per minute and a full scale of 2,000 pounds. Load elongation curves were automatically plotted on a chart recorder. The elongation observed is the sum of the specimen elongation and that of the testing system. Its value is therefore comparative but not absolute. Average load elongation curves for the different series are plotted in Appendix C, Figures C1 to C4.

Relevant results on load at the first structural crack (through the matrix crack), maximum postcracking load, and the energy absorbed at failure are given in Table B2, Appendix B. Due to the stress concentration at the tip of the notched sections, the stress at first crack is expected to be a more relative than absolute value. Discussion and correlation of observed results with theoretical predictions are in 6.

Series	Fiber diam. inch	Fiber** length inch	Aspect ratio ℓ/ϕ	Specimen type	Percent* fibers by weight	Percent fibers by volume	Mean # of fibers /cubic inch	Mean # of fiber intersections /sq.inch	Mean spacing in plane inch	Mean spacing in space inch [81]
A	0.010	0.50	50.	A1	3.41	1.	256	64	0.125	0.138
				A2	6.65	2.	512	128	0.0884	0.097
				A3	9.78	3.	768	192	0.0722	0.079
B	0.010	0.75	75.	B1	3.41	1.	170	64	0.125	0.138
				B2	6.65	2.	340	128	0.0884	0.097
				B3	9.78	3.	510	192	0.0722	0.079
C	0.010	1.0	100.	C1	3.41	1.	128	64	0.125	0.138
				C2	6.65	2.	256	128	0.0884	0.097
				C3	9.78	3.	384	192	0.0722	0.079
D	0.006	0.50	83.3	D1	3.41	1.	708	177	0.0751	0.083
				D2	6.65	2.	1416	354	0.053	0.058
				D3	9.78	3.	2124	531	0.043	0.048

* Based on specific gravity of 140 lbs/cub.ft. for mortar and 490 lbs/cub.ft. for steel

** Brass plated, round, low carbon high strength steel fibers

TABLE 1 Reinforcement Parameters - Tensile Tests

5.4 Cleavage Specimens.

The geometry and the dimensions of the double cantilever cleavage type beam used are shown in Fig. 18. This particular design was chosen after a number of less successful trials. The longitudinal reinforcing rods were provided in order to avoid flexural type cracks during testing and to supply enough shear resistance at the gripping supports. Note that the compliance of the specimen is modified by only a few percent due to the presence of the steel reinforcement. The notches shown were cut before testing using a diamond saw under wet conditions. The larger notch was necessary to allow for enough light for observation during testing.

The testing apparatus and a typical specimen under test are shown in Fig. 19. Note the simplicity and effectiveness of the gripping system. A 5x magnifier was used to follow the extension of the crack along the beam, during loading. The load rate applied on the INSTRON testing machine was chosen equal to 0.01 inch per minute.

As these experiments were mainly intended to devise a reliable testing method in order to determine some fracture properties of the material, no attempt has been made to perform a complete and systematic experimental program. Only six beams containing 3%

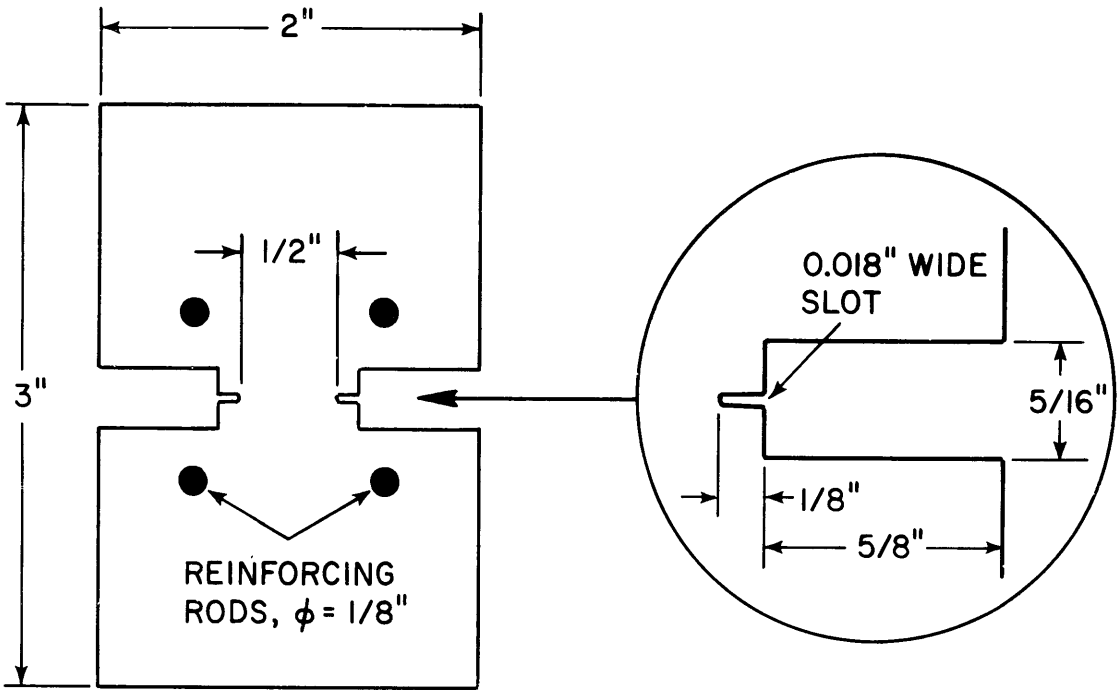

CROSS SECTION

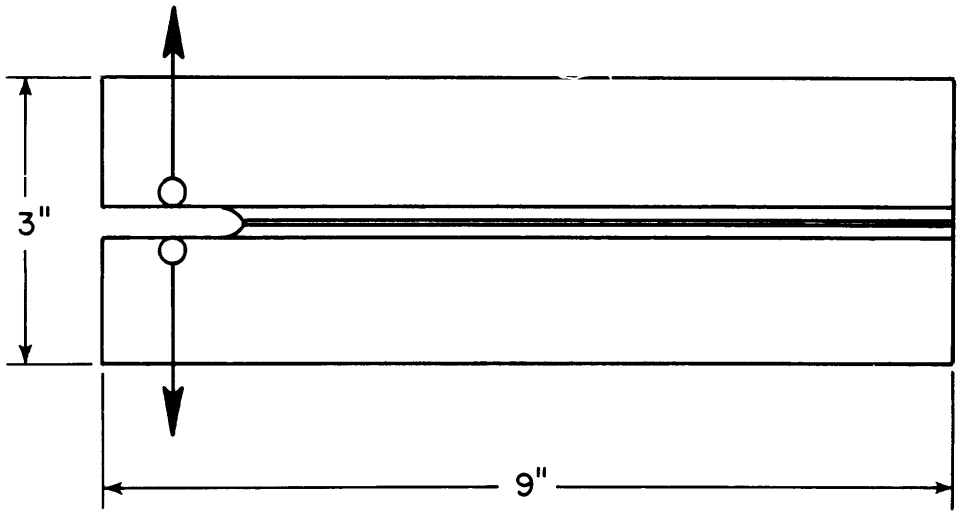

FIG. 18. CLEAVAGE SPECIMEN.

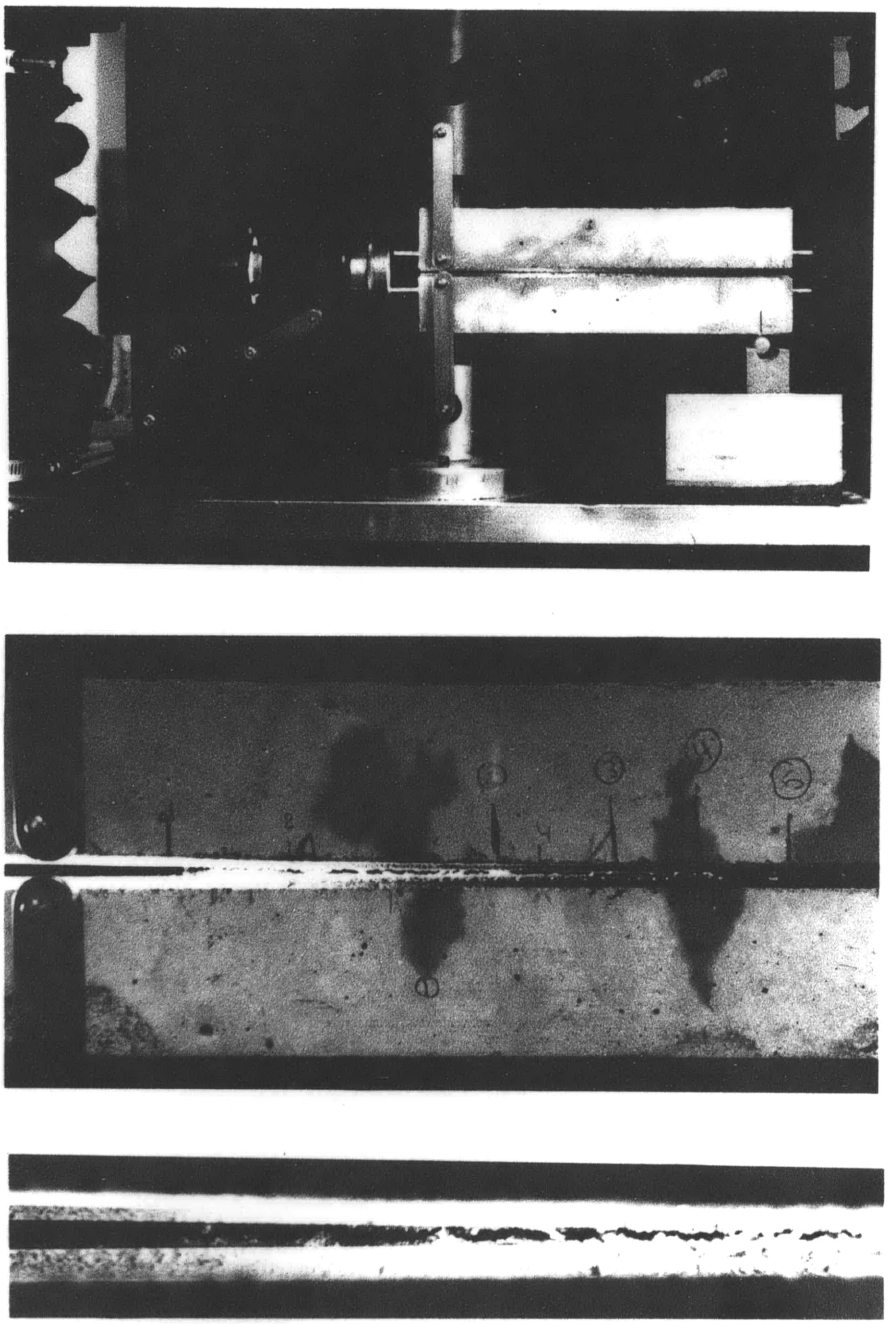

Fig. 19 View of Double Cantilever Cleavage Type Beam under Test

fibers of the following characteristics were used: (ϕ = 0.010", ℓ = 0.50"), (ϕ = 0.010", ℓ = 0.75"), and (ϕ = 0.006", ℓ = 0.5"). A typical load displacement curve is presented in 6.

CHAPTER 6

EXPERIMENTAL RESULTS - DISCUSSION AND CORRELATION WITH MODEL'S PREDICTIONS

This chapter presents the results of the experimental program described in Chapter 5. The first section is devoted to pull-out tests. The second section presents the tensile test results correlating them with those predicted by the model and using observed differences as feadback information to restructure some of the model's underlying assumptions. A third section deals with the cleavage beam tests.

6.1 Results of Pull-Out Tests.

Pull-out experiments were performed in order to provide information on the average bond or shear strength at the fiber matrix interface and to clarify the relation between the pull-out load and the angle of orientation of the fiber. These results are presented in detail in Table 1 Appendix B.

The average value of bond strength observed from 54 pull-out specimens with orientation angle $\theta = 0$ is found equal to 380 psi. Typical pull-out load versus pull-out distance curve is plotted on the upper part of Fig. 20. It is observed that, after reaching a peak value, the load decreases drastically, and tends slowly to zero. On the

lower part of Fig. 20 is shown a typical pull-out load versus pull-out distance curve for an oriented fiber with $\theta = 30^{o}$. It can be seen that here, after reaching its peak value, the load decreases and levels off to a kind of plateau value before dropping suddenly to zero at complete pull-out. The "final plateau value" of the load is due to a pseudo "pulley" action that bends the fiber and induces a friction point during pull-out operation. Similar behavior is observed for all $\theta > 0$. In Fig. 21 the peak value and the final plateau value of the pull-out load (or associated bond stress) are plotted versus the angle of orientation θ. Note that the final plateau value increases linearly with θ while the peak value follows an unpredictable path. It is rather difficult to interpret this behavior. A number of parameters seem to be involved such as the flexibility of the particular fiber under pull-out, the local resistance of the matrix, and a possible change in the bond failure mode due to the fiber orientation. Finally, on the same Figure is plotted in dashed form the theoretically assumed variation of peak load versus the angle of orientation θ. It is of

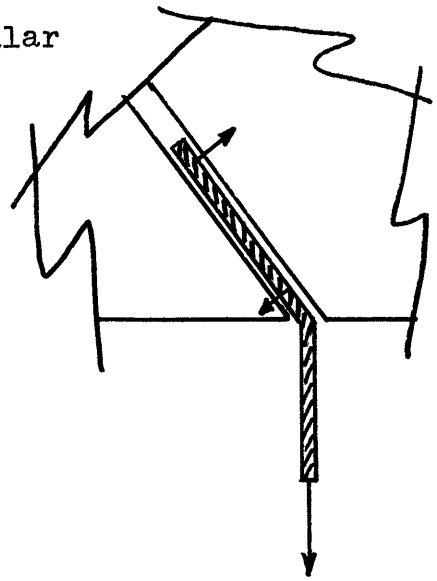

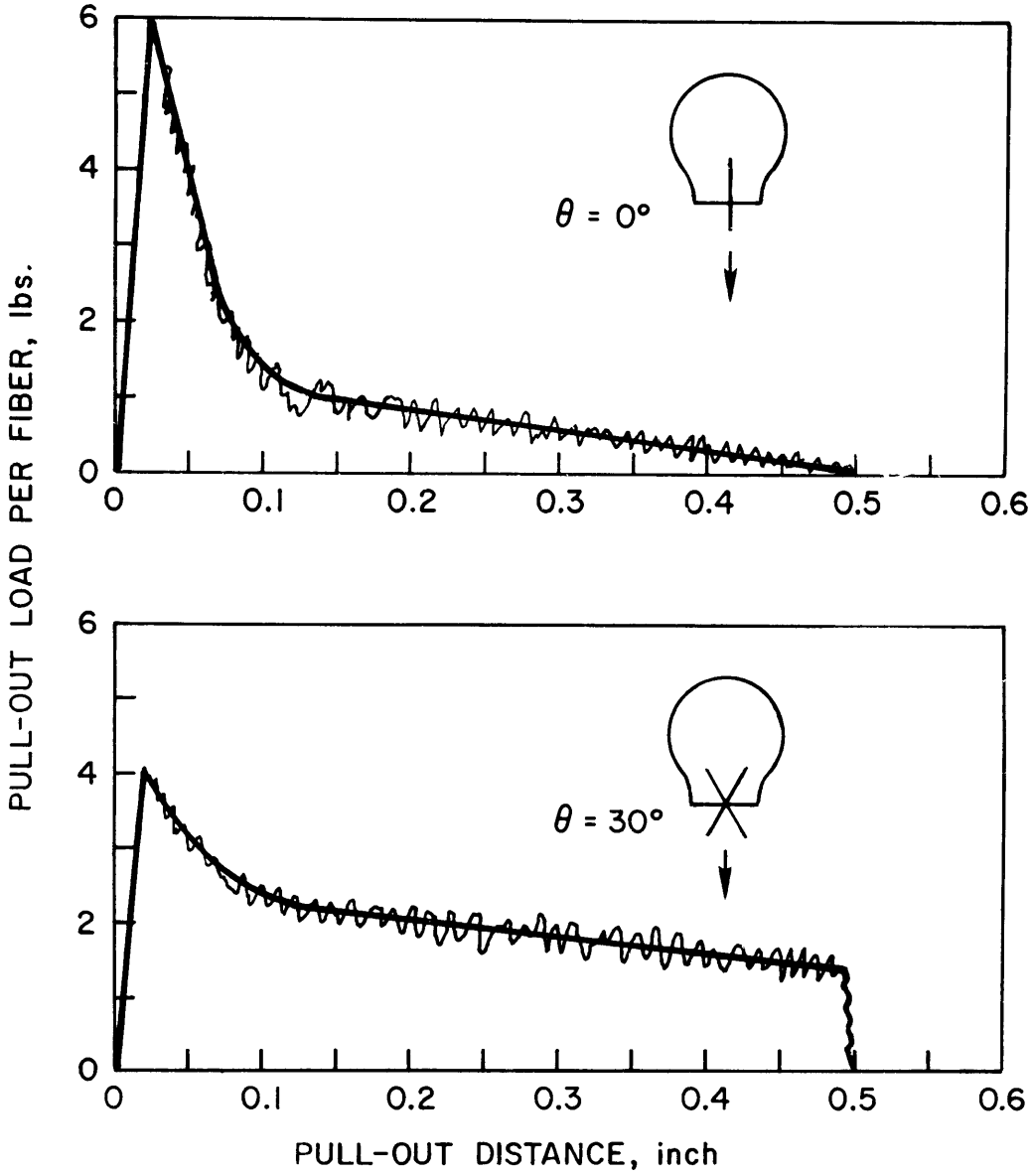

FIG. 20. TYPICAL FIBER PULL-OUT CURVES FOR 0° AND 30° ORIENTATION ANGLES.

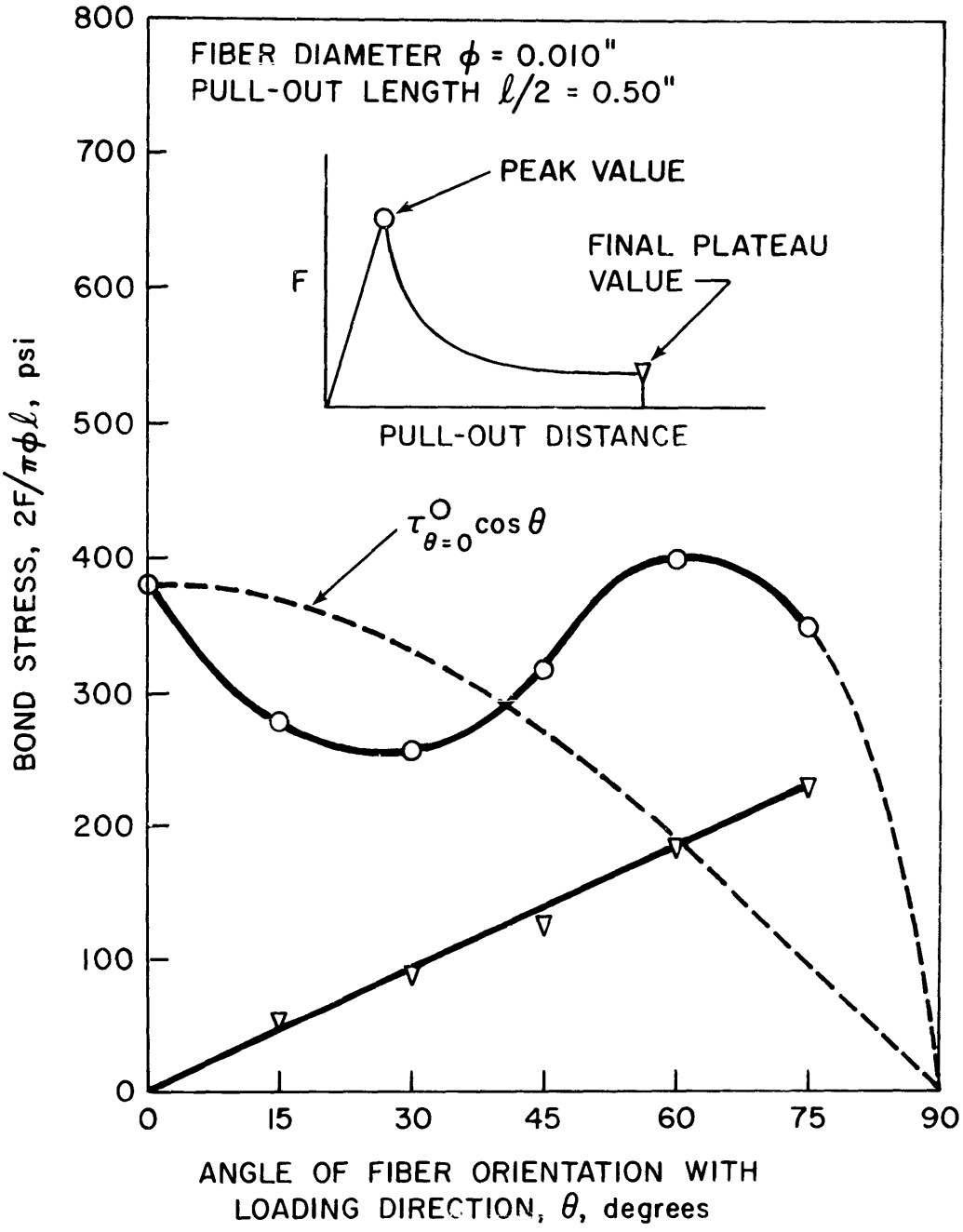

FIG. 21. VARIATION OF BOND STRENGTH WITH FIBER ORIENTATION.

the form $F_\theta = F_{\theta=0} \cos\theta$ where $\cos\theta$ represents the efficienty factor of orientation. By comparing the theoretical and the observed curve, it can be seen that the expected values of bond strength for a randomly oriented fiber as derived from either curve are not very different. This somewhat simplified observation is made more attractive for practical purposes when one observes the scatter of the experimental results, Table 1 Appendix B. In some cases the standard deviation is as high as 50% of the mean value observed, indicating that care must be excercised in using and interpreting the results. In fact, if the mean theoretical value of bond strength for a randomly oriented fiber is close to the observed mean value, it is not because the assumed theoretical mode of failure is exact. It is only because the pull-out load for inclined fibers is influenced by some additional action - the "pulley" action described earlier - and that on the average the results turned out to be similar. Also note that, for example, for $\theta = 15^o$, Fig. 21, where the "pulley" action is less important, the peak load observed drops drastically and in a very different way from the $\cos\theta$ variation theoretically predicted.

Finally, note that these experiments were conducted on only one or two symmetrical fibers, pulling out from a one square inch cross section of the matrix. If the density of fibers pulling out increases to about 100 or 200 fibers, the

expected value of bond strength per fiber may decrease drastically due to local failures in the resistance of the surrounding matrix and other possible stress concentration effects. In the next section we will see how this can influence the observed postcracking strength of the composite.

6.2 Description of Global Results on Tensile Tests.

In describing the observed behavior of fiber reinforced concrete under tensile loading a distinction must be made between the precracking state and the postcracking state which are separated by the occurrence of the first structural crack. On the load elongation curve the first crack occurrence induces a drastic change in material response (Figures C1 to C4, Appendix C). Before the first crack the composite may be described as an elastic material. After cracking the fibers bridging the cracked surfaces pull out under load and the material is in a somewhat pseudo-plastic state. Theoretically the postcracking strength may be lower or higher than the cracking strength. In general it is higher for long or continuous fibers. Consequently, in characterizing the strength of the composite one must specify whether it is equal to the recorded cracking or maximum postcracking stress. This distinction has been made in the manner tensile test results are presented.

The observed values of average cracking and postcracking strengths for the four aspect ratios tested are plotted versus the volume fraction of fibers, in Figures 22 and 23. They are also plotted versus the aspect ratio for a given volume fraction of fibers in Figures 24 and 25. Finally, in Figure 26 the surface energy of the composite is plotted versus the volume fraction of fibers for the four aspect ratios used. As only one crack developed at fracture the surface energy per unit nominal cracked area has been derived from the total energy absorbed as corresponding to the area under the load elongation curve. Detailed computations are shown in Table B3 Appendix B.

6.3 Discussion and Correlations with the Model's Predicted Values of Tensile Strengths.

In this section we will try to compare the average observed values of cracking strength, postcracking strength, and energy absorbed with those predicted by the model proposed in Chapter III. Similarities will be noted and discrepancies will be explained to the best possible extent. They will be used as feedback information to restructure some of the assumptions used in the model.

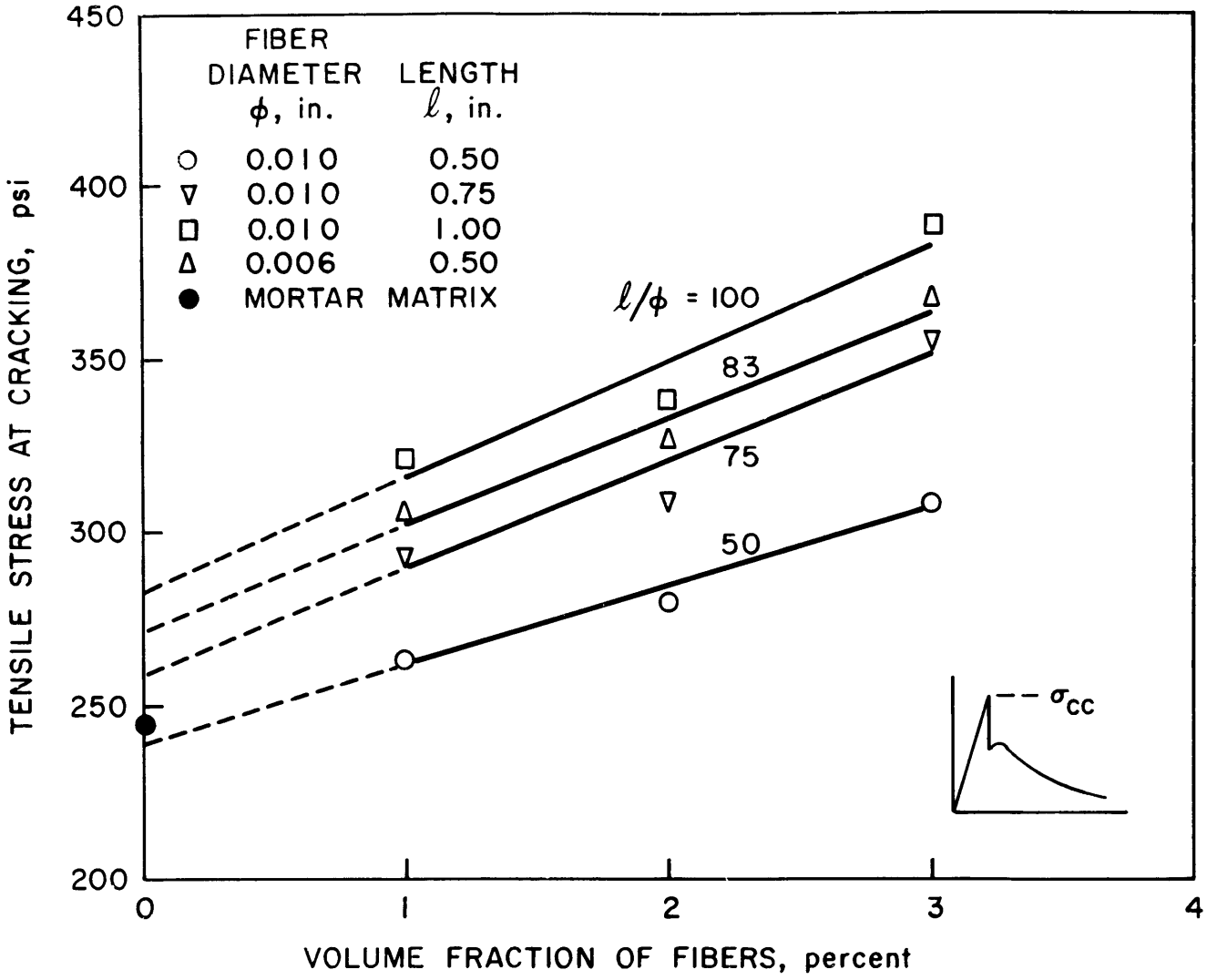

FIG. 22. TENSILE STRESS AT CRACKING - LEAST SQUARE FITTING LINES IF MORTAR MATRIX POINT IS NOT INCLUDED.

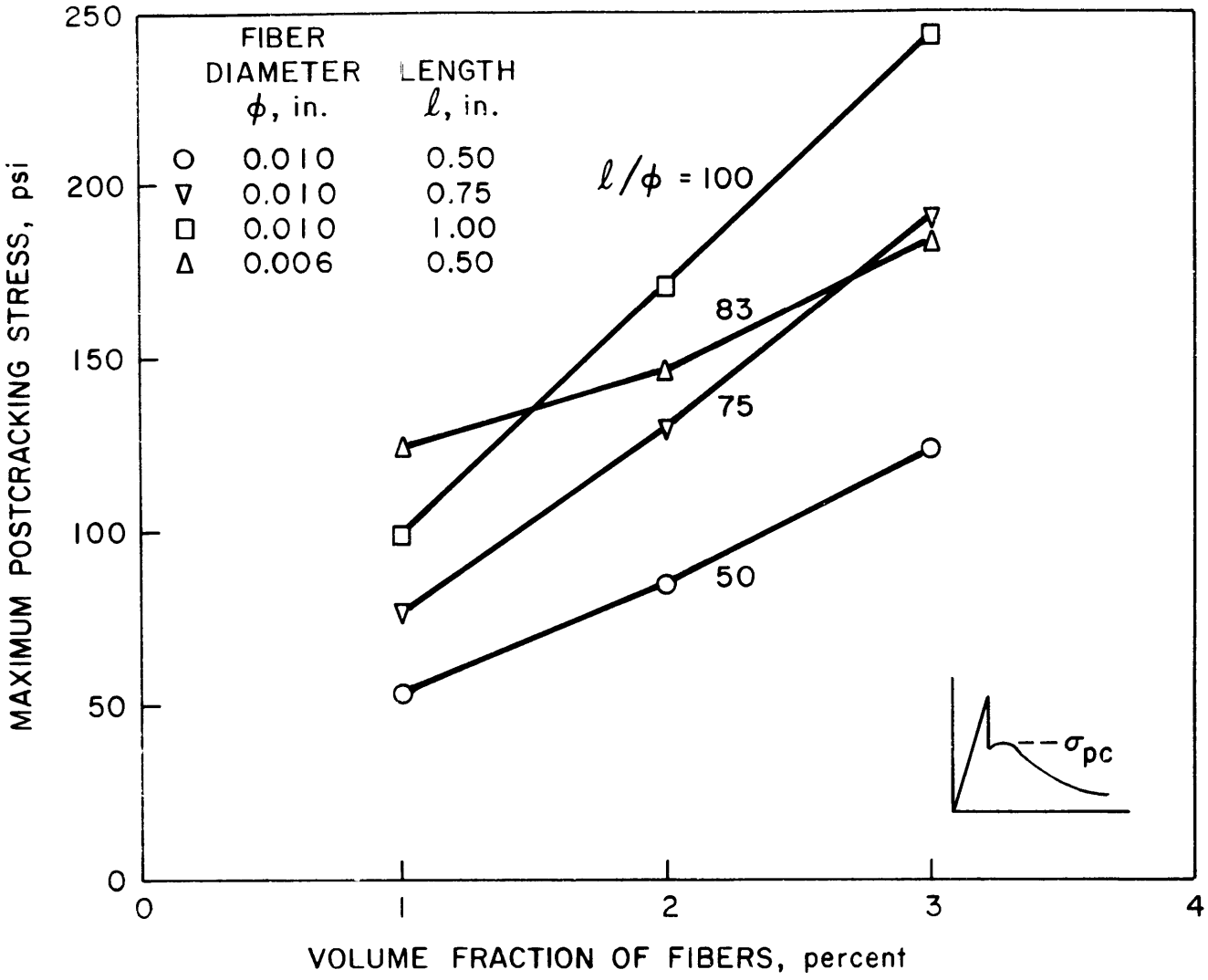

FIG. 23. MAXIMUM POSTCRACKING STRESS vs. VOLUME FRACTION OF FIBERS.

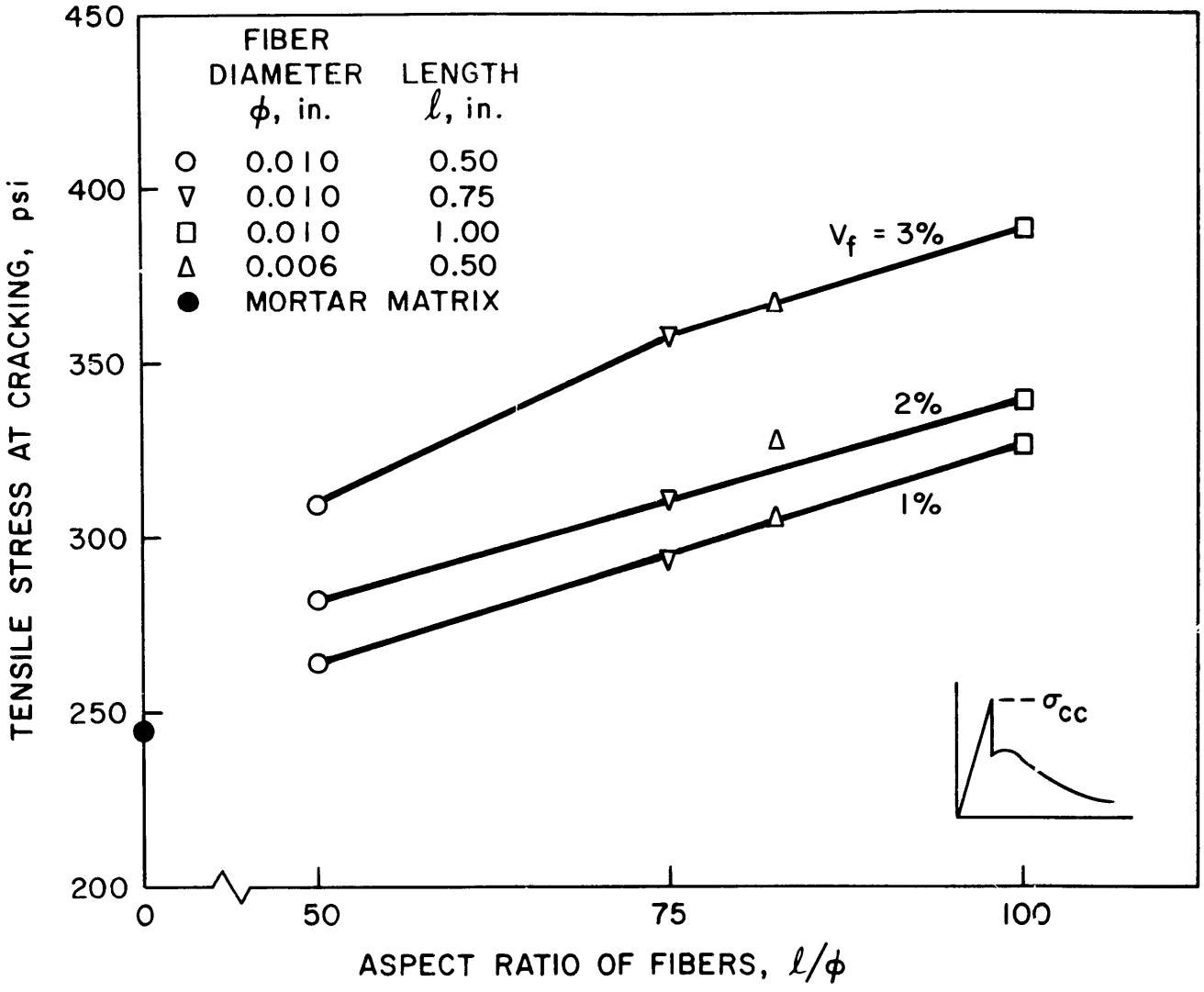

FIG. 24. TENSILE STRESS AT CRACKING vs. ASPECT RATIO OF FIBERS.

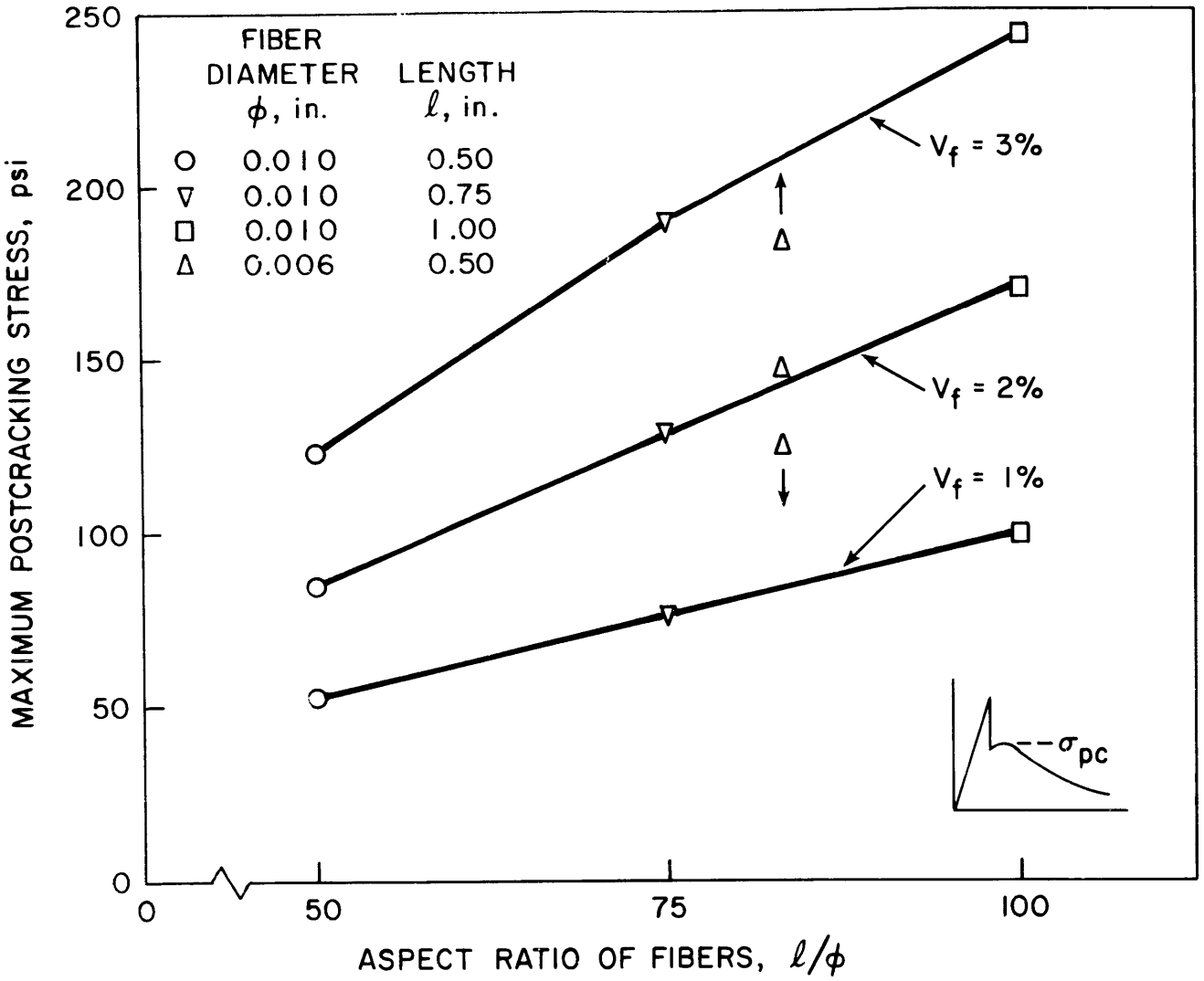

FIG. 25. MAXIMUM POSTCRACKING STRESS vs. ASPECT RATIO OF FIBERS.

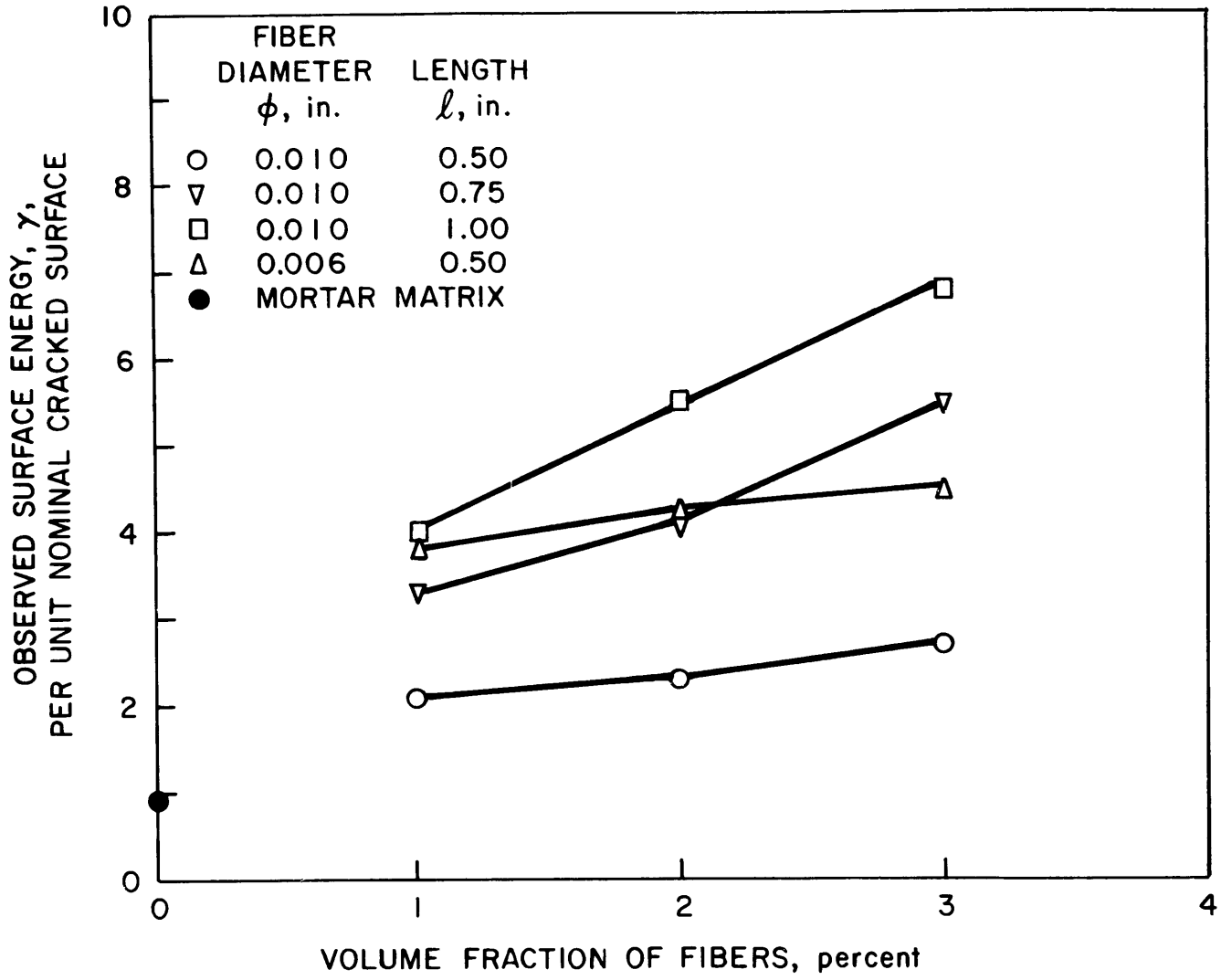

FIG. 26. ENERGY ABSORBED TO FAILURE vs. VOLUME FRACTION OF FIBERS.

6.3.1 On the Postcracking Strength.

Let us reproduce here equation 3.16 that predicts the postcracking link strength of the composite, that is

$$\bar{\sigma}_{cu} = \frac{1}{\pi} \bar{\tau} V_f \frac{\ell}{\phi} .$$

This relation suggests that for a given $\bar{\tau}$ and ℓ/ϕ the postcracking strength varies linearly with the volume fraction of fibers and similarly, given $\bar{\tau}$ and V_f, $\bar{\sigma}_{cu}$ varies linearly with ℓ/ϕ. These theoretical trends are strikingly reflected in the experimental observations on series A, B, C using fibers of the same diameter with aspect ratios of 50, 75, and 100 (Figures 23, 25). Results of series D using a fiber diameter of 0.006 and an aspect ratio of 83.3, follow the linear trend but do not seem to fit between those of series B and C with aspect ratios of 75 and 100, as they should theoretically do. Looking back at Table 1 it can be noted that an important consequence of the difference in fiber diameter between series A, B, C, and series D is apparent in the average number of fiber intersections per square inch of composite. For a given V_f, this number is almost three times higher in series D than in series A, B, and C. Equivalently this also means that the average number of fibers pulling out from the fracture surface of a type D specimen is almost

three times higher than that associated with a type A, B, or C specimen. Having this observation in mind, it has been hypothesized that the difference between theoretically predicted and observed postcracking strengths may be a direct consequence of a decrease in the pull-out resistance per fiber when the density of fibers per square inch increases. This hypothesis is furthermore supported by observing that the composite fracture surfaces sustain a very high matrix deterioration which takes place at the base of the fibers (Fig. 27). One can almost correlate this deterioration to the crushed particles of the matrix that separate from the fracture surface by collecting and weighing these particles.

The theoretical mean values of postcracking link strength as given by equation 3.16, and the corresponding three link chain strengths are derived in Table 2, for series A, B, C, and D, assuming $\bar{\tau} = 380$ psi as in section 6.2. The chain strength values obtained are plotted in Figure 28 for series A, B, C versus fraction volume of fibers and compared to observed experimental results. Predicted results are consistently higher than observed ones, and the difference seems to increase with the volume fraction of fibers. If we attribute these differences, as hypothesized earlier, to a deterioration in the pull-out load or bond strength per fiber due to a high density of fibers, some useful empirical relation to the bond deterioration can be assessed. In Table 3 a $\Delta\tau$ decrease in bond

(a)

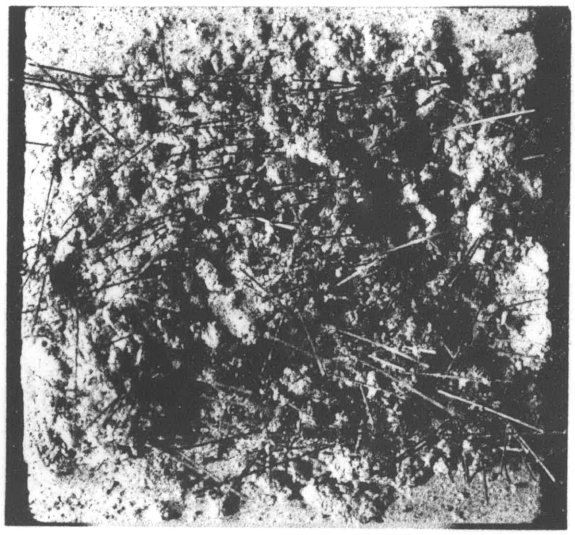

ϕ = 0.010" ℓ = 1" V_f = 3%

(b)

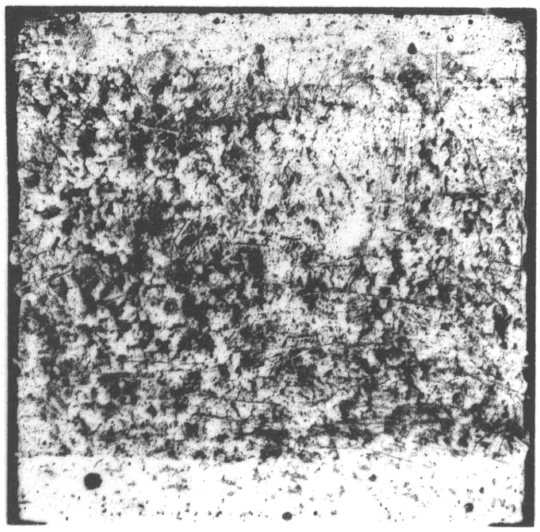

ϕ = 0.006" ℓ = 0.50" V_f = 2%

Fig. 27 Typical Fracture Surfaces of Fiber Reinforced Concrete Showing Matrix Disruption at the Base of the Fibers.

Specimen type	Fiber aspect ratio ℓ/ϕ	Volume fract. V_f %	Link - Theoret.		Chain(3 links) Theor.			Chain - observed	
			$E(\sigma_{cu})$ psi (a)	$SD(\sigma_{cu})$ psi (b)	$\sigma_{5\%}$ fract. psi (c)	$\sigma_{95\%}$ fract. psi (d)	$E(\sigma_{cu})$ psi (e)	$E(\sigma_{cu})$ psi	$SD(\sigma_{cu})$ psi
A1	50	1.	60.5	7.4	44.7	62.9	54.5	53.3	26.
A2		2.	121.	11.	97.6	124.6	112.	85.	57.
A3		3.	181.5	12.8	154.3	185.7	171.5	124.	52.
B1	75	1.	90.7	8.6	72.4	93.5	83.7	77.	49.
B2		2.	181.4	12.2	155.	185.4	171.4	130.	33.
B3		3.	272.2	15.	240.	277.2	260.	191.	63.
C1	100	1.	121.	15.	89.	126.	109.	100.	75.
C2		2.	242.	21.	197.	249.	225.	172.	75.
C3		3.	363.	26.	308.	371.6	342.	243.	82.
D1	83.3	1.	100.8	7.4	85.	103.2	95.	125.	63.
D2		2.	201.6	10.4	184.	203.2	196.	147.	61.
D3		3.	302.4	12.7	281.	306.	292.	184.	95.

(a) $E(\sigma_{cu})_{N=1} = \frac{1}{\pi} \bar{\tau} V_f \frac{\ell}{\phi}$. $\bar{\tau} = 380$ psi

(b) $SD(\sigma_{cu})_{N=1}$ as per equations 3.(15), 3.(12) and 3.(8) for A = 3 sq.inches.

(c) Corresponds to normalized variable $z = -2.13$, $z = \frac{\sigma - E(\sigma_{cu})_{N=1}}{SD(\sigma_{cu})_{N=1}}$ = Fig. 9 & 10

(d) Corresponds to normalized variable $z = 0.33$, " = Fig. 9 & 10

(e) Corresponds to normalized variable $z = -0.8$, " = Fig. 9 & 10

TABLE 2 Derivation of the Theoretical Chain Postcracking Strength

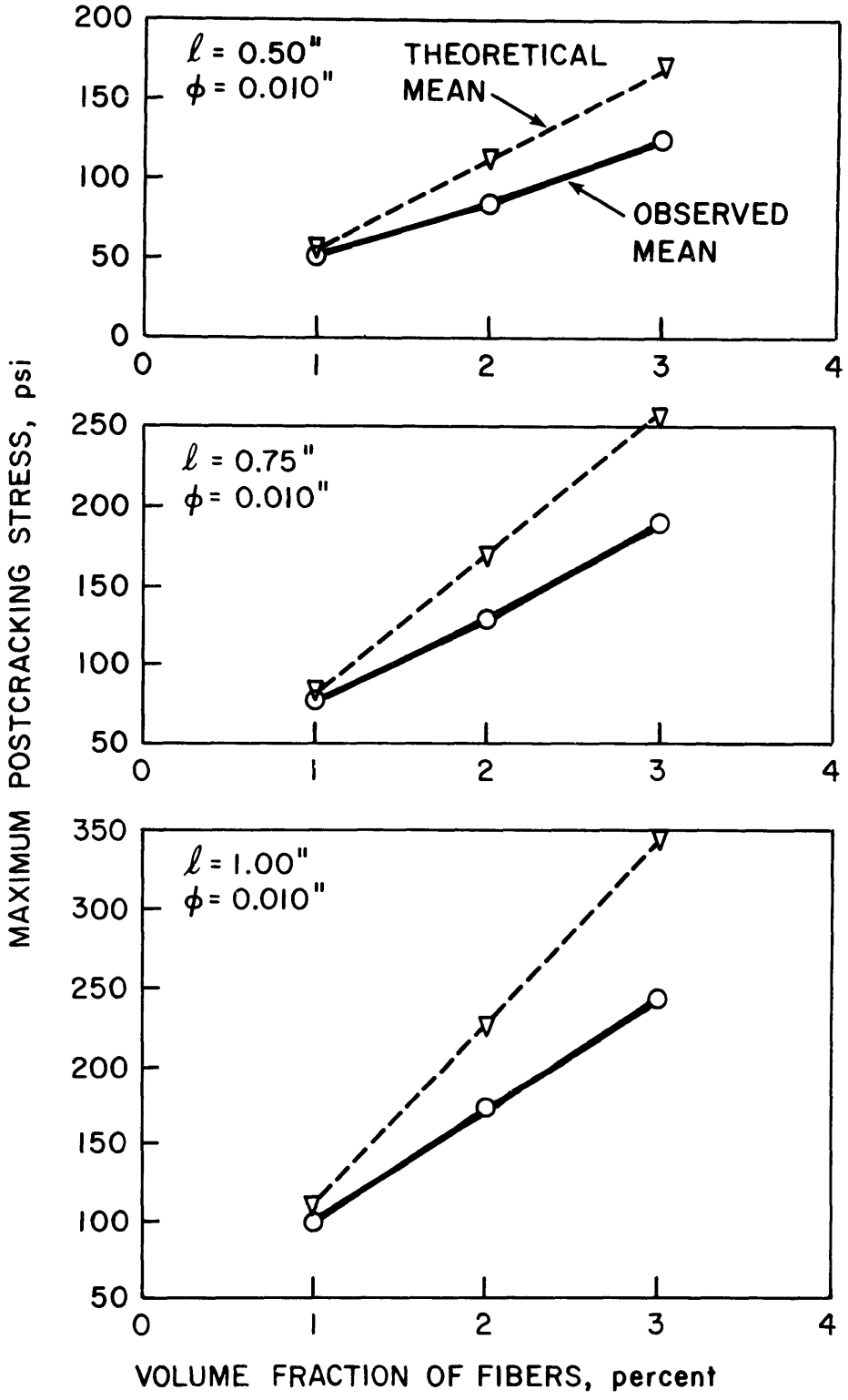

FIG. 28. COMPARISON OF PREDICTED AND OBSERVED POSTCRACKING STRENGTH.

Specimen Type	Theor. chain strength (a)	Observ. chain strength (b)	Differ. $\Delta\sigma$ (a)-(b) psi	* $\Delta\tau$ psi	Fiber density N_s /square inch	Suggested average relationship
A1	54.5	53.3	1.2	7.5	64	N_s $\Delta\tau$ 0 0 64 21 128 85 192 100
A2	112.	85.	27.	85.	128	
A3	171.5	124.	47.5	100.	192	
B1	83.7	77.	6.7	28.	64	$\bar{\tau}^* = \bar{\tau} - 0.52N_s \geq 0$
B2	171.4	130.	41.4	87.	128	
B3	260.	191.	69.	97.	192	$\bar{\tau}$ measured from pull-out test on one fiber
C1	109.	100.	9.	28.	64	
C2	225.	172.	53.	83.	128	
C3	342.	243.	99.	104.	192	
D1	95.	125.	-30.	-113.	64	Fitting line suggests that $\bar{\tau}$ for the 0.006 inch diameter fiber $\simeq$ 600 psi
D2	126.	147.	49.	92.	128	
D3	292.	184.	108.	135.	192	

* $\Delta\tau = \frac{\pi \Delta \sigma}{V_f \ell/\phi}$ from Equation 3.16

TABLE 3 Assessment of Empirical Relation between Bond Detioration and Density of Fibers N_s

strength has been caluculated from the $\Delta\sigma$ difference in strength observed between theoretical and experimental results. Also, a column is devoted to showing the average number of fiber intersections per square inch, N_s, for each specimen. It can be noticed that for series A, B, and C which use the same fiber diameter, the $\Delta\tau$ calculated decreases consistently when N_s increases. An average value of $\Delta\tau$ versus N_s for series A, B, C is then calculated.

The upper part of Figure 29 shows a plot of the actual bond strength $\overline{\tau}^* = \overline{\tau}_{N_s=1} - \Delta\tau = 380 - \Delta\tau$ to be associated with one fiber versus the density of fibers N_s per square inch, for the 0.01" fiber diameter used. The lower part of Figure 29 shows a similar relation derived from results on series D that uses a 0.006" fiber diameter. Both curves indicate a linear behavior.

In general the decrease in bond strength as a function of the density of fibers N_s is expected to depend on a number of parameters such as the flexibility of the fiber, its length and the local resistance of the matrix. Therefore some prior experimental observations must accompany any specific composite design. From the particular results of series A, B, C with the 0.01" fiber diameter used, the empirical relation that will predict the bond strength to be assessed versus the density of fibers per square inch

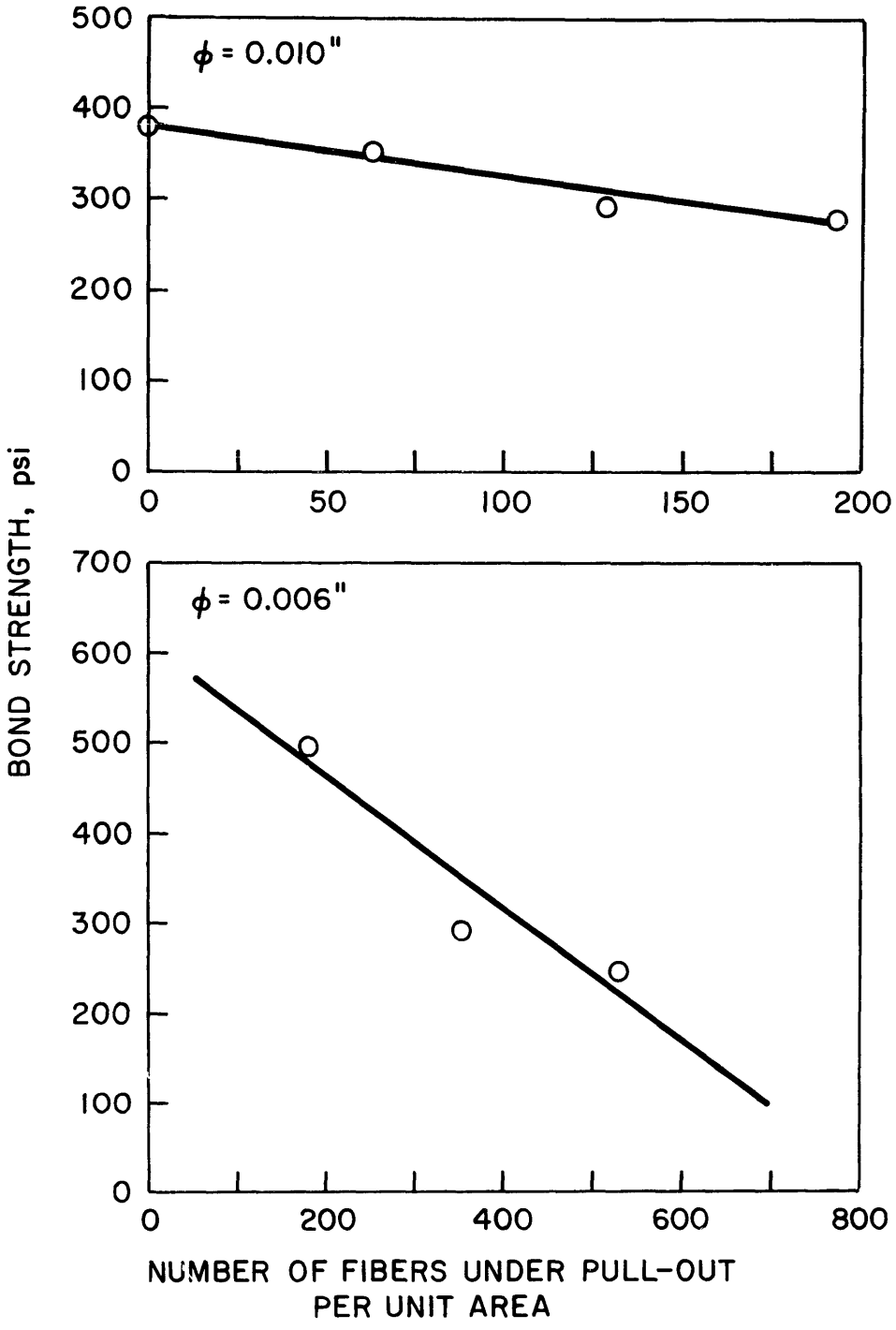

FIG. 29. BOND DETERIORATION WITH DENSITY OF FIBERS.

seems to be well approximated by

$$\bar{\tau}^* = \bar{\tau} - 0.52\ N_s$$

where $\bar{\tau}^*$ = modified bond strength to be used ≥ 0 psi

$\bar{\tau}$ = average measured bond strength from pull-out tests on one fiber psi

N_s = number of fiber intersections per square inch, $= 2V_f/\pi\phi^2$.

So far we have mainly discussed similarities and differences between experimental and theoretical mean values. A word on their respective spread seems to be necessary. In general the observed coefficient of variation defined as the ratio of the standard deviation to the mean value was, contrary to theoretical predictions, very high and of the order of 50%. Theoretical and observed spreads are shown schematically in Figure 30 for the results of series A experiments.. The drastic difference between them can only be explained by variations such as mixing, pouring or curing procedures and the inherent variability of strength encountered in Portland cement concrete matrices.

6.3.2 On the Cracking Strength.

The two formulas of interest derived in Chapter 3 concerned with predicting the composite cracking strength

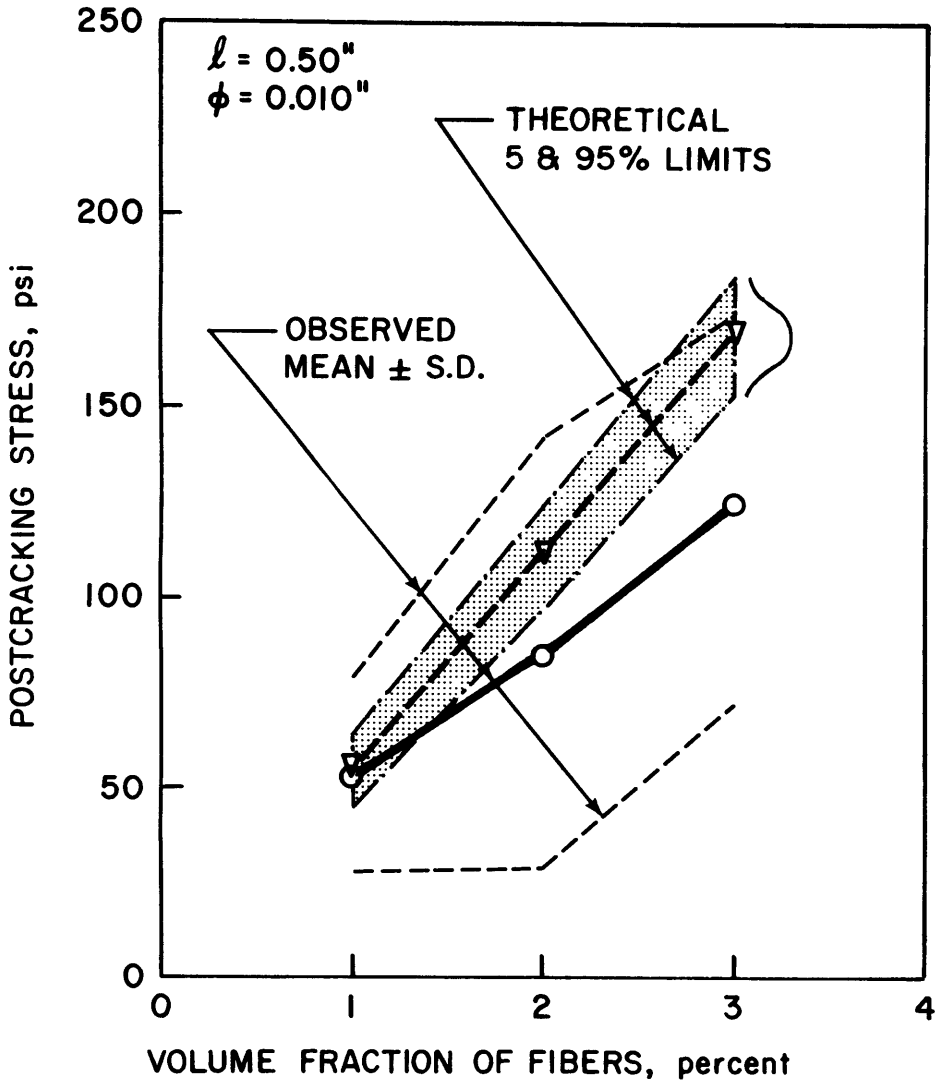

FIG. 30. POSTCRACKING STRENGTH WITH TYPICAL LIMITS OF THEORETICAL AND OBSERVED VARIATIONS.

are

$$3.(27) \qquad \bar{\sigma}_{cc} = \bar{\sigma}_{mu}(1-V_f) + \alpha\, \bar{\tau}\, V_f \frac{\ell}{\phi}$$

and/or

$$3.(29) \qquad \bar{\sigma}_{cc} = \bar{\sigma}^*_{mu}(1-V_f) + \alpha\, \bar{\tau}\, V_f \frac{\ell}{\phi} \,.$$

These relations are linear functions of $\bar{\tau}$, V_f or ℓ/ϕ, respectively. They are different in that 3.(27) does not take into consideration the modification of the ultimate tensile strain of the matrix due to the presence of the fibers while 3.(29) does. The second term of these equations represents the fiber contribution to the cracking strength. It has been suggested in 3.6 that the value of σ^*_{mu} and α be determined experimentally.

Referring back to Figures 22 and 24 where the average observed cracking strength for series A, B, C, D has been plotted versus volume fraction V_f and aspect ratio of fibers ℓ/ϕ, note that the linear trends predicted by the theory as to the influence of the fiber contribution are strikingly verified. Contrary to what was observed on the postcracking behavior, there is no apparent deterioration of strength due to an increase in the density of fibers per unit area or volume. Results of series D, using a fiber diameter of 0.006 inch and an aspect ratio of 83.3, fall well between those of series B and C using 0.010 inch fiber

diameter and aspect ratios of 75 and 100. Bond strength deterioration as a function of the number of fibers pulling out per unit cracked area (described in 6.3.1) seems to be characteristic of the state and conditions of pull-out. Apparently it is not felt in the precracking or elastic state.

Figure 22 shows the least square regression lines that have been fitted to the results from which the tensile strength of the non-reinforced mortar matrix have been excluded. The purpose was to find out from the intercepts of these lines the modified matrix strength as given in 3.(29). The equations of these lines are given below:

Series	ℓ/ϕ	Least Square Lines - Cracking Strength
A	50	$y = 240. + 2250.\ V_f$
B	75	$y = 259. + 3100.\ V_f$
D	83.3	$y = 273. + 3050.\ V_f$
C	100	$y = 283. + 3350.\ V_f$

and 3.(29) $\bar{\sigma}_{cc} = \bar{\sigma}^*_{mu}(1-V_f) + \alpha\, \bar{\tau}\, \frac{\ell}{\phi}\, V_f$

where $a = \alpha\, \bar{\tau}\, \frac{\ell}{\phi}$ = slope of lines.

Assuming that $(1-V_f) \simeq 1$ as V_f is in general less than 5% for steel fiber reinforced mortar, one can plot the increase in matrix tensile strength versus the aspect ratio of the fibers as extrapolated to $V_f = 0$, that is $\Delta\sigma_{mu} = \bar{\sigma}^*_{mu} - \bar{\sigma}_{mu}$. Figure 31 shows the results to be an

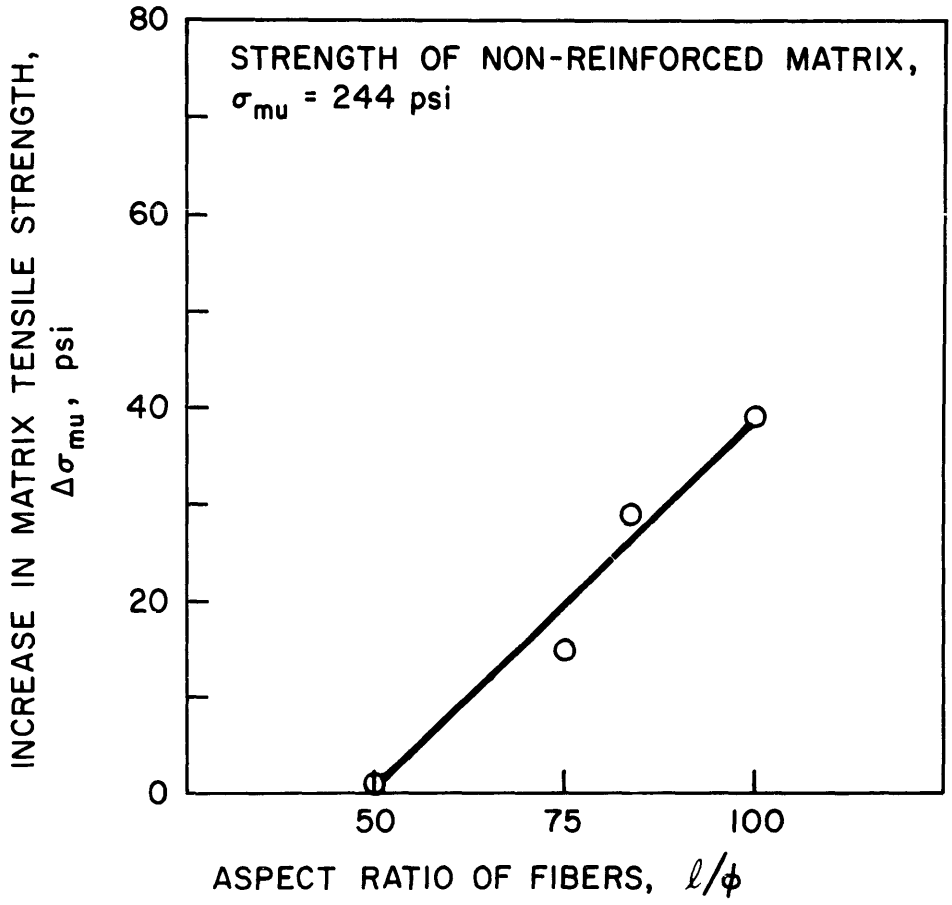

FIG. 31. APPARENT INCREASE IN MATRIX TENSILE STRENGTH DUE TO THE PRESENCE OF FIBERS, EXTRAPOLATED TO $V_f = 0$.

almost linear relation. For $\ell/\phi = 50$, $\Delta\sigma_{mu} \simeq 0$ such that apparently for $\ell/\phi \leq 50$ it can be stated that no significant improvement in matrix strength is incurred. Figure 31 also suggests that for very high aspect ratios of fiber reinforcement the modified matrix tensile strength or strain may show drastic increases.

In fact, it is difficult, in practice, to incur a wide range of variation in the reinforcing parameters V_f and ℓ/ϕ, without changing the matrix properties by addition of water in order to maintain workability. Furthermore, for current values of ℓ/ϕ of less than 100, the preceding results indicate that the apparent increase in matrix strength is less than 18% of the non-modified mortar matrix. These observations suggest that for practical purposes and within the limitations described, it may be more useful to use equation 3.(27) in which it is assumed that the tensile ultimate strain or strength of the matrix remain constant with the addition of fibers.

In Figure 32 cracking strength results for series A, B, C, D are plotted again and fitted by least square regression lines, including the matrix point. Equations of these lines are given as follows:

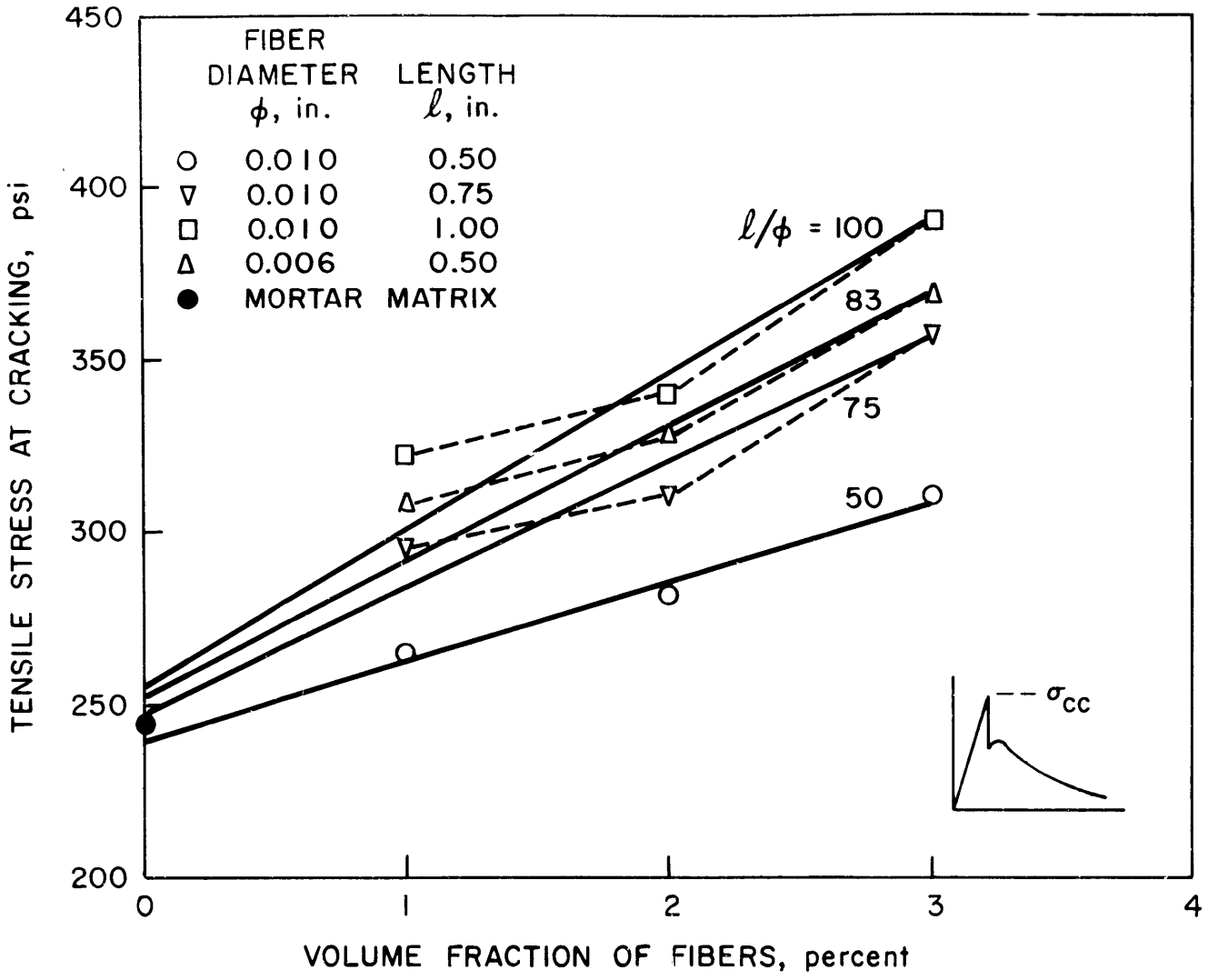

FIG. 32. TENSILE STRESS AT CRACKING - LEAST SQUARE FITTING LINES IF MORTAR MATRIX POINT IS INCLUDED.

Series	ℓ/ϕ	Least Square Lines - Cracking Strength
A	50	$y = 243. + 2150.\ V_f$
B	75	$y = 248. + 3550.\ V_f$
D	83.3	$y = 252.8 + 3930.\ V_f$
C	100	$y = 255.7 + 4520.\ V_f$

and 3.(27) $\bar{\sigma}_{cc} = \sigma_{mu}(1-V_f) + \alpha\ \bar{\tau}\ \frac{\ell}{\phi}\ V_f$

where $a = \alpha\ \bar{\tau}\ \frac{\ell}{\phi}$ = slope of lines.

Note that the slopes of these lines seem to increase linearly with ℓ/ϕ (Fig. 33) and another least square line has been used to represent the relation between them, that is

$$a = -28. + 46.3\ \frac{\ell}{\phi} \simeq 46.3\ \frac{\ell}{\phi}\ .$$

as in general $\ell/\phi \geq 40$.

Therefore, if we replace a by $46.3\ \ell/\phi$ we end up with

$$46.3\ \frac{\ell}{\phi} = \alpha\ \bar{\tau}\ \frac{\ell}{\phi} \Rightarrow \alpha = \frac{46.3}{380} \simeq 0.122.$$

Therefore, the empirical value of the coefficient α that best fits the results leads to the following relation:

$$\bar{\sigma}_{cc} = \bar{\sigma}_{mu}(1-V_f) + 0.122\ \bar{\tau}\ V_f\ \frac{\ell}{\phi}\ .$$

Note that in this formula the bond strength $\bar{\tau}$ is not modified by the density of fibers, and therefore $\bar{\tau}$ should

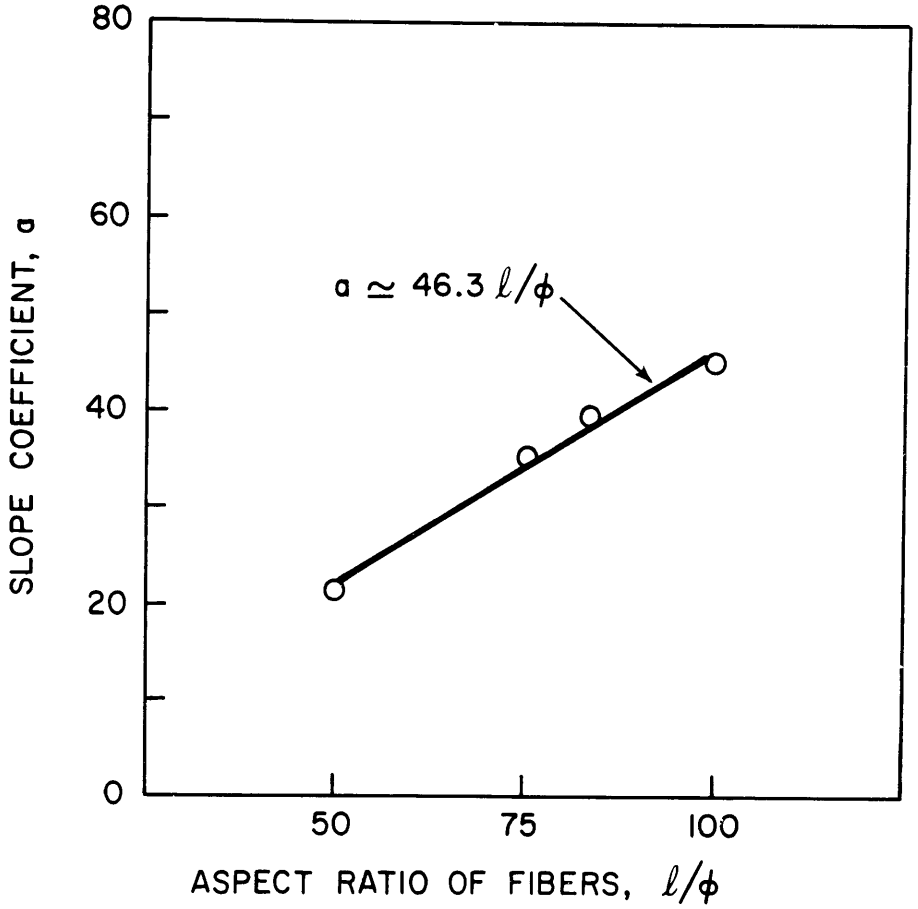

FIG. 33. LEAST SQUARE FITTING LINE OF SLOPE COEFFICIENTS vs. ASPECT RATIO OF FIBERS.

be used directly as observed from pull-out tests on single fibers.

6.3.3 On the Energy Absorbed at Failure.

It has been explained in 3.5 that the energy absorbed at failure of the composite is made out of two terms corresponding to the matrix and the fiber contribution. The fiber contribution consists of the work of friction of the fibers during the pull-out process. Therefore the relation between pull-out load and pull-out distance is of importance. This relation has been assumed to be linear in 3.5. On the other hand pull-out tests on fibers have suggested another type of relation. Both are plotted for the average random fiber as derived from the pull-out experiments in Figure 34. It can be seen that even though these relations are conceptually different, they lead to almost the same value of energy as the energy is measured by the area under the curve. Therefore, the value predicted by equation 3.(21) can be used for practical purposes to estimate the fiber contribution in the energy term, that is:

$$G_{ps} = \frac{1}{6\pi} \bar{\tau}^* V_f \frac{\ell^2}{\phi} = \bar{\sigma}_{cu} \frac{\ell}{\phi} .$$

Note that in this equation we have used the modified value

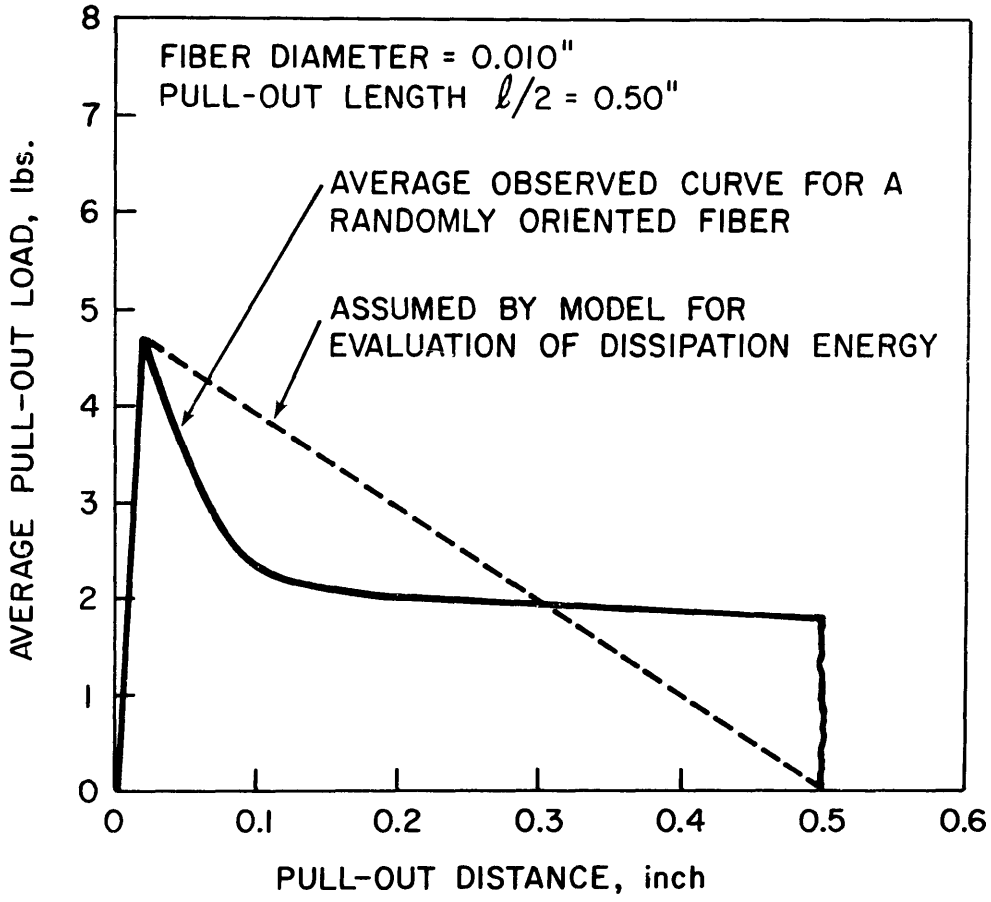

FIG. 34. AVERAGE OBSERVED AND ASSUMED PULL-OUT LOADS vs. DISTANCE.

of the bond strength $\bar{\tau}^*$ as influenced by the density of fibers under pull-out per unit cracked area.

6.4 Results on Double Cantilever Cleavage Beams.

The objective of these tests was to devise a method by which the fracture toughness of the material as well as the pseudo-plastic zone R as defined in this study, can be measured experimentally. This goal was successfully achieved using double cantilever cleavage type beams as described in Chapter 5.

A typical load displacement curve is shown in Figure 35. (Also reproduced in Figure C5 Appendix C, is the first part of the curve, amplified.) It can be seen that the test did not provide all the information that it usually does. The crack in the matrix extended all the way along the beam, that is 8 inches before complete pull-out of the fibers at the tip of the crack. For this particular specimen, the corresponding opening at the crack tip was approximately .1 inch. By extrapolation one can say that for an opening of 0.25 inch, corresponding to a complete pull-out, the crack will travel approximately 20 inches. This result suggests that the pseudo-plastic zone extension R is of the order of 20 inches and that beam lengths of at least twenty inches shall be used in future investigations using a-half-inch long fibers. One

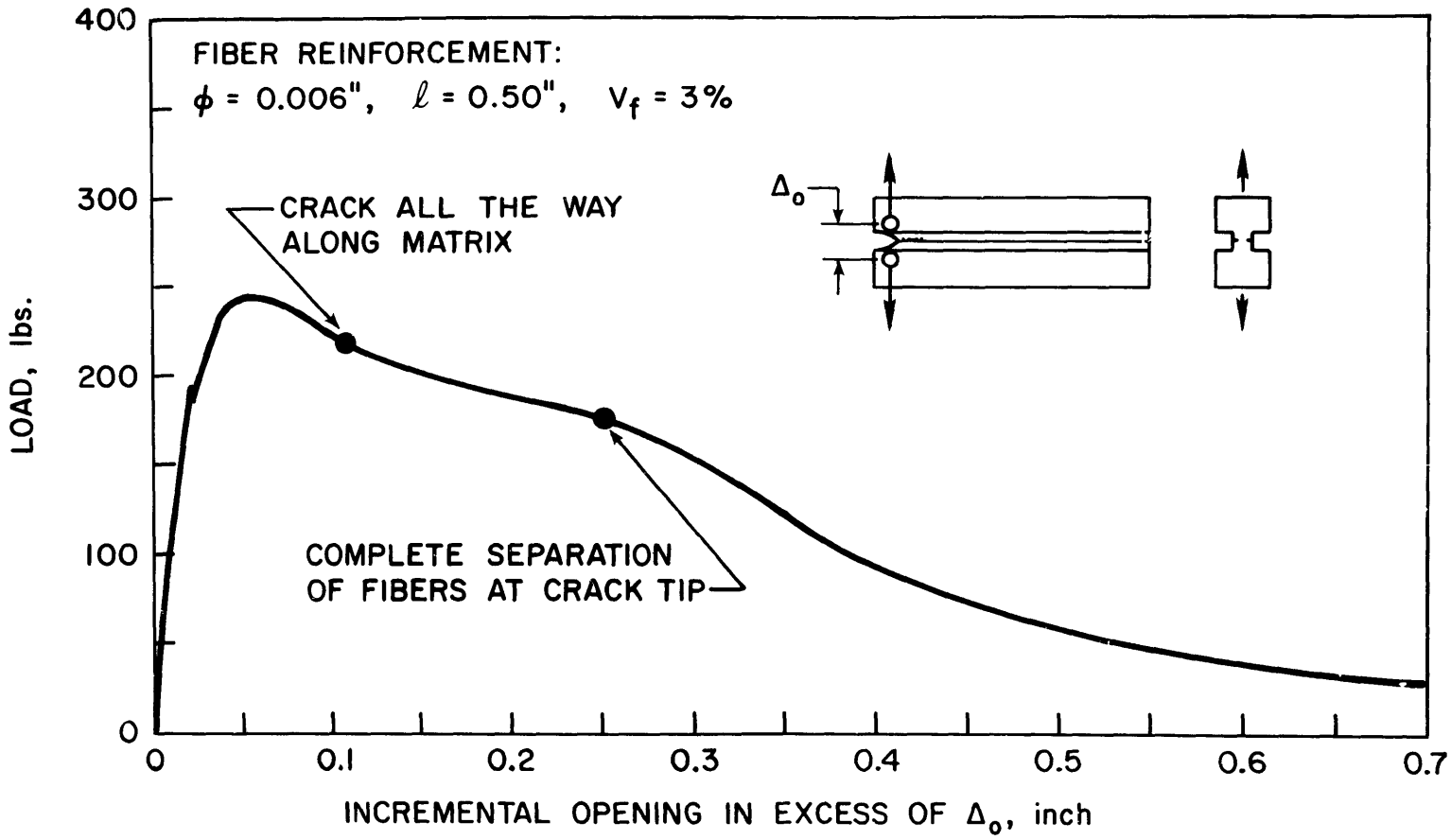

FIG. 35. TYPICAL LOAD-DISPLACEMENT CURVE OF CLEAVAGE SPECIMEN UP TO COMPLETE SEPARATION.

can argue that fracture properties K_{Ic} or γ can be assessed using notched tensile specimens similar to the tensile tests used in this study. However, the determination of R is not possible by the tensile test method. Moreover, one cleavage specimen provides as much information as several tensile specimens combined and is therefore more efficient [67,96].

For fiber reinforced cementitious materials, such as asbestos cements, full testing efficiency can be achieved using the double cantilever beam method as the pseudo-plastic zone radius R is expected to be small. In conventional steel fiber reinforced concrete the method will be useful only if the size of the member is important enough. For in-between cases the equations predicting the strength in Chapter 3 can be used as a close upper bound estimation to the composite strength. Note however that an advantage of the cleavage test is that by determining the average surface energy $\overline{\gamma}$, it automatically takes into consideration parameters such as bond strength, bond deterioration, fiber orientation, volume fraction, aspect ratio and so on, as discussed in 6.3.

6.5 Recapitulation of Major Results as per Chapters 3 and 6.

The average value of the composite postcracking strength, assuming one link, can be predicted as follows:

$$\bar{\sigma}_{cu} = \frac{1}{\pi} \bar{\tau}^* V_f \frac{\ell}{\phi} \qquad \text{psi}$$

where V_f = volume fraction of fibers

ℓ/ϕ = aspect ratio of fibers

$\bar{\tau}^*$ = modified bond strength as a function of the average number of fibers pulling out per unit cracked area psi

Example: $\bar{\tau}^* = \bar{\tau} - 0.52\ N_s$

$\bar{\tau}$ = average bond strength as derived from pull-out tests on single fibers psi

The mean cracking strength of the composite can be predicted by

$$\bar{\sigma}_{cc} = \bar{\sigma}_{mu}(1-V_f) + 0.122\ \bar{\tau}\ V_f \frac{\ell}{\phi} \qquad \text{psi}$$

where $\bar{\sigma}_{mu}$ is the average tensile strength of the matrix psi.

The average surface energy of the composite can be assessed by

$$\bar{\gamma}_c = \tfrac{1}{2}[\bar{\gamma}_{mu} + \frac{1}{6\pi} \bar{\tau}^* V_f \frac{\ell^2}{\phi}] = \tfrac{1}{2}[\bar{\gamma}_{mu} + \bar{\sigma}_{cu} \frac{\ell}{6}]$$

where $\bar{\gamma}_{mu}$ = matrix surface energy pound/inch.

CHAPTER 7

CONCLUSIONS

7.1 Conclusions.

The conclusions can be conveniently categorized into two groups, the first dealing with the advantages and validity of the proposed analytical model, the second dealing with the results of the experimental program and their correlation with the model's predicted values.

The following features characterize the mathematical model developed to simulate the response of fiber reinforced concrete under tensile loading.

1. The model provides a full understanding of the composite behavior under loading by identifying the relevant variables and parameters involved.
2. It takes into consideration the statistical nature of these variables.
3. It distinguishes between ductile and brittle fractures which are observed in real fiber reinforced cementitious materials, and solves each case using relevant criteria of composite materials and fracture mechanics studies.
4. For the ductile type failure, it identifies the pre-cracking and the postcracking states and in each case points out the influencing parameters on observed strength.

5. For the brittle type failure it introduces a new concept related to the statistical distribution of inherent weak areas (i.e. areas without fibers) in a discontinuous fiber reinforced composite, and discusses the potential effect of these areas on the composite strength.
6. After assessing the characteristic strength of the material it accounts for size effects by introducing the weakest link concept in the analytical formulation.
7. The analytical formulation is flexible enough to allow possible modifications in the distribution functions of major variables.
8. It finally provides reasonably realistic and simple expressions predicting mean strengths and toughness of the composite as a function of the characteristics of the components.
9. By providing the full distribution functions of the predicted design properties it allows for a better understanding of statistical variations observed in experimental results.

The experimental program features per se a number of tests that are relatively new in the area of fiber reinforced concrete: these are, for example, pull-out tests on symmetrically oriented fibers, pure tensile tests on notched prisms simulating a chain member, and the double

cantilever beam or cleavage tests. On the basis of the experimental results the following conclusions are drawn:

a) It can be assumed with reasonable confidence that the random distribution of the fibers in the concrete mass is described by a Poisson process.

b) The bond or shear strength observed at the fiber matrix interface in fiber reinforced concrete shows a large variation and therefore cannot be considered as a constant.

c) The pull-out load of a fiber oriented at an angle θ is not necessarily smaller than that of an aligned fiber. The effect of an additional term associated with a pseudo "pulley" action under load and with the fiber flexibility suggests that a randomly oriented fiber may be as or more efficient than an aligned one.

d) There is strong evidence that the bond strength which is measured from a pull-out test on one fiber decreases if the density of fibers increases. As a first approximation, the relation describing this behavior is linear. It is therefore recommended to take into account in the design the so modified value of the bond strength.

e) Cleavage type specimens can be used to measure some fracture properties of fiber reinforced concrete and mainly estimate the size of a pseudo plastic zone

corresponding to an area where the matrix is cracked, the fibers are pulling out and the crack tip opening is equal to half the fiber length.

f) For a fiber of 0.5 inch length the observed pseudo plastic zone radius in fiber reinforced concrete is found to be of the order of 20 inches. This suggests that, unless shorter fibers are used, the solution simulating brittle type failure applies only to rather large size structures.

g) Experimental results indicate, in close correlation with the model's predictions, that the cracking and the postcracking strength of fiber reinforced concrete increase linearly with the volume fraction and aspect ratio of the fibers.

h) Trends predicted by the model have been in general observed in the experimental results. Even when discrepancies exist, the model is flexible enough to allow a feedback process, a refinement of the assumptions and an adaptation of major relations to simulate more closely the experimental observations.

i) The overall solutions proposed to simulate the brittle or ductile failure seem to provide rather realistic bounds on strength predictions that can be beneficially used for design purposes.

7.2 Recommendations.

The field of fiber reinforced cementitious materials is still in its initial stage of investigation, therefore, recommendations in this section will be restricted to only those topics which have become evident during the course of this particular study.

1. The variation of the bond strength versus the fiber orientation should be investigated for a full range of values covering variations of fiber diameters and lengths as well as matrix properties.
2. The deterioration of bond strength per fiber due to an increase in the density of fibers pulling out from a unit area must be characterized in order to take full advantage of the model's predictions on strength and toughness.
3. The results presented in Chapter 4 of this study must be substantiated by further testings, particularly with larger test specimens or shorter fibers.
4. The use of double cantilever type beams to characterize the fracture properties of concrete and fiber reinforced concrete presents some promising capabilities and should be widely investigated in future experiments.
5. It may be of interest to extend the formulation of Chapter 4 to the case where the plastic zone size R and the fracture toughness K_{Ic} are considered as

random variables with distributions that can be determined experimentally.

6. The chain weakest link model of a tensile member should be validated on fiber reinforced concrete specimens by testing tensile members of different length, i.e. having various number of links.
7. The analytical representation of the proposed model is supposed to simulate the behavior of fiber reinforced cementitious and ceramics matrices. It should be extended to fiber reinforced polymeric matrices that show in general ductile properties.
8. The model developed in this study assumes that a constant stress is applied on the composite. Extending it to the case where stresses are stochastic in the time domain will lead to a realistic assessment of the reliability of a given structure.

BIBLIOGRAPHY

1. Abolitz, A.L., Agbim, C.C., Untrauer, R.E., Works, R.E., "Discussion of paper on tensile strength of concrete affected by uniformly distributed and closely spaced short length of wire reinforcement," American Concrete Institute Journal, Dec. 1964.

2. American Society of Metals, "Fiber composite materials," 1965.

3. Amirbayat, J., Hearle, J.W.S., "Properties of unit composites as determined by the properties of the interface," Parts I, II and III, Fiber Science & Technology, vol. 2, July 1969.

4. Argon, A., "Fracture of composites," to appear in Treatise on Materials Science, vol. 1, Academic Press.

5. Ashton, Halpin, Petit, Primer on Composite Materials Analysis, Stamford Conn., Technomic Publ. Co., 1969.

6. ASTM STP 381, Fracture Toughness Testing and Its Application, 1965.

7. ASTM STP 410, Plane Strain Crack Toughness Testing of High Strength Metallic Materials, 1966.

8. ASTM STP 438, Metal Matrix Composites, 1967.

9. ASTM STP 542, Interfaces in Composites, 1968.

10. ASTM STP 460, Composite Materials: Testing and Design, 1969.

11. ASTM STP 463. Review of Developments in Plane Strain Fracture Toughness, Ed. W.F. Brown, Jr., 1970.

12. Ball, Claire, G., "The fatigue behavior of steel-fiber-reinforced concrete," M.S. Thesis, October 1967, Clarkson College of Technology, Civil Engineering Department.

13. Berard, A., "Artificial Stone," U.S. Patent no. 157 903, December 15, 1874.

14. Benjamin, J.R., Cornell, A.C., Probability Statistics and Decision for Civil Engineers, McGraw-Hill, 1970.

15. Biryu kovitch, K.L. et al., "Steklotsement," transl. by Civil Engineering Research Association, London, 1964 CERA Translation no. 12.

16. Bowen, D.H., "Fiber reinforced ceramics," Fiber Science and Technology, vol. 1, 1968.

17. Brooks, A.E., Newman, K., editors, The Structure of Concrete and its Behavior under Load, Proceedings of an International Conference, London, 1965, Cement and Concrete Association.

18. Broutman and Krock, Modern Composite Materials, Addison-Wesley, Reading, MA., 1967.

19. Coleman, B.D., "Statistics and time dependence of mechanical breakdown in fibers," J. of Appl. Physics, vol. 29 no. 6, 1958.

20. "Concrete Year 2000," Report of ACI Ad Hoc Board Committee on Concrete, ACI Journal, August 1971.

21. Cornell, A.C., "Stochastic process models in structural engineering," Technical Report no. 34, Department of Civil Engineering, Stanford University, May, 1964.

22. Corte, H., Kallmes, O.J., "Statistical geometry of a fibrous network," in Formation and Structure of Paper, ed. by F. Bolam, Transactions of the Oxford Symposium, 1961.

23. Cox, F.B., Gemayer, H.G., "Expedients reinforcement for concrete for use in Southeast Asia," Report no. 1 Preliminary Tests of Bamboo, U.S. Army Engineer Waterways Experiment Station, TR C-69-3, February 1969.

24. Cox, H.L., British Journal of Applied Physics, vol. 3 no. 72.

25. Cratchley, D., "Experimental aspects of fiber reinforced metals," Metallurgical Review, vol. 10, no. 37, 1965.

26. Crow, E., Davies, F.A., Maxfield, M.W., Statistics Manual, Dover Publications, Inc., New York, 1960.

27. Daniels, H.E., "The statistical theory of the strength of bundles of threads," Proceedings of the Royal Society, London, 1945, 183A495.

28. Dehoff, R.T., Rhines, F.M., Quantitative Miscroscopy, McGraw-Hill Book Co., 1968.

29. Deltheil, R., Probabilités géometriques, Gautier-Villars, Paris, 1926.

30. Dow, N.F., G.E.C. Missile and Space Division Report no. R63SD61,

31. Drake, A., Fundamentals of Applied Probability Theory, McGraw-Hill, New York, 1967.

32. Edgington, J., Hannant, D.J., "Steel fiber reinforced concrete: the effect on fiber orientation of compaction by vibration," Matériaux et Constructions, vol. 5 no. 25, 1972.

33. Epstein, B., "Application of the theory of extreme values in fracture problems," J. of the Amer. Stat. Assoc., vol. 42, 1948, pp.403-412.

34. Epstein, B., "Statistical aspects of fracture problems," J. of Appl. Physics, vol. 19, 1948, pp.140-147.

35. Fishburn, C.C., "Physical properties of some samples of asbestos-cement siding," Building Materials and Structures Report 122, U.S. Dept. of Commerce, July, 1951.

36. Glucklich, J., "Fracture of plain concrete," J. of the Eng. Mechanics Div., ASCE, vol. 89 no. EM6, 1963.

37. Goldfein, S., "Fibrous reinforcement for Portland cement," J. of Modern Pastics, April 1965.

38. Goudsmit, S., "Random distribution of lines in a plane," Review of Modern Physics, no. 17 pp. 321-323.

39. Gray, B.H., "Fiber reinforced concrete, a general discussion of field problems and applications," M-1 Construction Engineering Research Lab., Champaign, Illinois, April 1972.

40. Gray, B.H., Rice, J.L., "Fibrous concrete for pavement applications," Report M13, CERL, Champaign, Ill., April 1972.

41. Griffith, A.A., "The phenomena of rupture and flow in solids," Philosophical Transactions, Royal Society, London, Series A, vol. 221, 1920.

42. Grimer, F.J., Ali, M.A., "The strength of cements reinforced with glass fibers," Magazine of Concrete Research, March 1969.

43. Gumbel, E.J., Statistics of Extremes, Columbia University Press, New York, 1958.

44. Hammersly, J.M., Hanscombe, D.C., Monte Carlo Methods in Applied Probability and Statistics, Methuen, London, 1965.

45. Haynes, J., "Investigation of fiber reinforcement methods for thin shell structures," U.S. Naval Civil Engineering Lab., Ocian Eng. Div., Port Hueneme, California.

46. Hoagland, R.G., "On the use of double cantilever beam specimens for determining the plane strain fracture toughness of metals," ASME J. of Basic Engineering, September 1967.

47. Holister & Thomas, Fiber Reinforced Materials, Elsevier Publ. Co., London, 1966.

48. Holliday, L., Composite Materials, Elsevier Publ. Co., London, 1966.

49. Howard, W.J., "Chain reliability, a simple failure model for complex mechanisms," The Rand Corporation, R.M. 1058, March 1953.

50. Hsu, T.T.C. et al., "Microcracking of plain concrete and shape of the stress strain curve," J. of the ACI, 1963.

51. Kabaila, A.P., Warner, R.F., "Monte Carlo simulation of variable material response," Proc. of the Southampton 1969 Civil Eng. Materials Conf., Wiley, Interscience, 1971.

52. Kallmes & Corte," The statistical geometry of an ideal two dimensional fiber network," Technical Assoc. of the Pulp & Paper Industry (TAPPI), vol. 43 p.737, errata vol. 44 p.448.

53. Kallmes & Corte, "The structure of paper II: the statistical geometry of a multiplanar fiber network," TAPPI, no. 44, p.519.

54. Kaplan, M.F., "Strains and Stresses of concrete at initiation of cracking near failure," J. of the ACI, July 1963.

55. Kelly, A. & Davies, G.J., "The principles of the fiber reinforcement of metals," Metallurgical Review, vol. 10 no. 37, 1965.

56. Kelly, A., Strong Solids, Clarendon Press, Oxford, 1966.

57. Kelly, A., "Interface effects and the work of fracture of a fibrous composite," Proc. Royal Soc. London, Oct. 1970.

58. Kelly A., "Reinforcement of structural materials by long strong fibers, ASM Symposium, Boston, May 1972.

59. Kendall, M.G., Moran, P.A., Geometrical Probability, C. Griffin & Co., London, 1964.

60. Krenchell, H., Fiber Reinforcement, Akademisk Forlag, Copenhagen, Denmark, Engl. translation, 1964.

61. Liebowitz, H., Fracture, An Advanced Treatise, vol. 2 Academic Press, New York, 1968.

62. Lowry, G.G., Markov Chains and Monte Carlo Calculations in Polymer Science, Marcel Dekker Inc., New York, 1970.

63. Mack, C., "The expected number of clumps formed when convex areas or bodies are placed at random in two or three dimensions," Proc. Cambridge Philosophical Soc., vol. 50, 1954.

64. Majumdar, A.J., "Determining bond strength in fiber reinforced composites," Magazine of Concrete Research, vol. 20, Dec. 1968.

65. Majumdar, A.J. & Ryder, J.F., "Glass fiber reinforcement of cement products," Glass Technology, vol. 9-78, 1968.

66. Mandell. J.F., "Fracture toughness of fiber reinforced plastics, M.I.T. Ph.D. Thesis, 1971.

67. McGarry, F.J., Course Notes on Composite Materials and Strength of Structural Materials, M.I.T., Civil Engineering Department.

68. Moavenzadeh, F., Kuguel, R., "Fracture of concrete," J. of Materials, vol. 4 no. 3, 1969.

69. Monfore, G.E., "A review of fiber reinforcement of Portland cement paste, mortar, and concrete," J. of the Portland Cement Association, September 1968.

70. Naaman, A.E., "Reinforcing mechanisms in ferro-cement," M.S. Thesis, M.I.T. Civil Eng. Dept., September 1970.

71. Naaman, A.E., McGarry, F.J., Sultan, J., "Developments in fiber reinforcement for concrete," M.I.T. Civil Eng. Dept. Report R72-28, May 1972.

72. Olster, E.F., Jones, R.C., "Toughening mechanisms in fiber reinforced metal matrix composites," Civil Eng. Dept. M.I.T. R70-75, November 1970.

73. Orowan E., "Energy criteria of fracture," The Welding Journal Research Supplement, March 1955.

74. Orowan, E., "Experiments of brittle fracture of steel plates," The Welding Journal Research Supplement, November 1955.

75. Peirce, F.T., "Tensile tests for cotton yarns, V: the weakest link," J. of Textile Institute Transactions, vol. 17 p.355, 1926.

76. Pellini, W.S., "Evolution of engineering principles for fracture-safe design of steel structures, Naval Research Laboratory Report NRL 6957, September 1969.

77. Proceedings of the Royal Society, Discussion of Strong Fibrous Solids, London, October 1970.

78. Rauch, Sutton, McCreight, Refractory Materials, a series of monographs, vol. 3: Ceramic Fibers and Fibrous Composite Materials, Academic Press, New York, 1968.

79. Riley, V.R., "Fiber/Fiber Interaction," J. of Composite Materials, vol. 2 no. 4, October 1968 p.436.

80. Roberts, Norman H., Mathematical Methods in Reliability Engineering, McGraw-Hill, New York, 1964.

81. Romualdi, J.P., and Batson, G.P., "Behavior of reinforced concrete beams with closely spaced reinforcement," J. of the ACI, June 1963.

82. Romualdi, J.P., and Mandel, J.A., "Tensile strength of concrete affected by uniformly distributed closely apaced short length of wire reinforcement," J. of the ACI, June 1964.

83. Romualdi, J.P., Ramey, M., Sanday, S.C., "Prevention and control of cracking by use of short random fibers," Paper no. 10, Sp. Publ. no. 20, ACI, 1968.

84. Romualdi, J.P., "Two phase concrete and steel materials, U.S. Patent no. 3, 439,094, February 25, 1969.

85. Rosen, B.W., "Tensile failure of fibrous composites," AIAA J., vol. 2 no. 11, November 1964.

86. Rosen, B.W., "Thermomechanical properties of fibrous composites," Proc. of the Royal Society, October, 1970.

87. Rosen, B.W., Dow, B.F., Hashin, Z., "Mechanical properties of fibrous composites," NASA Report CR 31, April 1964.

88. Rothwell, A., "Optimum fiber orientation for the buckling of thin plate of composite material," Fiber Science & Technology, vol. 2, 1969.

89. Saibel, E., Size Effect in Fracture: Structure Solids Mechanics and Engineering Design, Proc. of the Southampton 1969 Civil Eng. Materials Conference, ed. by M. Te'eni, Wiley Interscience, 1971.

90. Sanchez, R., "Building materials in developing countries," M.S. Thesis, M.I.T. Dept. of Civil Eng., June 1972.

91. Scop, P., Argon, A.S., "Statistical theory of strength of laminated composites," J. of Composite Materials, vol. 1, 1967, p.92.

92. Shah, S.P., and Rangan, R.V., "Some micromechanical properties of fiber reinforced concrete," M.I.T. Research Report R69-72, December 1969, Dept. of Civil Engineering, Materials Division.

93. Shah, S.P., Rangan, B.V., McKee, C., Romualdi, J.P., Sinno, R.R., "Discussion of a paper on fiber reinforced concrete properties," J. of the ACI, August 1971.

94. Sneddon, I.N., "The distribution of stress in the neighborhood of a crack in an elastic solid," Proc. of the Royal Soc. of London, vol. A-187, 1946.

95. Snyder, M.J. Lankard, D.R., "Factors affecting the flexural strength of steel fibrous concrete," J. of the ACI, February 1972.

96. Sultan, J.N., McGarry, J.F., "Microstructural characteristics of toughened thermoset polymers," M.I.T. Civil Eng. Dept. Report R69-59, October 1969.

97. Sundara, K.T., Viswanatha, C.S., "Discussion of the paper by Wai-Fah Chen and J.L. Carson, 'Stress-strain properties of random wire reinforced concrete'," J. of the ACI, June 1972, p.346.

98. Tetelman, A.S., Fracture Processes in Fiber Composite Materials, ASTM STP 460, 1969.

99. Tetelman, A.S., McEvily, A.J., Fracture of Structural Materials, J. Wiley & Sons, New York, 1967.

100. Warner, R.F., Kabaila, A.P., "Monte Carlo study of structural safety," J. of the Structural Division, ASCE 94, no. ST12, 1968.

101. Weibull, W., "A statistical distribution function of wide applicability," J. of Appl. Mechanics, vol. 18, 1953.

102. Weibull, W., Ing. Vetenskaps Akad. Handl. no. 151, 1939.

103. Williamson, G.R., "Response of fibrous reinforced concrete to explosive loading," Tech. Report no. 2-40, May 1965, U.S. Army Engineer Division, Ohio River.

104. Williamson, G.R., "Response of fibrous reinforced concrete to explosive loading," Technical Report no. 2-48, January 1966, U.S. Army Engineer Division, Ohio River.

105. Zweben, C., Tensile Strength of Fiber Composites: Basic Concepts and New Developments, ASTM STP 460, 1969.

106. RILEM, Proceedings of the Symposium on Bond and Crack Formation in Reinforced Concrete, Stockholm, 1957.

BIOGRAPHY - Antoine E. Naaman

Personal: Born July 19, 1940 in Beirut Lebanon
Parents Clotilde and Elie Naaman
Married to Ingrid Schneider of Berlin, Germany
One son, Patrice.

Education: French and Lebanese Baccalaureates, with major in Science, Notre Dame College, Beirut, Lebanon, 1959.

Diplomed Engineer, Ecole Centrale des Arts et Manufactures, Paris, France, June 1964.

Specialist in Reinforced and Prestressed Concrete, Centre des Hautes Etudes de la Construction, Paris, France, June 1965.

M.S., Massachusetts Institute of Technology, September 1970.

Ph.D., Massachusetts Institute of Technology, August 1972.

During his graduate studies at M.I.T. the author was research assistant, Division of Sponsored Research, from 1969 to 1970 and a full-time teaching assistant in the Department of Civil Engineering from 1970 to 1972.

Professional Experience:

In 1965 the author joined the Executive Council for Large Projects in Beirut, Lebanon, where he held the position of field engineer and was responsible for the supervision of a highway construction segment and related bridges in reinforced concrete. Late in 1966 he worked for Potenco Inc., Montreal, Canada supervising and coordinating prestressed concrete operations for Habitat 67, at the Montreal World Exhibition. During the second quarter of 1967 he joined Lalonde, Valois & Associates, Consulting Engineers, Montreal, Canada, where he worked mainly as a structural and computer-oriented engineer on large projects involving design of highway bridges, interchanges and tunnels in reinforced and prestressed concrete. Before entering M.I.T. in 1969 he was a Registered Professional Engineer in Lebanon and Quebec,

BIOGRAPHY - continued

Canada. He is currently a member of the Sigma Xi Society, the American Concrete Institute, the Prestressed Concrete Institute and the American Society of Civil Engineers.

Publications:

(with S. P. Shah) "Tensile Tests of Ferro-Cement," Journal of the American Concrete Institute, September 1971.

"Computer Program for Selection and Design of Simple Span Prestressed Concrete Highway Bridges," Journal of the Prestressed Concrete Institute, Vol. 17, no. 1, Jan.-Febr. 1972.

(with F. McGarry and J. Sultan) "Developments in Fiber-Reinforcement for Concrete," Civil Eng. Dept. M.I.T. Report no. R72-28, May 1972.

APPENDIX A

A.1 The Weakest Link Concept and Weibull's Approach.

A.2 Mathematical Basis to the Distribution of Fibers in the Concrete Mass Following a Poisson Process.

A.3 The χ^2 Goodness-of-Fit Test Used to Validate the Assumption on the Poisson Distribution of Fibers.

A.4 On the Cracking Strength of Fiber Reinforced Concrete.

A.1 The Weakest Link Concept and Weibull's Approach.

The weakest link theory is an extreme value theory in statistics. It assumes that a system (in our study a tensile member) is made like a chain of a series of consecutive links. The strength of each link is characterized by a statistical distribution function and it is assumed that the chain will break when the weakest link breaks.

Let us consider a population described by a probability density function $f(x)$ and its cumulative function:

$$F(x) = \text{Prob}(X \leq x) = \int_{-\infty}^{x} f(x)dx \ .$$

Similarly: $\text{Prob}(X \geq x) = 1. - F(x)$.

Let us assume that we take a sample of size n drawn independently and at random from this population, say $(x_1, x_2, \ldots, x_n)$. Let us now define y_n as the smallest value of x in the sample. We have thus generated a new population y_n, the distribution of which is found as follows:

$$\begin{aligned} \text{Prob}(y_n > y) &= \text{Prob}(\text{All } x > y) \\ &= \text{Prob}(x_1 > y,\ x_2 > y, \ldots, x_n > y) \\ &= [1. - F(y)]^n \ . \end{aligned}$$

Then we define the cumulative function of y as given by

$$G_n(y) = \text{Prob}(y_n \leq y) = 1. - [1. - F(y)]^n$$

and the probability distribution function of y is obtained by differentiation:

$$g_n(y) = G_n'(y) = n\, f(y)\, [1. - F(y)]^{n-1}.$$

We have thus generated the probability distribution and cumulative functions of the chain variable of interst, knowing those of the link and the number of links. In our case, the variable of interest is the strength of the tensile member under consideration, say σ.

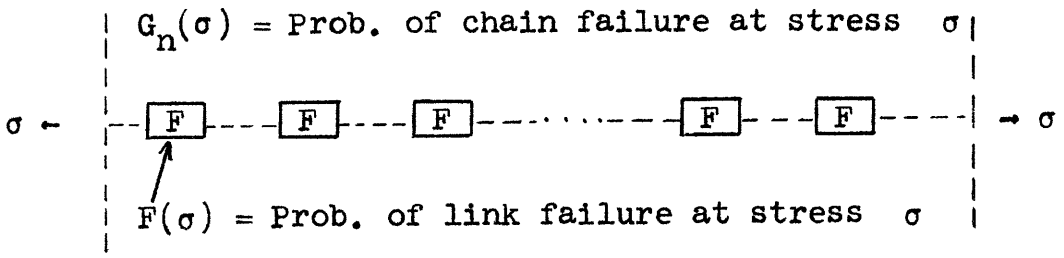

Weibull derived the probability distribution function of the material strength considering the following point of view.

Assuming $\text{Prob}(\Sigma \leq \sigma) = F(\sigma)$

Weibull chooses to express the function $F(\sigma)$ as

$$F(\sigma) = 1 - e^{-\Phi(\sigma)}\ .$$

Therefore

$$[1 - F(\sigma)]^n = e^{-n\Phi(\sigma)} = e^{-n \log(1 - F(\sigma))} .$$

The chain cumulative function becomes

$$G_n = 1 - e^{-n\Phi(\sigma)} .$$

Weibull defined $-n\Phi(\sigma) = -n \log [1 - F(\sigma)]$ as the risk of failure R and he assumed that the risk of failure dR of an infinitesimal volume dV can be written as $dR = f(\sigma)dV$; since $(1. - F(\sigma))$ depends only on the stress. For the whole specimen

$$R = \int_V f(\sigma)dV$$

and so the probability of failure of the whole specimen is

$$G_n(\sigma) = 1 - \text{Exp}(-\int_V f(\sigma)dV) .$$

Weibull further assumed that the function $f(\sigma)$ has the following form

$$f(\sigma) = \left(\frac{\sigma - \sigma_u}{\sigma_o}\right)^m$$

where σ_u = stress below which there is a zero probability of failure

σ_o = measure of the density of flaws in the material

m = measure of the variability of flaws.

Note: σ_o and m are material constants.

This is the fundamental approach of Weibull's theory. In the case of a pure tensile test, the stress is assumed constant throughout the specimen and consequently

$$G_n(\sigma) = 1 - \text{Exp} \left[-\left(\frac{\sigma - \sigma_u}{\sigma_o}\right)^m V \right]$$

and it can be easily shown that for two specimens from the same material with different volumes V_1 and V_2, we have the following result

$$\left(\frac{\sigma_1}{\sigma_2}\right)^m = \frac{V_2}{V_1}$$

where σ_1 and σ_2 can be considered as the median tensile strength for specimens of different volumes.

A.2 Mathematical Basis to the Distribution of Fibers in the Concrete Mass Following a Poisson Process.

Probability theory can best be applied to random or independent events. In this study we will assume that the fibers of a composite volume are formed into a network by a random process which is fulfilled by the following conditions:

a. The fibers are deposited in the mass independent of each other.

b. The fibers have an equal probability of landing at all portions of the mass.

c. The fibers have an equal probability of making all possible angles with any arbitrary chosen fixed axis; that is the fibers have a random orientation.

It can be stated equivalently that, in relation with conditions (a) and (b), the points of intersections of the fibers with a cutting plane occur independently of each other and have equal probability of landing on any part of the plane.

Considering, for example, a cutting area of size A square inches, divided into $A \times 1$ squares, let us assume that a fiber is represented by its point of intersection with that area and let us materialize this point by a small disk. When a given disk is dropped into the area of interest by a

random process, the probability that its center lands within and outside a given square are $(\frac{1}{A})$ and $(1-\frac{1}{A})$, respectively. If a large number of disks N_L is dropped onto the area, the probability that R fibers land within the given square is given by the binomial distribution

$$p(R) = \binom{N_L}{R} \left(\frac{1}{A}\right)^R \left(1 - \frac{1}{A}\right)^{N_L - R}$$

If N_L is large and $\frac{1}{A}$ is relatively small, $\frac{N_L}{A} = N_S$ would represent the mean number of fiber intersections per square inch and $p(R)$ reduces to the Poisson approximation of the binomial distribution, that is

$$p(R) = \frac{N_S^R \, e^{-N_S}}{R!} \quad .$$

Note that $p(R)$ is the probability of finding R fiber intersections knowing that N_S is the average number of intersections.

We can equivalently define N_V as being the mean number of fibers per unit volume of the composite, and, following the same reasoning, end up with

$$p(Q) = \frac{N_V^Q \, e^{-N_V}}{Q!} \quad .$$

$p(Q)$ is the probability of finding Q fibers in a volume containing on the average N_V fibers.

In view of the above assumptions, it seems a priori very realistic to assume a Poisson type distribution for the fibers in a fiber reinforced concrete member. This assumption is furthermore made attractive as the average number of fibers per unit volume N_V is easily derived from the given independent and exogeneous variables of interest, the fraction volume V_f, the length ℓ, and the diameter ϕ of the fibers. Experimental justification of the Poisson like distribution of fibers is made in Appendix A.3 .

A.3 The χ^2 Goodness-of-Fit Test Used to Validate the Assumption on the Poisson Distribution of Fibers.

The χ^2 goodness-of-fit test was used in this study to determine whether a sample representing the fiber intersections of a cross sectional area comes from a population having a distribution of Poisson form.

Let us call $p_\lambda(x) = \frac{\lambda^x e^{-\lambda}}{x!}$ the theoretical Poisson distribution function. Given a sample of observed data represented by a histogram, one has to decide, at the significance level α, whether these data constitute a sample from the population with distribution function $p_\lambda(x)$.

Suppose the experimental sample values fall into r categories. To compare the observed frequencies n_i with the expected theoretical frequencies x_i we compute

$$\chi^2 = \sum_{i=1}^{r} \frac{(n_i - x_i)^2}{x_i} .$$

Let us state our null hypothesis H_o as follows: the fiber intersections are Poisson distributed in the cross sectional area of the material. If the calculated value χ^2 exceeds $\chi^2_{\alpha,f}$ for f degrees of freedom, as given in standard tables, we reject at the significance level α the null hypothesis.

The value of f is given as $f = r - 1 - g$. If we can specify the type and form of $p_\lambda(x)$ before the experiment,

but cannot specify it completely, then g stands for the number of quantities necessary to complete the specification. These quantities are obtained as estimates from the experimental data themselves. In our case, we determine from the experimental data the mean value of fiber intersections per square, and we choose that value as the λ parameter of the theoretical distribution $p_\lambda(x)$. Therefore for our test, $g = 1$ and $f = r - 2$.

Let us finally note that the α level of significance of the test means that if the null hypothesis is true, there is an $\alpha\%$ probability that we will reject it (Type I error). In practice, usual values of α are taken as 10%, 5%, and 1%.

Let us give an example of how the χ^2 test has been applied to validate the Poisson distribution of fibers. For that we analyze a slice taken from specimen C3 (identified as slice 1 top face). We put on that section a grid containing $8 \times 8 = 64$ small squares of dimensions 0.2×0.2 inches. We count the fibers inside each square (Table 1) and plot the histogram. In order to show the importance of the range r we run the test for two values of r, one corresponding to one fiber interval and the other to two fiber intervals (Tables 2 and 3). The result may be a striking difference in the apparent goodness-of-fit of the histogram as shown in Fig. A1 and 5 . Also on these figures are shown the theoretical distribution curve

for the experimental mean observed and the theoretical curve for the theoretical mean.

TABLE 1

Number of fiber intersections observed in grid

5	1	2	3	8	11	10	6
4	4	3	7	5	4	2	2
6	5	4	4	5	4	4	6
6	5	6	6	6	4	8	13
5	3	7	5	1	8	3	10
3	7	11	7	4	8	4	7
3	3	8	8	7	2	7	7
1	3	5	4	6	4	4	7

The observed mean number per square is $\lambda_o = 5.3$

The theoretical mean number per square is $\lambda_t = 7.6$

So the curves drawn on Fig. A1 and 5.

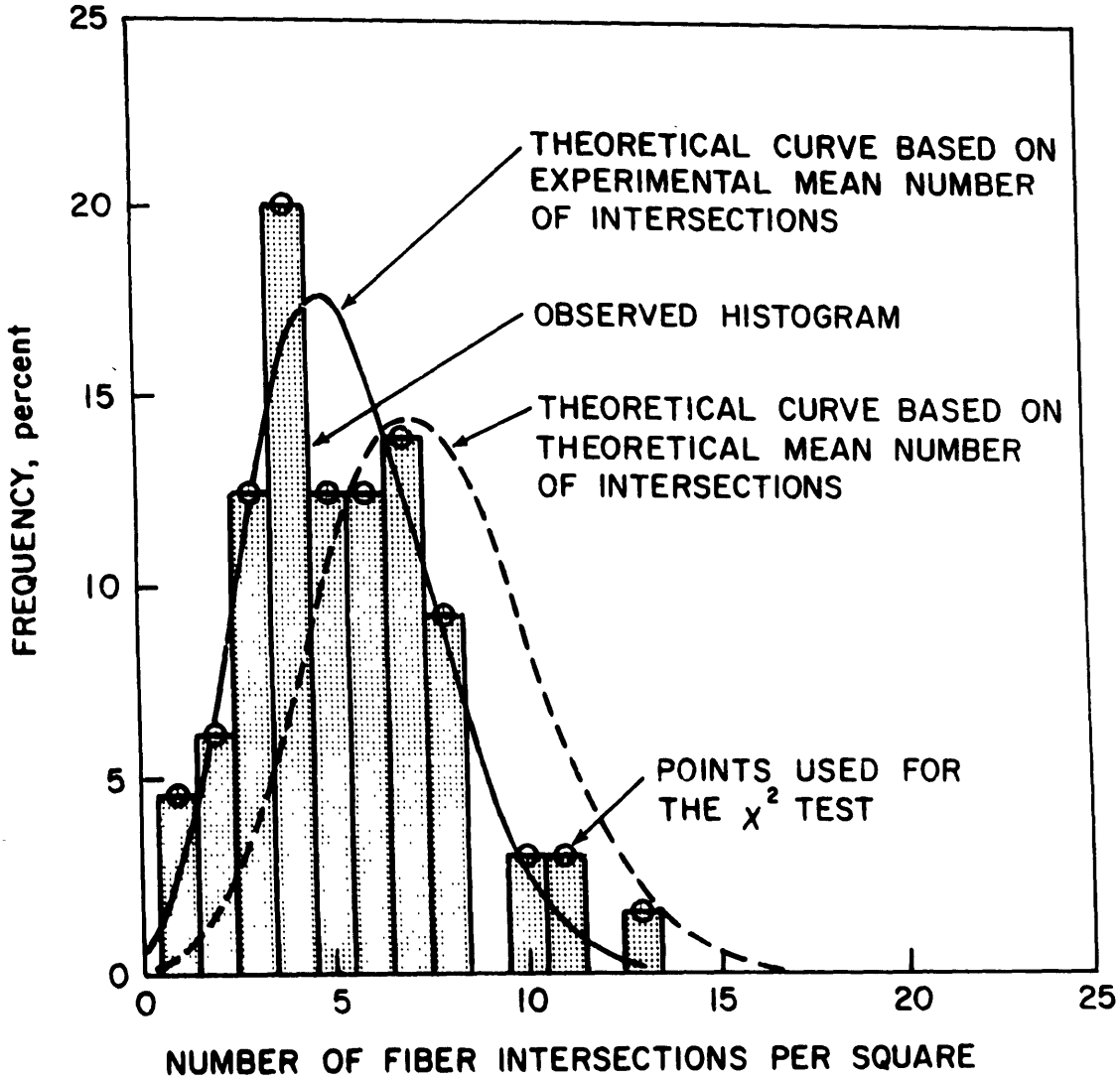

FIG. A1. POISSON-LIKE DISTRIBUTION OF THE FIBER INTERSECTIONS IN A CROSS SECTION.

TABLE 2

χ^2 test results for $r = 13$ categories and an interval of one fiber intersection

Number of fiber intersections	Observed number of occurrences n_i	Normalized theoretical occurrences x_i	Normalized square deviation $\frac{(n_i - x_i)^2}{x_i}$
0	0	0.30	0.30
1	3.	1.70	1.00
2	4.	4.48	0.051
3	8.	7.83	0.003
4	13.	10.50	0.595
5	8.	11.20	0.920
6	8	9.82	0.337
7	9	7.45	0.322
8	6	4.94	0.228
9	0	2.95	2.95
10	2	1.54	0.125
11	2	0.75	2.080
12	0	0.32	0.320
13	1	0.20	3.20
	$\Sigma = 64$	$\Sigma = 64$	$\chi^2 = 12.43$

The $\chi^2_{0.10,11} = 17.3$ $\chi^2 = 12.43 < \chi^2_{0.10,11} = 17.43$

So with 90% confidence we cannot reject the null hypothesis.

TABLE 3

χ^2 test for $r = 7$ categories and an interval of 2 fiber intersections

Number of fiber intersections	Number of occurrences observed n_i	Normalized theoretical occurrences x_i	Normalized square deviation $\frac{(n_i - x_i)^2}{x_i}$
0 and 1	3.	2.02	0.475
2 - 3	12.	12.40	0.013
4 - 5	21	21.66	0.020
6 - 7	17	17.30	0.005
8 - 9	6	7.80	0.005
10 - 11	4	2.28	1.300
12 - 13	1	0.54	0.392
	64	64	$\chi^2 = 2.21$

$$\chi^2 = 2.21 < \chi^2_{0.10,5} = 9.24$$

So with 90% confidence we cannot reject the null hypothesis.

A.4 On the Cracking Strength of Fiber Reinforced Concrete

The approach described herein is similar to that of Kelly and Davies [55], but takes into consideration the randomness of the fiber orientation and distribution in space.

The model proposed simulates the composite by considering a small matrix prism containing one fiber. The component's fraction volumes in the prism are identical to those of the real material. Furthermore, it is assumed that if a tensile strain (or stress) is applied on the matrix, it will be high enough to develop the full value of shear or bond strength at the fiber matrix interface.

Assume first that the fiber is oriented in the loading direction. Let us apply a load P_c on the composite (model). We then have

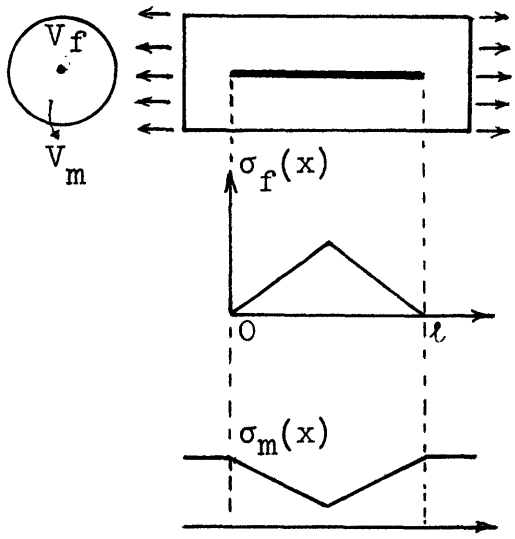

$$P_c = P_f + P_m$$

where the subscripts f and m stand for fiber and matrix, respectively. Along the fiber we have

$$P_c = A_f\sigma_f(x) + A_m\sigma_m(x). \tag{1}$$

Note that x is the abcissa from the edge of the fiber and $0 \leq x \leq \ell/2$.

That is, the stress in the matrix decreases with x while it increases in the fiber.

$$(2) \qquad \frac{dP_c}{dx} = 0 = A_f \, d\sigma_f(x) + A_m \, d\sigma_m(x).$$

The analysis of a pull-out load test on a fiber leads to the following result

$$A_f d\sigma_f(x) = \pi \phi \bar{\tau} \, dx$$

and for $$A_f = \frac{\pi \phi^2}{4}$$

$$d\sigma_f(x) = \frac{4\bar{\tau}}{\phi} \, dx$$

and from (2) $$d\sigma_m(x) = - \frac{A_f}{A_m} \frac{4\bar{\tau}}{\phi} \, dx.$$

Note that the ratio $\frac{A_f}{A_m} = \frac{V_f}{V_m} = \frac{V_f}{1-V_f}$. We are interested in the value of x for which the matrix will crack. That is the decrease in matrix stress from the point $x = 0$ should be at least equal to the ultimate tensile strength of the matrix.

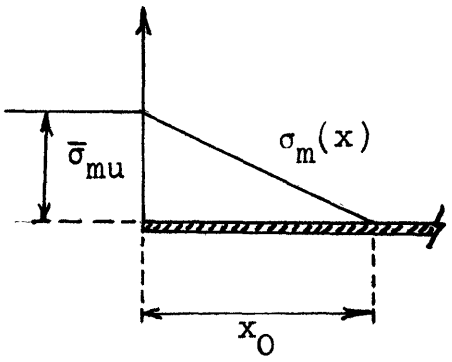

The stresses in the fibers and in the matrix along the fiber can be written as

$$(3) \qquad \begin{cases} \sigma_f(x) = \dfrac{4\bar{\tau}}{\phi}\, x \\ \sigma_m(x) = \sigma_m - \dfrac{A_f}{A_m}\, \sigma_f(x) \end{cases}$$

where σ_m is the stress in the matrix outside the region covered by the fiber. We are interested in the value of x for which $\sigma_m = \bar{\sigma}_{mu}$, i.e. for which the matrix will crack, and for $\sigma_m(x) = 0$. Therefore

$$\sigma_m(x) = 0 = \bar{\sigma}_{mu} - \frac{A_f}{A_m} - \frac{4\bar{\tau}}{\phi}\, x_0$$

and

$$x_0 = \frac{\phi}{4\bar{\tau}}\ \bar{\sigma}_{mu}\left(\frac{1-V_f}{V_f}\right) .$$

The critical length of the fiber is defined by symmetry equal to $2x_0$.

So $\ell_{co} = \bar{\sigma}_{mu}\, \dfrac{\phi}{2\bar{\tau}}\left(\dfrac{1-V_f}{V_f}\right)$.

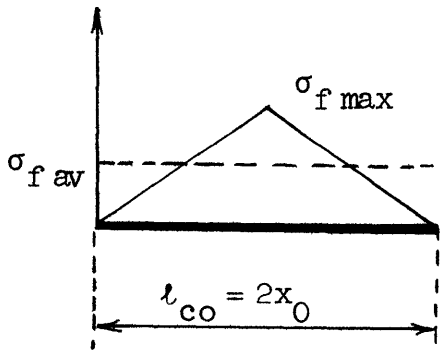

Note that the subscript o in ℓ_{co} refers to the fact that we have been considering a fiber oriented in the loading direction i.e. with $\theta = o$.

A fiber oriented at an angle θ to the loading direction will have a modified critical length. In the matrix $\sigma_{m\theta} = \sigma_{mo} \cos^2 \theta$, that means that the matrix will apparently break at a lower stress relatively to the fiber.

The critical length in this case is given by

$$(4) \qquad \boxed{\ell_{c\theta} = \bar{\sigma}_{mu} \frac{\phi}{2\bar{\tau}} \left(\frac{1-V_f}{V_f}\right) \cos^2 \theta = \ell_{co} \cos^2 \theta \ .}$$

We are now interested in assessing the contribution of the fiber to the cracking strength of the composite. For this we need to calculate first the average stress in the fiber, then multiply it by the expected number of fibers intersecting per square inch of material. This is done, step by step, in the following procedure.

Procedure Leading to the Determination of the Composite Cracking Strength

a) Calculate $\ell_{co} = \bar{\sigma}_{mu} \frac{\phi}{2\bar{\tau}} \left(\frac{1-V_f}{V_f}\right)$.

b) If $\ell \geq \ell_{co} \geq \ell_{c\theta}$, we have for a fiber oriented at θ

$$\sigma_{fmax} = \frac{2\tau}{\phi} \ell_{c\theta}$$

$$\sigma_{fav} = \sigma_{fmax}\left(1 - \frac{\ell_{c\theta}}{2\ell}\right) = \frac{2\bar{\tau}}{\phi} \ell_{c\theta}\left(1 - \frac{\ell_{c\theta}}{2\ell}\right) .$$

The expected value of σ_{fav} can be written as follows:

$$E(\sigma_{fav})\Big|_{0\leq\theta\leq\pi/2} = \bar{\sigma}_{fav} = \frac{2\bar{\tau}}{\phi} E\left[\ell_{c\theta} - \frac{\ell_{c\theta}^2}{2\ell}\right] .$$

The expected load taken by the fibers per square inch

of composite

$$E(F_s) = N_s A_f \bar{\sigma}_{fav} = \frac{2V_f}{\pi\phi^2} \frac{\pi\phi^2}{4} \bar{\sigma}_{fav} = \frac{V_f}{2} \bar{\sigma}_{fav}$$

and the composite's expected cracking strength will be

$$E(\sigma_{cc}) = \bar{\sigma}_{cc} = \bar{\sigma}_{mu}(1-V_f) + \frac{V_f}{2} \bar{\sigma}_{fav}.$$

c) If $\ell < \ell_{co}$ then there exists certainly a θ value, say θ_0, below which $\ell \geq \ell_{c\theta}$ as $\ell_{c\theta} = \ell_{co} \cos^2 \theta$, and $0 \leq \cos^2 \theta \leq 1$. To determine θ_0 calculate

$$\cos^2 \theta_0 = \frac{2\bar{\tau}\,\ell\,V_f}{\phi\,\bar{\sigma}_{mu}(1-V_f)} \Rightarrow \theta_0 .$$

i) For $0 \leq \theta \leq \theta_0$ $\ell \leq \ell_{c\theta}$.

Therefore $\sigma_{fmax} = \frac{2\bar{\tau}}{\phi} \frac{\ell}{\cos^2 \theta}$

$$\sigma_{fav} = \tfrac{1}{2} \sigma_{fmax}$$

$$E(\sigma_{fav})\Big|_{0\leq\theta\leq\theta_0} = E(\frac{\bar{\tau}}{\cos^2 \theta} \frac{\ell}{\phi}) = \bar{\sigma}^{(1)}_{fav} .$$

ii) For $\theta_0 \leq \theta \leq \pi/2$ $\ell \geq \ell_{c\theta}$

$$\sigma_{fmax} = \frac{2\bar{\tau}}{\phi} \ell_{c\theta}$$

$$\sigma_{fav} = \frac{2\bar{\tau}}{\phi} \ell_{c\theta}(1 - \frac{\ell_{c\theta}}{2\ell})$$

$$E(\sigma_{fav})\Big|_{\theta_0 \leq \theta \leq \pi/2} = \bar{\sigma}^{(2)}_{fav} \cdot$$

iii) The overall expected average fiber stress to be used is given by

$$\bar{\sigma}_{fav} = \frac{\theta_0}{\pi/2}\,\bar{\sigma}^{(1)}_{fav} + \frac{\pi/2 - \theta_0}{\pi/2}\,\bar{\sigma}^{(2)}_{fav}$$

and the expected value of the cracking strength of the composite will be

$$\bar{\sigma}_{cc} = \bar{\sigma}_{mu}(1-V_f) + \frac{V_f}{2}\,\bar{\sigma}_{fav} \cdot$$

Application to the Special Case of Concrete

The maximum possible stress in the fiber corresponds to the case where we have the same strain in the fiber and the matrix, like in continuous reinforcement. Therefore

$$\sigma_f = \frac{E_f}{E_m}\,\sigma_m$$

and at cracking of the matrix, we have an upper bound

$$\sigma_f^* = \frac{E_f}{E_m}\,\bar{\sigma}_{mu} \cdot$$

For average concrete we will have

$$\sigma_f^* \simeq \frac{30.10^6}{3.10^6}\ 300 = 3000 \text{ psi} \cdot$$

An example of σ_{fmax} as derived from the model assuming $\frac{\ell}{\phi} = 50$ and $\bar{\tau} = 300$ psi gives

$$\sigma_{fmax} = 2\bar{\tau} \frac{\ell}{\phi} \simeq 30{,}000 \text{ psi} .$$

This is an order of magnitude higher than the possible σ_f^* and the model does not seem useful here. Note that this discrepancy is due to the fact that we assumed that enough strain is applied on the composite to develop the full shear strength at the fiber matrix interface. If on the other hand we put a limitation on the strain applied, it will not be possible to assess how much of the bond is developed along the fiber. An experimental investigation and analysis of observed results, as was done in this thesis, may provide a more realistic answer to the problem.

APPENDIX B

TABLES OF RESULTS

TABLE B1

Results of Pull-out Tests on Fibers

Type	Spec. no.	Peak Load Pounds	Spec. no.	Peak Load Pounds	Results of Interest
1 Fiber Straight Pull-out	1	10.3	28	9.5	Mean Load = 5.97 pounds St. Dev. = 3.27 pounds Mean Bond Stress = 380 psi St. Dev. = 208 psi
	2	2.0	29	5.9	
	3	2.6	30	6.5	
	4	1.4	31	9.2	
	5	1.3	32	7.5	
	6	2.3	33	7.6	
	7	7.6	34	11.8	
	8	5.9	35	8.1	
	9	1.2	36	9.5	
	10	3.8	37	9.8	
	11	1.3	38	7.3	
	12	2.1	39	5.3	
	13	8.3	40	4.2	
	14	1.8	41	10.2	
	15	6.6	42	9.8	
	16	1.4	43	13.2	
	17	7.4	44	9.8	
	18	3.5	45	10.3	
	19	4.6	46	8.	
	20	5.0	47	12.	
	21	3.9	48	6.1	
	22	6.6	49	4.4	
	23	9.1	50	6.7	
	24	2.6	51	3.0	
	25	2.6	52	2.4	
	26	2.8	53	6.8	
	27	3.9	54	5.9	

TABLE B1 continuation

Type	Peak Load Pounds	Final Load (Plateau) Pounds	Results of Interest Normalized per Fiber
2 Fib. oriented at 15°	8.9 7.1 7.8 11.6 7.1 20.0 8.0 20.6 5.9 3.8 3.0 1.6 16.8 3.3 4.9 17.5 6.7 4.3	.8 * 1.8 2.0 2.8 2.0 2.9 4.0 .8 1.0 .6 1.0 1.6 1.4 1.6 * 1.6 1.4	Peak Load Mean Load = 4.41 lbs Standard Deviation = 2.98 lbs Corresp. Mean Bond = 280. psi Stan. Dev. Bond Stress = 189 psi Final Plateau Value Mean Load = 0.85 lbs Standard Deviation = .45 lbs Mean Bond Stress = 54. psi Stan. Dev. Bond Stress = 28. psi
2 Fib. oriented at 30°	11.5 4.6 5.7 5.7 10.5 12.8 7.4 12.5 3.6 11.4 3.7 11.3 6.0	1.8 2.0 2.0 1.8 2.0 5.0 3.6 5.2 2.8 2.6 2.4 2.4 *	Peak Load Results: Mean Load = 4.1 lbs Standard Deviation = 1.75 lbs Mean Bond Stress = 261. psi Standard Deviation = 114. psi Final Plateau Results: Mean Load = 1.4 lbs Standard Deviation = 0.59 lbs Mean Bond Stress = 89. psi Standard Deviation = 37. psi

TABLE B1 continuation

Type	Peak Load Pounds	Final Load (Plateau) Pounds	Results of Interest Normalized per Fiber
2 fib. oriented at 45°	8.8	3.9	Peak Load Results:
	9.2	4.1	Mean Load = 5.0 lbs
	8.9	4.0	Standard Deviation = 1.03 lbs
	12.0	4.0	Mean Bond Stress = 318. psi
	13.2	4.0	Standard Deviation = 65. psi
	8.0	3.6	Final Plateau Results:
			Mean Load = 1.97 lbs
			Standard Deviation = 0.09 lbs
			Mean Bond Stress = 125. psi
			Standard Deviation = 6. psi
2 fib. oriented at 60°	10.6	6.0	Peak Load Results:
	12.5	6.2	Mean Load = 6.25 lbs
	15.3	*	Standard Deviation = .83 lbs
	12.6	7.0	Mean Bond Stress = 398. psi
	11.5	4.0	Standard Deviation = 52.8 psi
			Final Plateau Results:
			Mean Load = 2.9 lbs
			Standard Deviation = .64 lbs
			Mean Bond Stress = 184. psi
			Standard Deviation = 40. psi
2 fib. oriented at 75°	12.2	8.0	Peak Load Results
	10.6	8.0	Mean Load = 5.5 lbs
	10.6	7.0	Standard Deviation = .44 lbs
	10.0	6.0	Mean Bond Stress = 350. psi
	11.6	*	Standard Deviation = 28. psi
			Final Plateau Results:
			Mean Load = 3.62 lbs
			Standard Deviation = .48 lbs
			Mean Bond Stress = 230. psi
			Standard Deviation = 31. psi

(*) One fiber broke before end of test.

TABLE B2

Results of Tensile Tests on Fiber-Reinforced Concrete Prisms

Specimen Type	Reinforcement Parameters	Cracking Load Pounds	Maximum Post-cracking Load Pounds	Descriptors Mean Values and Standard Deviations psi
A1	ℓ = 0.50" ϕ = 0.01" V_f = 1%	925 985 780 520 620 625 960 950	160 50 130 90 240 170 300 140	Cracking stress = 265 SD = 62 Postcracking stress = 53.3 SD = 26
	Aver. SD	796 185	160 79	
A2	ℓ = 0.50" ϕ = 0.01" V_f = 2%	1025 950 645 520 570 1000 970 1085	560 130 140 95 460 130 265 270	Cracking stress = 282 SD = 76 Postcracking stress = 85 SD = 57
	Aver. SD	847 227	256 171	
A3	ℓ = 0.50" ϕ = 0.01" V_f = 3%	540 875 1070 1030 1270 800	530 280 340 600 190 300	Cracking stress = 310 SD = 69 Postcracking stress = 124 SD = 52
	Aver. SD	932 207	373 158	

TABLE B2 continued

Specimen Type	Reinforcement Parameters	Cracking Load Pounds	Maximum Post-cracking Load Pounds	Descriptors Mean Values and Standard Deviations
B1	ℓ = 0.75"	1030	90	Cracking stress = 295 psi
		965	160	SD = 42 psi
		750	80	
	ϕ = 0.01"	1080	400	
		815	210	Postcracking
	V_f = 1%	730	120	stress = 77 psi
		850	395	SD = 49 psi
		880	460	
	Aver.	887	232	
	SD	127	147	
B2	ℓ = 0.75"	1110	240	Cracking stress = 311 psi
		1060	520	SD = 51 psi
	ϕ = 0.01"	1020	290	
	V_f = 2%	880	410	Postcracking
		820	480	stress = 130 psi
		720	410	SD = 33 psi
	Aver.	936	390	
	SD	152	108	
B3	ℓ = 0.75"	910	435	Cracking stress = 357 psi
		1400	532	SD = 76 psi
	ϕ = 0.01"	1050	470	
	V_f = 3%	930	850	Postcracking
				stress = 191 psi
				SD = 63 psi
	Aver.	1072	572	
	SD	227	189	

TABLE B2 continued

Specimen Type	Reinforcement Parameters	Cracking Load Pounds	Maximum Post-cracking Load Pounds	Descriptors Mean Values and Standard Deviations
C1	ℓ = 1" ϕ = 0.01" V_f = %	980 900 1000 1200 750 965	320 90 370 700 200 115	Cracking stress = 322 psi SD = 54 psi Postcracking stress = 100 psi SD = 75 psi
	Aver. SD	966 163	299 225	
C2	ℓ = 1" ϕ = 0.01" V_f = 2%	940 1090 920 1050 970 960 1200	690 630 720 690 300 460 140	Cracking stress = 339 psi SD = 34 psi Postcracking stress = 172 psi SD = 75 psi
	Aver. SD	1018 100	507 226	
C3	ℓ = 1" ϕ = 0.01" V_f = 3%	1130 1210 1160	500 700 990	Cracking stress = 389 psi SD = 13 psi Postcracking stress = 243 psi SD 82 psi
	Aver. SD	1167 40	730 246	

TABLE B2 continued

Specimen Type	Reinforcement Parameters	Cracking Load Pounds	Maximum Post-cracking Load Pounds	Descriptors Mean Values and Standard Deviations
D1	ℓ = 0.50" ϕ = 0.006" V_f = 1%	890 1175 1000 1050 630 920	480 430 610 190 170 375	Cracking Stress = 307 psi SD = 57 psi Postcracking stress = 125 psi SD = 63 psi
	Aver. SD	920 171	376 190	
D2	ℓ = 0.50" ϕ = 0.006" V_f = 2%	1165 1160 950 1130 780 720	310 240 630 450 690 330	Cracking stress = 328 psi SD = 66 psi Postcracking stress = 147 psi SD = 61 psi
	Aver. SD	986 198	442 183	
D3	ℓ = 0.50" ϕ = 0.006" V_f = 3%	960 1080 1260 1310 880 1140	340 530 420 1110 550 370	Cracking stress = 368 psi SD = 56 psi Postcracking stress = 184 psi SD = 95 psi
	Aver. SD	1105 167	553 285	

Specimen Type	Average area under load elong. curve	Correspon. total energy lbs.inch	Surface energy $\bar{\gamma}$ lbs/inch	Toughn. $\bar{G} = 2\bar{\gamma}$ lbs/inch	Comp. modulus E_c^* 10^6 psi	Fracture toughness $K_{1c} = \sqrt{\frac{2E_c\bar{\gamma}}{1-\nu_c^2}}$ psi$\sqrt{\text{inch}}$
A1	2.57	12.85	2.14	4.28	3.76	4200
A2	2.78	13.90	2.32	4.64	4.03	4410
A3	3.28	16.40	2.73	5.46	4.30	4940
B1	3.95	19.75	3.29	6.58	3.76	5070
B2	4.93	24.65	4.11	8.22	4.03	5880
B3	6.62	33.10	5.51	11.02	4.30	7040
C1	4.85	24.25	4.04	8.08	3.76	5610
C2	6.70	33.50	5.58	11.16	4.03	6850
C3	8.20	41.	6.83	13.66	4.30	7820
D1	4.60	23.	3.83	7.66	3.76	5470
D2	5.11	25.55	4.25	8.50	4.03	5970
D3	5.43	27.15	4.52	9.04	4.30	6360
Contr. Matrix	1.15	5.75	.96	1.92	3.50	2640

* $E_c = E_m(1-V_f) + E_f V_f = 3.5(1-V_f) + 30.\ V_f$

* $\nu_c = 0.20$

TABLE B3 Surface Energy and Toughness of Fiber Reinforced Concrete as Deduced from Results of Tensile Tests.

APPENDIX C

ADDITIONAL FIGURES

Figs. C1 to C4. Typical Average Load Elongation Curves of Fiber Reinforced Concrete Specimens in Tension - Series A, B, C, D.

Figure C5. Typical Load Displacement Curve of Cleavage Type Specimen.

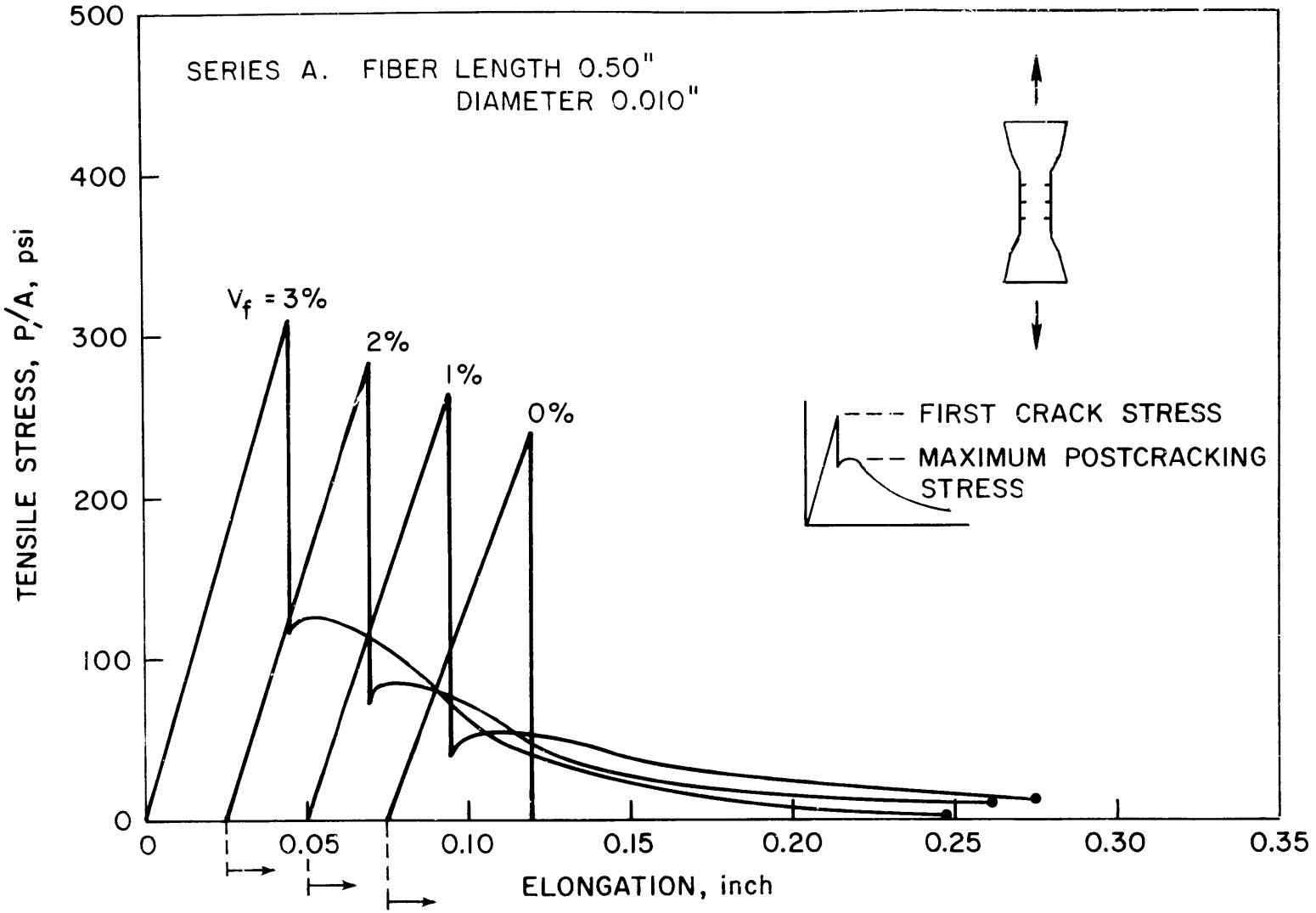

FIG. C1. TYPICAL AVERAGE LOAD ELONGATION CURVES OF FIBER-REINFORCED CONCRETE SPECIMENS IN TENSION.

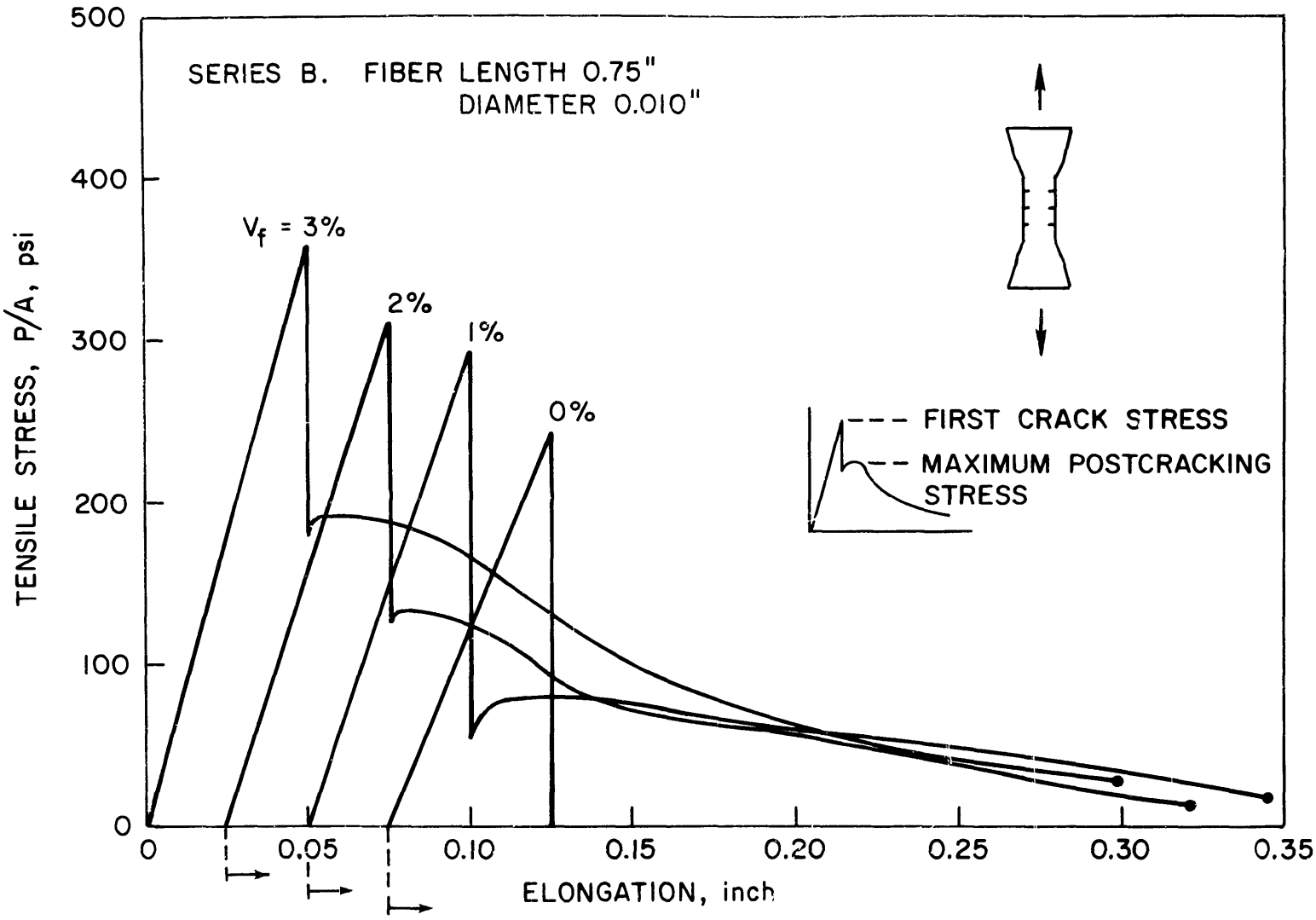

FIG. C2. TYPICAL AVERAGE LOAD ELONGATION CURVES OF FIBER-REINFORCED CONCRETE SPECIMENS IN TENSION.

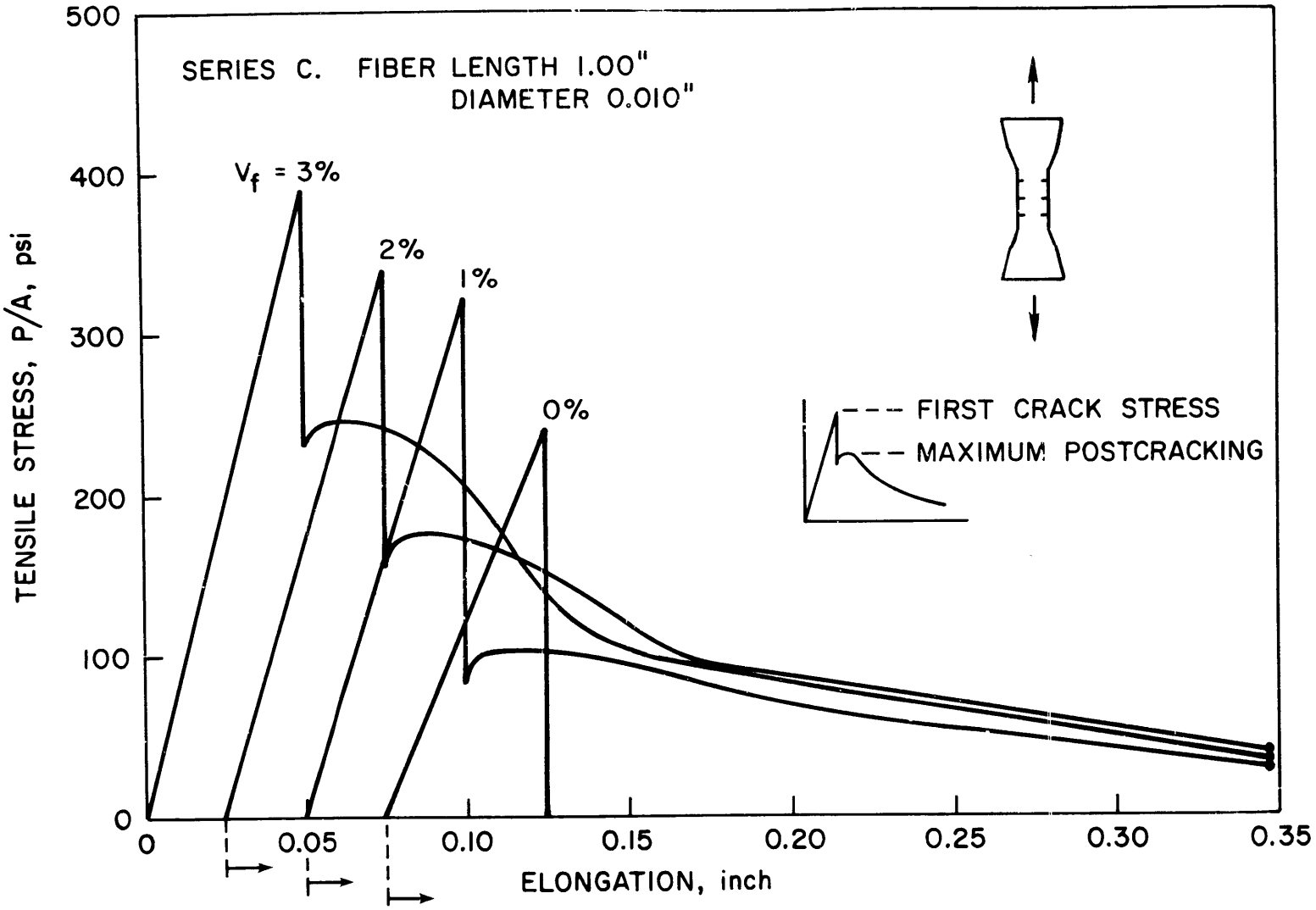

FIG. C3. TYPICAL AVERAGE LOAD ELONGATION CURVES OF FIBER-REINFORCED CONCRETE SPECIMENS IN TENSION.

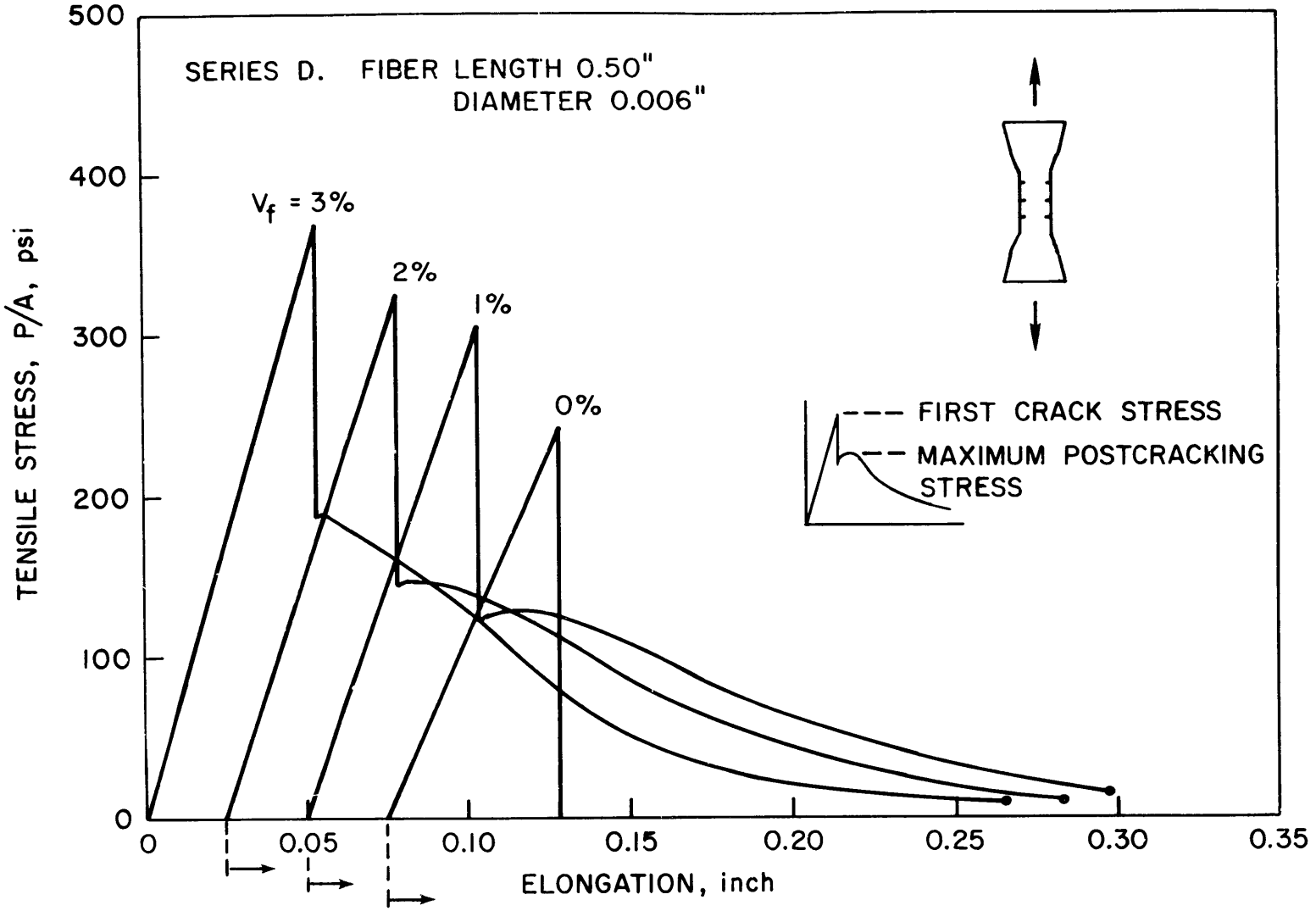

FIG. C4. TYPICAL AVERAGE LOAD ELONGATION CURVES OF FIBER-REINFORCED CONCRETE SPECIMENS IN TENSION.

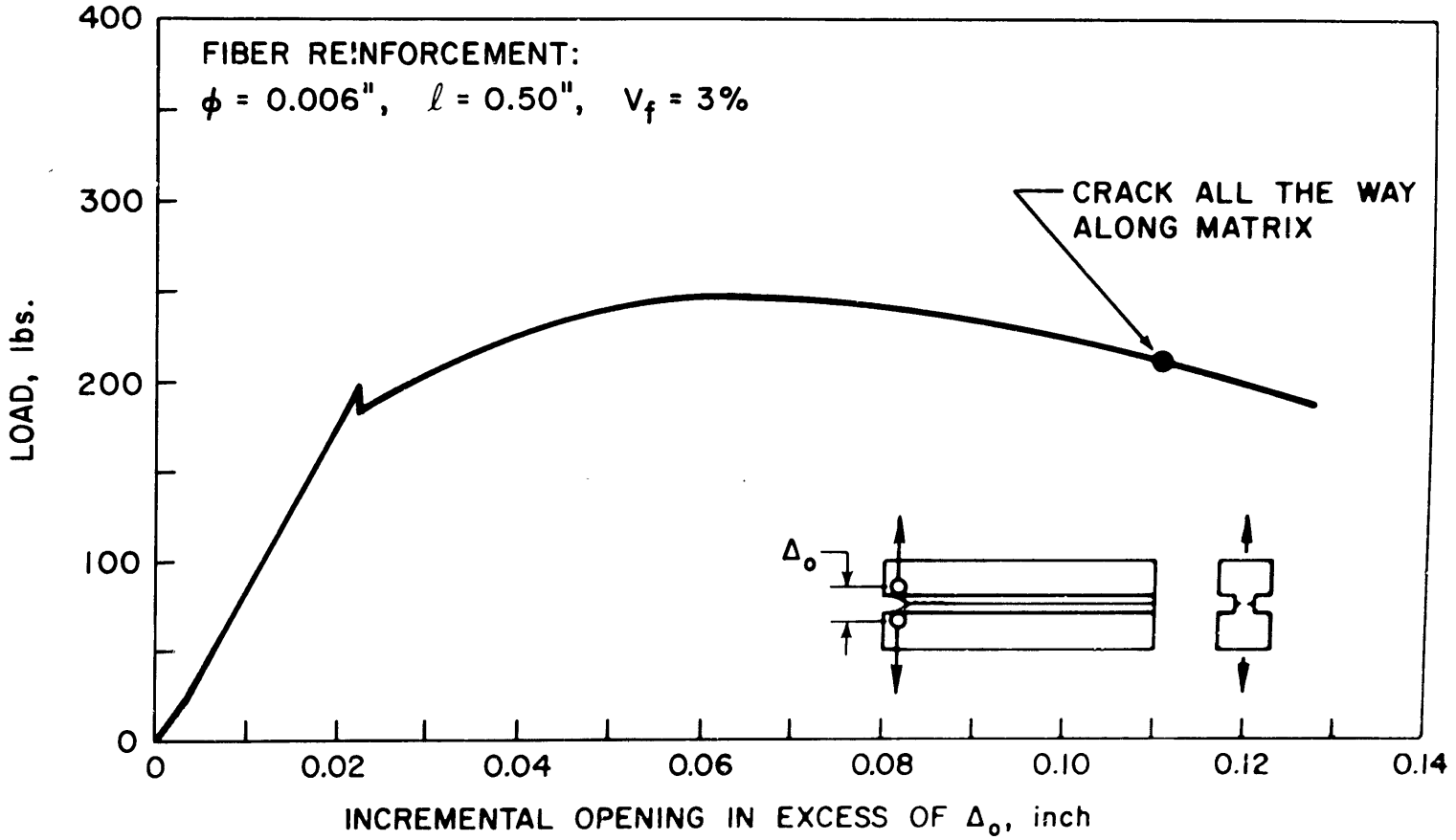

FIG. C5. TYPICAL LOAD-DISPLACEMENT CURVE OF CLEAVAGE SPECIMEN.